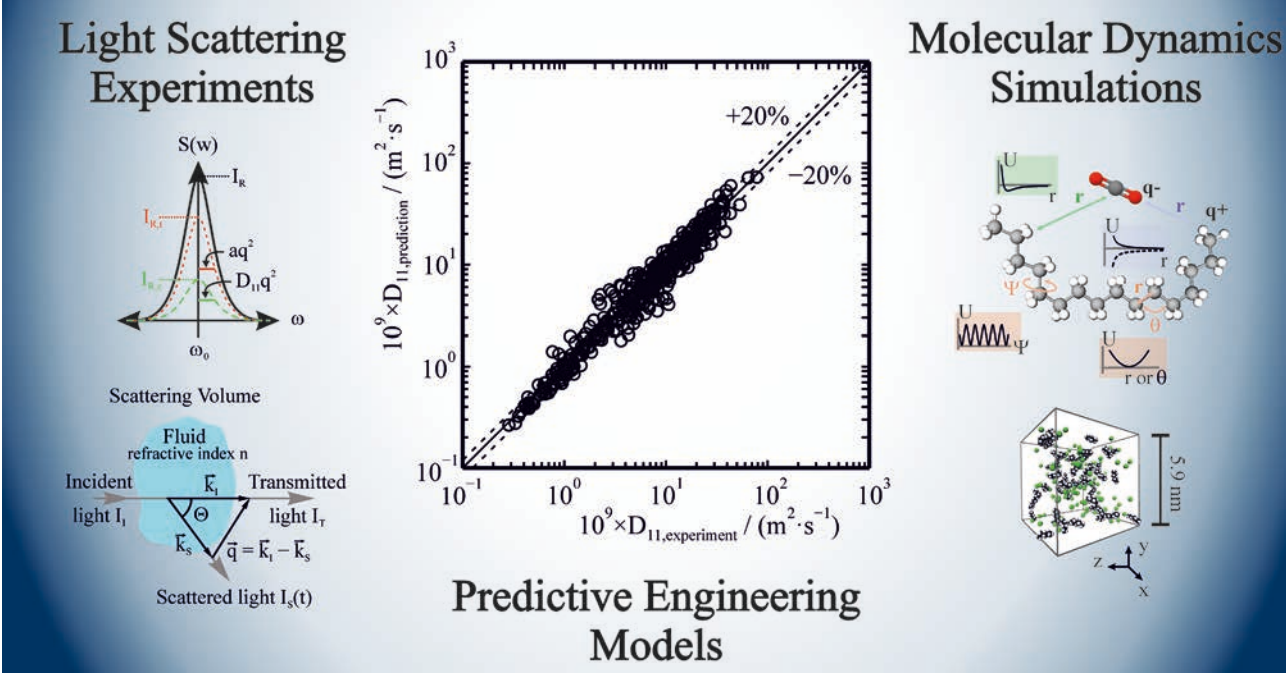

FAU Studies Chemical and Biological Engineering 3

Frances Daggett Lenahan

Diffusion in Liquids with Dissolved Gases by Dynamic Light Scattering Experiments, Equilibrium Molecular Dynamics Simulations, and Prediction Models

FAU University Press

Frances Daggett Lenahan

Diffusion in Liquids with Dissolved Gases by Dynamic Light Scattering Experiments, Equilibrium Molecular Dynamics Simulations, and Prediction Models

FAU Studies Chemical and Biological Engineering

Band 3

Herausgeber/-innen:
Prof. Dr. Kathrin Castiglione
Prof. Dr.-Ing. habil. Andreas Paul Fröba

Frances Daggett Lenahan

Diffusion in Liquids with Dissolved Gases by Dynamic Light Scattering Experiments, Equilibrium Molecular Dynamics Simulations, and Prediction Models

Erlangen
FAU University Press
2024

Bibliografische Information der Deutschen Nationalbibliothek:
Die Deutsche Nationalbibliothek verzeichnet diese Publikation in der Deutschen Nationalbibliografie; detaillierte bibliografische Daten sind im Internet über http://dnb.d-nb.de abrufbar.

Kontakt: Frances Daggett Lenahan, Friedrich-Alexander-Universität Erlangen-Nürnberg (ROR https://ror.org/00f7hpc57), https://orcid.org/0000-0001-5117-640X

Bitte zitieren als
Lenahan, Frances Daggett. 2024. *Diffusion in Liquids with Dissolved Gases by Dynamic Light Scattering Experiments, Equilibrium Molecular Dynamics Simulations, and Prediction Models.* FAU Studies Chemical and Biological Engineering Band 3. Erlangen: FAU University Press. DOI: 10.25593/978-3-96147-727-2.

Das Werk, einschließlich seiner Teile, ist urheberrechtlich geschützt.
Die Rechte an allen Inhalten liegen bei ihren jeweiligen Autoren.
Sie sind nutzbar unter der Creative-Commons-Lizenz BY.

Der vollständige Inhalt des Buchs ist als PDF über OPEN FAU
der Friedrich-Alexander-Universität Erlangen-Nürnberg abrufbar:
https://open.fau.de/home

Verlag und Auslieferung:
FAU University Press, Universitätsstraße 4, 91054 Erlangen

Druck: Docupoint

ISBN: 978-3-96147-726-5 (Druckausgabe)
eISBN: 978-3-96147-727-2 (Online-Ausgabe)
ISSN: 2940-6986
eISSN: 2940-6994
DOI: 10.25593/978-3-96147-727-2

Diffusion in Liquids with Dissolved Gases by Dynamic Light Scattering Experiments, Equilibrium Molecular Dynamics Simulations, and Prediction Models

Diffusion in Flüssigkeiten mit darin gelösten Gasen durch dynamische Lichtstreuexperimente, Gleichgewichtsmolekulardynamik-simulationen und Vorhersagemodelle

Der Technischen Fakultät der
Friedrich-Alexander-Universität Erlangen-Nürnberg

zur Erlangung des Doktorgrades Dr.-Ing.

vorgelegt von

Frances Daggett Lenahan, M.Sc.

Als Dissertation genehmigt
von der Technischen Fakultät
der Friedrich-Alexander-Universität Erlangen-Nürnberg (FAU)
Tag der mündlichen Prüfung: 17.11.2023

Gutachter: Prof. Dr.-Ing. habil. Andreas Paul Fröba
Prof. Dr.-Ing habil. Jadran Vrabec

Acknowledgement

At first, I would like to thank Prof. Dr.-Ing. habil Jadran Vrabec of the Technische Universität Berlin for acting as a reviewer to this thesis. I gratefully acknowledge the financial support of the German Research Foundation (Deutsche Forschungsgemein-schaft, DFG) via the project grants FR 1709/15-1 and FR 1709/11-2 as well as the Erlangen Graduate School in Advanced Optical Technologies (SAOT) funded by the Bavarian State Ministry for Science and Art. I would also like to acknowledge the support and computing resources provided by the Erlangen Regional Computing Center (RRZE).

A special thank you goes to my doctoral advisor Prof. Dr.-Ing. habil. Andreas P. Fröba, for not only giving me the opportunity to pursue my doctorate and reviewing this thesis but also for providing guidance, support, and encouragement during my time at his institute. The environment of AOT-TP is certainly one I'll miss. While I am incredibly grateful of all team members, only a few of you made the cut to get your names mentioned. I would like to thank Dr.-Ing. Thomas M. Koller for his expert teaching and supervision during my first year as well as Ziwen Zhai Msc., who was a tremendous help to me in the lab. I am grateful to Maritta Lechler who has always been enthusiastically supportive and is always available for a chat. I am especially grateful to Maximilian Piszko Msc. for performing all the DLS measurements to my simulations and stopping by from time to time to check in. Finally, I thank Dr.-Ing. Tobias Klein for being my mentor, for challenging me, and for being a friend. Your energy is contagious. Hopefully your positivity is too.

This thesis is dedicated to everyone who made the last few years possible. To my friends, who got me out of the house and away from work, so that we may discuss food, culture, history, and life. To my family, who encourage my selfish pursuit of life. You let me know that you are proud of everything I do and there is no greater motivation. To my colleagues, who understand. The workload. The deadlines. The confusion.

To my cat, Cookie, and in loving memory of Cocoa and my grandmother, Virginia Doty Daggett.

Abstract

As energy demand continues to deplete global resources, it is imperative that new materials and methods for both efficient and environmentally conscious industrial-scale processes are investigated. For this reason, there is an increasing interest in working fluids which constitute a liquid with dissolved gas. Such mixtures are used in gas separation or synthesis processes, refrigeration cycles, energy storage and transport, etc. Knowledge on the thermophysical properties of corresponding working fluids will strongly influence the design and optimization of such processes. In particular, the mutual diffusion coefficient, which describes diffusive mass transport in a fluid, is required for several dimensionless numbers in engineering to characterize convective mass transfer. Knowledge on molecular diffusion is also necessary for understanding e.g. de-mixing processes in refrigeration cycles, or for determining the rate-limiting step of chemical processes. The sheer number of possible working fluids or thermodynamic state points makes it impossible to screen candidates using experimental methods. Therefore, this thesis aims to characterize the diffusion process by utilizing experimental data for the validation and improvement of simulation methods and for the development of simple predictive engineering models. Although industrial scale processes typically involve multicomponent mixtures across a wide composition range, the Fick diffusion coefficients discussed in this thesis are for binary mixtures consisting of a liquid solvent with a dissolved gas solute close to the infinite dilution regime. This is done to isolate the causes driving diffusion and characterize the process to better identify where predictive methods can be improved. The concentration dependence of diffusion is also explored by investigating mixtures over a wide concentration range for select mixtures. The experimental diffusivity data of these mixtures at the lowest solute concentrations are included in this thesis along with a discussion on how to verify their proximity to the infinite dilution regime using simulations.

Investigations are performed over temperatures from (298 to 423) K and pressures up to 10.86 MPa. In total, 451 binary Fick diffusion coefficients spanning 89 mixture combinations, 17 liquid solvents, and 11 dissolved gases are evaluated to assess the influence of molecular characteristics on diffusion. The solvents vary by fluid class considering *n*-alkanes with N_c = (6 to 28), 1-alcohols with N_c = (2 to 10), cyclic molecules, branched alkanes, an acid, an ester, and ionic liquids. The dissolved gasses vary by molecular weight from M_{H_2} = 2.02 g·mol^{-1} to M_{R236fa} = 152 g·mol^{-1}, as well as by size, shape, and polarity.

Equilibrium molecular dynamics (EMD) simulations show a systematic underprediction of diffusion coefficients compared to experimental dynamic light scattering (DLS) results. However, they are generally within combined uncertainty and accurately predict the observed trends, leading to a reliable analysis of fluid behavior on a molecular level. To improve the predictive capabilities of EMD simulations, a transferable force field (FF) modification was developed which only requires the critical temperature of the substance and is applicable up to a reduced temperature $T_R = T/T_c$ of 0.98. Additionally, the cyclohexane FF is modified to improve predictions of the dynamic viscosity and self-diffusivity up to 448 K.

One important finding arising from the cumulation of results is the close relationship between viscosity and D_{11} over an extended viscosity range. It could be demonstrated that the relationship is dependent on solute type and weakens with increasing solvent viscosity. Based on the large amount of D_{11} data from experiments and simulations, an exceptionally simple predictive engineering model could be developed. This model is empirically fit to the 451 aforementioned diffusivities with a total bias and average absolute relative deviation (AARD) of (0.08 and 19)%. It is then applied to a further 314 diffusivities acquired from the literature considering 49 mixture combinations, which include 11 binary gaseous mixtures. Overall, the numerical values of this data span seven orders of magnitude. The bias and average absolute relative deviation is (6.7 and 23)%. Considering all 765 binary Fick diffusion coefficients, the bias and AARD are (2.8 and 21)%. The wide applicable range of this model coupled with its exceptional ease of implementation and reasonable accuracy make it a valuable tool for the prediction of Fick diffusivities at the limit of infinite dilution.

The combination of reliable Fick diffusion coefficients from DLS experiments and EMD simulations have led not only to an enhanced fundamental understanding of diffusive mass transport, but also to improvements in the accuracy of EMD simulation results and to the development of a simple, predictive engineering model. Future work following this thesis would include further expanding the available database to novel substances, including more diverse or complex real systems. Additionally, the applicability of the new model could be tested beyond the infinite dilution limit with use of the mixture thermodynamic factor or to multi-component mixtures, provided they may be treated as a binary system. This could extend the scope of this work to many of the working fluids of industrial processes.

Kurzdarstellung

Im Zuge des anhaltenden Energiebedarfs, der globale Ressourcen erschöpft, ist es unerlässlich, dass neue Materialien und Methoden für effiziente und umweltbewusste industrielle Prozesse untersucht werden. Aus diesem Grund wächst das Interesse an Arbeitsfluiden, die aus Flüssigkeiten mit darin gelösten Gasen bestehen. Solche Gemische werden unter anderem in Gastrenn- oder Syntheseprozessen, Kühlkreisläufen und Energiespeicherung sowie transport eingesetzt. Die thermophysikalischen Eigenschaften entsprechender Arbeitsfluide beeinflussen maßgeblich das Design und die Optimierung solcher Prozesse. Insbesondere der Diffusionskoeffizient, der den molekularen Massentransport in einer Flüssigkeit hervorgerufen durch einen Gradienten in der Zusammensetzung beschreibt, wird zur Berechnung mehrerer dimensionsloser Zahlen zur Charakterisierung des Massentransports benötigt. Kenntnis über die molekulare Diffusion ist zudem erforderlich, um beispielsweise Misch-prozesse in Kältemittelkreisläufen zu verstehen oder um geschwindigkeitslimitierende Schritte innerhalb chemischer Prozesse zu bestimmen. Aufgrund der großen Anzahl möglicher Arbeitsfluide und thermodynamischer Zustandspunkte ist es nicht möglich, alle relevanten Kombinationen mit experimentellen Methoden zu untersuchen. Ziel dieser Arbeit ist es daher, den Diffusionsprozess durch die Nutzung experimenteller Daten zur Validierung und Verbesserung von Simulationen sowie zur Entwicklung von Vorhersagemodellen zu charakterisieren. Obwohl industrielle Prozesse meist Gemische mehrerer Komponenten in einem weiten Zusammensetzungsbereich umfassen, bezieht sich ein Großteil der in dieser Arbeit diskutierten Fick'schen Diffusionskoeffizienten auf binäre Gemische bestehend aus einem flüssigen Lösungsmittel mit einem darin gelösten Gas im Bereich der unendlichen Verdünnung des Gases. Dadurch sollen die treibenden Mechanismen der Diffusion isoliert werden, um zu identifizieren, wo Vorhersagemethoden verbessert werden können. Für ausgewählte Gemische wurden auch Untersuchungen zur Konzentrationsabhängigkeit des Diffusionskoeffizienten durchgeführt. Die experimentell bestimmten Diffusionsdaten dieser Gemische bei der geringsten Konzentration des Gases sind in der vorliegenden Arbeit zusammen mit einer Diskussion zur Verifizierung des Bereiches unendlicher Verdünnung mittels Simulationen eingebunden.

Die Untersuchungen wurden bei Temperaturen zwischen (298 und 423) K und Drücken bis zu 10,86 MPa durchgeführt. Insgesamt wurden 451 Diffusionskoeffizienten für 89 Gemische bestehend aus 17 flüssigen

Lösungsmitteln und 11 gelösten Gasen untersucht, um den Einfluss der molekularen Eigenschaften auf die Diffusion zu ermitteln. Die Lösungsmittel umfassen mehrere Flüssigkeitsklassen und beinhalten lineare Alkane mit einer Anzahl an Kohlenstoffatomen N_c = (6 bis 28), 1-Alkohole mit N_c = (2 bis 10), ringförmige Moleküle, verzweigte Alkane, eine Säure, ein Ester und ionische Flüssigkeiten. Die gelösten Gase variieren in ihrem Molekulargewicht von M_{H_2} = 2,02 g·mol^{-1} bis M_{R236fa} = 152 g·mol^{-1} sowie in ihrer Größe, Form und Polarität.

Gleichgewichtsmolekulardynamische (equilibrium molecular dynamics, EMD) Simulationen zeigen eine systematische Unterschätzung der Diffusionskoeffizienten im Vergleich zu experimentellen Ergebnissen der dynamischen Lichtstreuung (DLS). Meist lässt sich allerdings eine Übereinstimmung innerhalb der kombinierten Unsicherheit feststellen und zudem sind die Simmulationen in der Lage, die im Experiment beobachteten Tendenzen korrekt vorherzusagen, was eine zuverlässige Analyse des Flüssigkeitsverhaltens auf molekularer Ebene erlaubt. Um die Vorhersagefähigkeiten von EMD Simulationen zu verbessern, wurde eine übertragbare Kraftfeldmodifikation entwickelt, die nur die kritische Temperatur der Substanz erfordert und bis zu einer reduzierten Temperatur $T_R = T/T_c$ von 0,98 anwendbar ist. Darüber hinaus wird das Kraftfeld für Cyclohexan modifiziert, um die Vorhersagen der dynamischen Viskosität und des Selbstdiffusionskoeffizienten bis zu einer Temperatur von 448 K zu verbessern.

Eine wichtige Erkenntnis aus der Zusammenstellung der Ergebnisse ist der enge Zusammenhang zwischen dem Diffusionskoeffizienten und der Lösungsmittelviskosität über einen weiten der letzteren Größe. Es konnte festgestellt werden, dass dieser Zusammenhang von der Art des gelösten Stoffs abhängt und mit zunehmender Lösungsmittelviskosität schwächer ausgeprägt ist und dadurch eine Schwierigkeit für die Entwicklung einer Vorhersagemodells darstellt. Mit Hilfe der breiten Datenbasis an Diffusionskoeffizienten aus Experiment und Simulation, konnte ein einfaches Vohersagemodell entwickelt werden. Dieses Modell ist empirisch an die 451 oben genannten Diffusivitäten angepasst, mit einer mittleren relativen Abweichung und einer mittleren absoluten relativen Abweichung (AARD) von (0,08 und 19)%. Die Übertragbarkeit des Modells wird durch die Anwendung zur Vorhersage von 314 Diffusionskoeffizienten aus der Literatur, welche 49 Gemische bestehend aus Flüssigkeiten mit darin gelösten Gasen und 11 Gasgemische beinhalten, überprüft. Insgesamt umfasst dieses Testset Diffusionskoeffizienten über sieben Größen-

ordnungen hinweg. Die mittlere relative Abweichung und die AARD für das Testset betragen (6,7 und 23)%. Unter Berücksichtigung aller 765 binären Diffusionskoeffizienten betragen die mittlere relative Abweichung und die AARD (2,8 und 21)%. Der breite Anwendungsbereich dieses Modells in Verbindung mit seiner besonders einfachen Implementierung und seiner angemessenen Genauigkeit machen es zu einem wertvollen Modell für die Vorhersage von Diffusionskoeffizienten im Bereich der unendlichen Verdünnung.

Die Kombination von zuverlässigen Diffusionskoeffizienten aus der DLS und aus EMD Simulationen hat nicht nur zu einem verbesserten grundlegenden Verständnis des diffusiven Massentransports geführt, sondern auch zu Verbesserung der Vorhersagegenauigkeit von EMD Simulationen und zur Entwicklung eines einfachen Vorhersagemodells. Zukünftige Arbeiten können durch eine Erweiterung der verfügbaren Daten hin zu neuartigen, komplexen und diverse Substanzen das Verständnis des diffusiven Massentransports und die Anwendbarkeit des Vorhersagemodells erweitern. Darüber hinaus könnte die Anwendbarkeit des neuen Modells über die unendliche Verdünnungsgrenze hinaus mithilfe des thermodynamischen Faktors der Mischung oder auf Mehrkomponentenmischungen getestet werden, sofern diese als binäres System behandelt werden können. Dies erlaubt es, den Anwendungsbereich des entwickelten Modells hinsichlich vieler weiterer industrie und prozessrelevanter Arbeitsfluide zu erweitern.

Table of Contents

Symbols, Indices, and Abbreviations

Latin Symbols

a	thermal diffusivity	$m^2 \cdot s^{-1}$
A	roughness factor	
b_i	equation constants	
c	molar concentration	$mol \cdot cm^{-3}$
c_s	speed of sound	$m \cdot s^{-1}$
D	diffusion coefficient	$m^2 \cdot s^{-1}$
D^*	dimensionless diffusion coefficient	
D_o	diffusion coefficient acquired from EMD simulations without finite-size corrections	$m^2 \cdot s^{-1}$
D_{11}	binary Fick diffusion coefficient	$m^2 \cdot s^{-1}$
D_{11}^*	effective diffusivity	$m^2 \cdot s^{-1}$
$Đ_{12}$	Maxwell-Stefan diffusion coefficient	$m^2 \cdot s^{-1}$
D_s	sound attenuation	$m^2 \cdot s^{-1}$
D_{self}	self-diffusion coefficient of a neat fluid	$m^2 \cdot s^{-1}$
$D_{self,i}$	self-diffusion coefficient of component i	$m^2 \cdot s^{-1}$
D_{SHS}	smooth hard-sphere self-diffusion coefficient	$m^2 \cdot s^{-1}$
$g_{ij}(r)$	radial distribution function between species i and j	
$G_{ij}(r)$	Kirkwood-Buff integral	$m^3 \cdot molecule^{-1}$
$G_{ij}^{\infty}(r)$	Kirkwood-Buff integral extrapolation to infinite volume	$m^3 \cdot molecule^{-1}$
h	cap height	nm
J_i	diffusion flux	$mol \cdot m^{-2} \cdot s^{-1}$
k	coverage factor	

k_B	Boltzmann constant	$m^2 \cdot kg \cdot s^{-2} \cdot K^{-1}$
k_r	force constant for bond vibrations	$N \cdot m^{-1}$
k_c	force constant for dihedral angle rotations	$N \cdot m^{-1}$
k_q	force constant for angle bending	$N \cdot m^{-1}$
l	bond length	nm
L	length of cubic simulation box edge	nm
Le	Lewis number	
m	intermediate parameter	nm
M	molar mass	$g \cdot mol^{-1}$
n	particle number density	m^{-3}
n_{fluid}	refractive index of the fluid	
$n_{\text{O-H}}$	number of hydrogen bonds	
n_{SE}	Stokes–Einstein number	
N	number of atoms, molecules, or species	
N_A	Avogadro constant	mol^{-1}
N_c	number of carbon atoms	
p	pressure	MPa
p_{ij}	component of the pressure tensor in row i, column j	MPa
$\vec{P}$	pressure tensor	MPa
$\vec{q}$	scattering vector	nm^{-1}
q	modulus of the scattering vector	nm^{-1}
q_i	partial charge of atom i	C
r	radius or radial distance	nm

$r_{i,k}$	center-of-mass position of the k-th molecule of species i	nm
r_{ij}	distance between particles i and j	nm
R	universal gas constant	$J \cdot mol^{-1} \cdot K^{-1}$
$S(w_f)$	scattered light spectrum	
t	time	ps
T	temperature	K
T_o	temperature at which force field development took place	K
T_c	critical temperature	K
U	potential energy	J
V	volume	cm^3
V_o	molar core volume	$cm^3 \cdot mol^{-1}$
$V_{o,i}$	molar core volume of species i	$cm^3 \cdot mol^{-1}$
$V_{o,12}$	average molar core volume of species 1 and 2	$cm^3 \cdot mol^{-1}$
$V_{o,12+}$	molar core volume addition between spheres 1 and 2	$cm^3 \cdot mol^{-1}$
V_b	molal volume at the normal boiling point	$cm^2 \cdot g^{-1} \cdot mol^{-1}$
$V_{cap,i}$	volume of a spherical cap of sphere i	$cm^3 \cdot mol^{-1}$
x	x-coordinate	m
x_i	mole fraction of component i	
y	y-coordinate	m
Y	capillary number	
z	z-coordinate	m

Greek Symbols

β	unity criteria	

χ	association factor	
ε_{ii}	energy parameter of the Lennard-Jones potential	$J \cdot mol^{-1}$
ε_o	permittivity in vacuum	$J \cdot V^{-2} \cdot m^{-1}$
γ	surface or interfacial tension	$N \cdot m^{-1}$
γ_{ij}	activity coefficient	
Γ_{11}	thermodynamic factor	
η	dynamic viscosity	mPa·s
λ_o	wavelength in vacuum	nm
Λ_{ij}	Onsager coefficient	$m^2 \cdot s^{-1}$
μ	dipole moment	D
ν	kinematic viscosity	$m^2 \cdot s^{-1}$
Θ_s	scattering angle	rad
ρ	mass density	$g \cdot cm^{-3}$
ρ_c	critical density	$g \cdot cm^{-3}$
σ	hard sphere core diameter	nm
σ_{eff}	effective diameter	nm
σ_{ij}	size parameter of the Lennard-Jones potential	nm
τ	correlation time	μs or ps
τ_C	mean fluctuation lifetime	μs
$\tau_{C,c}$	characteristic decay time of concentration fluctuations	μs
$\tau_{C,t}$	characteristic decay time of temperature fluctuations	μs
ω	acentric factor	

ω_f	frequency	ns^{-1}
ω_q	frequency of propagation of surface wave fluctuation	ns^{-1}

Abbreviations

AA	All-Atom
AAD	Absolute Relative Deviation
AARD	Average Absolute Relative Deviation
AMBER	Assisted Model Building with Energy Refinement
AOT-TP	Institute of Advanced Optical Technologies – Thermophysical Properties
CAS	Chemical Abstracts Service number
CHARM	Chemistry at HARvard Macromolecular Mechanics
COM	Center of Mass
DFG	Deutsche Forschungsgemeinschaft
DLS	Dynamic Light Scattering
DMIM	1-decyl-3-methylimidazolium
EMD	Equilibrium Molecular Dynamics
EMIM	1-ethyl-3-methylimidazolium
FAU	Friedrich-Alexander Universität
FF	Force Field
GROMACS	GROningen MAchine for Chemical Simulations
GWP	Global Warming Potential
HMIM	1-hexyl-3-methylimidazolium
IL	Ionic Liquid

L-OPLS	Optimized Potentials for Liquid Simulations for Long hydrocarbons
LJ	Lennard-Jones
LOHC	Liquid Organic Hydrogen Carrier
MD	Molecular Dynamics
MSD	Mean Squared Displacement
NEMD	Non-Equilibrium Molecular Dynamics
NMR	Nuclear Magnetic Resonance
NTf_2	bis(trifluoromethylsulfonyl)imide
ODP	Ozone Depletion Potential
OPLS	Optimized Potentials for Liquid Simulations
ORC	Organic Rankine Cycle
RDF	Radial Distribution Function
SLS	Surface Light Scattering
WGSR	Water-Gas Shift Reaction

Indices

calc	calculated
exp	experimental
R	reduced with respect to critical

1 Introduction

The rising threat of prolonged environmental damage is a driving force behind much of modern scientific advancement. Within the field of energy technology, considerable efforts have been made in the last decades on the adaptation of existing infrastructure and the development of new technologies to accommodate more efficient and environmentally friendly methods of energy conversion, transport, and storage. At the forefront of these developments is the careful selection and characterization of novel working fluids. For example, the phase-out of refrigerants known to have high global warming potential (GWP) and ozone depletion potential (ODP), due to the Montreal Protocol and its subsequent revisions, has led to research in and development of highly tunable synthetic oils compatible with existing technologies for mechanical compressors of heat-pump systems and refrigeration. When classified within the fluid class of natural hydrocarbon refrigerants, such oils are typically multi-component mixtures of long-chained branched hydrocarbons [1]. Due to overlapping operating conditions, refrigerants are often used as working fluids in organic Rankine cycles (ORC) as well, where plant specifications can be highly dependent on the working fluid employed. Unfortunately, the optimization of plant design and operation is often organized with limited experimental data [2]. Reference values are largely based on theoretical property predictions and estimations – especially for mixtures. Thermophysical property research could improve the fluid selection process. Yet, to experimentally investigate each qualified candidate is impossible. This is also a necessity to consider when identifying working fluids in the fuel sector, where significant research is focused on eliminating petroleum dependencies. An emerging technology, which allows for the storage and transport of hydrogen (H_2) produced from renewable energies, is the development of liquid organic hydrogen carriers (LOHCs) [3]. Most current LOHC candidates are hydrocarbon-based and have similar thermophysical properties to conventional liquid fuels. Therefore, the existing transport pipeline infrastructure will be available for use by these new working fluids once the conversion processes become commercially viable [4]. The list of candidates for this technology is long, and considerable research efforts are still required at each step of the conversion process [3]. Therefore, a significant challenge is the screening of potential candidates. For each of the technologies mentioned above and particularly for systems or

conditions where experimental methods may be difficult to realize due to concerns of safety or cost, computational and prediction methods could be utilized to predict the thermophysical properties of new candidates and, thus, refine the search.

Diffusive mass transport is a dynamic process which is known to govern mixing processes. For catalysis activities, it is often the rate-limiting step in chemical reactions. The diffusion coefficient is the thermophysical property describing diffusive mass transport and it is necessary for several dimensionless numbers used in engineering. For example, the Lewis number Le is the ratio between the mass and thermal diffusivity coefficients and therefore correlates heat flow and thermal conductivity with the transport of mass. Another important number in engineering is the Thiele modulus, which relates catalytic activity to the size of a particle undergoing reaction. For large-enough particles, only the surface will react and therefore, the reaction rate is limited by how quickly diffusion forces carry the product away from the surface. The Thiele modulus is a good measure of how effectively catalysis pellets perform. Reaction processes such as the Fischer-Tropsch process or the water-gas shift reaction (WGSR) process utilizing gas-liquid mixtures need to consider the diffusion processes present in the mixture in order to optimize product output.

This thesis cumulates work investigating how the molecular characteristics of mixture components influence the diffusive mass process. The aim is to contribute to a fundamental understanding of the relationship between mass diffusion and other fluid properties through the combination of experimental techniques, molecular dynamics simulations, and predictive engineering models. Here, the experimental results serve as validation for the improvement of simulation performance and the development of prediction models. In the following, author contributions to the included publications are identified. The following chapter includes a State of the Art discussing the availability of diffusivity data, experimental and simulation techniques for the determination of mass diffusion coefficients, and prominent prediction models in the literature. Then, the applied strategies and used methods pertaining to the below-publications are detailed, followed by a chapter highlighting the cumulative results of the work, where a simple predictive engineering model is presented for the first time. The final chapter of this thesis summarizes the work and provides an outlook for future investigations.

The contributing publications are as follows:

A. Tobias Klein, Frances D. Lenahan, Manuel Kerscher, Michael H. Rausch, Ioannis G. Economou, Thomas M. Koller, and Andreas P. Fröba, *Characterization of Long Linear and Branched Alkanes and Alcohols for Temperatures up to 573.15 K by Surface Light Scattering and Molecular Dynamics Simulations*. Journal of Physical Chemistry B **2020** *124* (20), 4146-4163, DOI: 10.1021/acs.jpcb.0c01740.

Author's contribution: Frances Lenahan was responsible for organization, execution, and analysis of the simulations. The experimental investigations of this work were performed by Tobias Klein and Manuel Kerscher. The planning and writing of the entire publication was performed by Tobias Klein. The author contributed to the structure and input of the manuscript as well as to the revision process.

B. Frances D. Lenahan, Michael Zikeli, Michael H. Rausch, Tobias Klein, and Andreas P. Fröba, *Viscosity, Interfacial Tension, and Density of Binary-Liquid Mixtures of n-Hexadecane with n-Octacosane, 2,2,4,4,6,-8,8-Heptamethylnonane, or 1-Hexadecanol at Temperatures between 298.15 and 573.15 K by Surface Light Scattering and Equilibrium Molecular Dynamics Simulations*. Journal of Chemical & Engineering Data **2021** *66* (5), 2264-2280, DOI: 10.1021/acs.jced.1c00108.

Author's contribution: Frances Lenahan was responsible for the execution and analysis of the experimental SLS results. The author was also responsible for coordinating and processing simulations performed by Michael Zikeli. The author planned and wrote all parts of the publication.

C. Maximilian Piszko, Frances D. Lenahan, Simon Hahn, Michael H. Rausch, Thomas M. Koller, Tobias Klein, and Andreas P. Fröba, *Diffusivities in Binary Mixtures of n-Hexane or 1-Hexanol with Dissolved CH_4, Ne, Kr, R143a, SF_6, or R236fa Close to Infinite Dilution*. Journal of Chemical & Engineering Data **2021** *66* (5), 2218-2232, DOI:10.1021/acs.jced.1c00084.

Author's contribution: Frances Lenahan was responsible for organization, execution, and analysis of the simulations. The experimental investigations in this work were performed by Maximilian Piszko. The author wrote all parts of the publication related to the simulations and participated in the planning and writing of the complete manuscript.

D. Frances D. Lenahan, Maximilian Piszko, Tobias Klein, and Andreas P. Fröba, *Diffusivities in Binary Mixtures of n-Decane, n-Hexadecane, n-Octacosane, 2-Methylpentane, 2,2-Dimethylbutane, Cyclohexane, Benzene, Ethanol, 1-Decanol, Ethyl Butanoate, or n-Hexanoic Acid with Dissolved He or Kr Close to Infinite Dilution*. Journal of Chemical & Engineering Data **2022** *67* (3), 622-635, DOI: 10.1021/acs.jced.1c00922.

Author's contribution: Frances Lenahan was responsible for organization, execution, and analysis of the simulations. The experimental investigations in this work were performed by Maximilian Piszko. The author planned the complete manuscript and wrote all parts of the publication with the exception of the experimental procedure.

E. Frances D. Lenahan, Ziwen Zhai, Chathura J. Kankanamge, Tobias Klein, and Andreas P. Fröba, *Viscosity and Interfacial Tension of Ternary Mixtures Consisting of Linear Alkanes, Alcohols, and/or Dissolved Gases Using Surface Light Scattering and Equilibrium Molecular Dynamics Simulations*. International Journal of Thermophysics **2022** *116* (43), DOI: https://doi.org/10.1007/s10765-022-03040-x.

Author's contribution: Frances Lenahan was responsible for the organization, execution, and analysis of the experimental SLS results, supported by Ziwen Zhai. The molecular dynamics simulations in this work were performed by Chathura J. Kankanamge. The author planned the complete manuscript and wrote all parts of the publication with the exception of the simulation procedure.

F. Maximilian Piszko, Frances D. Lenahan, Lukas Friedl, Tobias Klein, and Andreas P. Fröba, *Mutual and Thermal Diffusivities in Mixtures of Cyclohexane, n-Hexadecane, n-Octacosane, or n-Hexanoic Acid with Carbon Dioxide Obtained by Dynamic Light Scattering and Molecular Dynamics Simulations*. Journal of Chemical & Engineering Data **2022** *67* (10), 3059-3076, DOI: 10.1021/acs.jced.2c00487.

Author's contribution: Frances Lenahan was responsible for organization, execution, and analysis of the simulations. The experimental investigations in this work were performed by Maximilian Piszko. The author wrote all parts of the publication related to the simulations and participated in the planning and writing of the complete manuscript.

G. Maximilian Piszko, Frances D. Lenahan, Tobias Klein, and Andreas P. Fröba, *Diffusivities in Binary Mixtures of Cyclohexane or Ethyl Butanoate with Dissolved CH_4 or R143a Close to Infinite Dilution*. Journal of Chemical & Engineering Data **2023** *68* (2), 339-348, DOI: 10.1021/acs.jced.2c00696.

Author's contribution: Frances Lenahan was responsible for organization, execution, and analysis of the simulations. The experimental investigations in this work were performed by Maximilian Piszko. The author wrote all parts of the publication related to the simulations and participated in the planning and writing of the complete manuscript.

H. Frances D. Lenahan, Maximilian Piszko, Tobias Klein, and Andreas P. Fröba, *Molecular Dynamics Simulations of Liquid Ethane Up to 298.15 K*. Molecular Physics **2023**, e2211401, DOI: 10.1080/00268976.2023.2211401.

Author's contribution: Frances Lenahan was responsible for organization, execution, and analysis of the simulations. The experimental investigation in this work was performed by Maximilian Piszko. The author planned the complete manuscript and wrote all parts of the publication with the exception of the experimental procedure in the Supporting Information.

I. Maximilian Piszko, Frances D. Lenahan, Tobias Klein, and Andreas P. Fröba, *Mutual and Thermal Diffusivities in Binary Mixtures of n-Hexane or 1-Hexanol with Krypton, R143a, or Sulfur Hexafluoride by Using Dynamic Light Scattering and Molecular Dynamics Simulations*. Accepted for publication in the Journal of Chemical & Engineering Data **2023,** DOI: 10.1021/acs.jced.3c00143.

Author's contribution: Frances Lenahan was responsible for organization, execution, and analysis of the simulations. The experimental investigations in this work were performed by Maximilian Piszko. The author wrote all parts of the publication related to the simulations and participated in the planning and writing of the complete manuscript.

2 State of the Art

In this chapter, the most recent developments in regard to mass-diffusion research in binary liquids consisting of a liquid with a dissolved gas are given. At first, the relevant system is characterized based on its thermodynamic state. Following this, a review of diffusion research is given, where the nomenclature is outlined with the theoretical basis behind mass diffusion. Here, as well, an overview of the currently available experimental reference data is discussed. Then different approaches for determining or predicting diffusion are addressed. These are divided into experimental methods, simulations, and prediction models.

Unless explicitly stated otherwise, all mixtures discussed in this work are binary mixtures consisting of a liquid solvent with a dissolved gas solute. The solvent will always have its melting point below the current temperature. When a gas is introduced to the liquid solvent, it is absorbed into the liquid phase, becoming the solute. The quantity of gas that can be absorbed by the liquid at a certain temperature and pressure is dependent on the solubility between the two components. This quality is not only highly dependent on the thermodynamic state point, but on the involved mixture components as well.

The IUPAC-NIST Solubility Database [5] contains over a hundred volumes worth of solubility data for gases dissolved in different solvents. Further solubility data specific to ionic liquids (ILs) can be found in the Ionic Liquid Database – ILThermo (v2.0) [6,7], which also contains data on further thermodynamic and thermochemical properties. At extremely small composition of one component, the mixture is said to be close to the infinite dilution limit. At this limit, it can be assumed that, since there are so few solute molecules in the mixture, they will never interact. The composition of the dilute component is essentially zero and the activity coefficient is one. All mixtures discussed in this thesis follow the assumptions of the infinite dilution limit.

2.1 Review of Diffusion Research of Liquids with Dissolved Gas

In 1855, Adolf Fick developed a fundamental law of diffusive mass transport in ideal mixtures with the first law of diffusion [8]. In a steady state, multicomponent mixture, the (N–1) independent fluxes J_i can be described by

the total molar concentration c_t, the (N–1) independent driving forces ∇x_i and the diffusion coefficient D_{ij} with

$$J_i = -c_t \sum_{j=1}^{N-1} D_{ij} \nabla x_j \,, \tag{2.1}$$

assuming a linear relationship between J_i and the corresponding driving forces in the form of the concentration gradients. Here, N is the number of mixture components and i =1, 2, ..., N–1 [9]. In a binary mixture, diffusive flux can be described by a single diffusion coefficient D_{11}. This classical representation of diffusion, relating diffusive mass flux to concentration gradients, is widely used because these are the diffusion coefficients which are easily accessible for binary mixtures through experiments. A different class of diffusion coefficients is the Stefan-Maxwell diffusion coefficient $Đ_{ij}$, which describes mass flux due to a gradient in the chemical potential. They can be related through the thermodynamic factor Γ_{ij}. Information on how intermolecular forces may influence mass transport and lead to non-ideal behavior is contained in Γ_{ij} and it is closely related to the fluid's activity coefficient γ_{ij}.

Molecular diffusion is the result of Brownian motion, which is to say, it is the result of random particle motion due to the particle's thermal energy, friction, and intermolecular repulsion and attraction. Looking only at Fickian diffusion in a binary mixture, there are several types of diffusion coefficients which exist, where the nomenclature should be clarified. Figure 2.1 shows an exemplary drawing of the diffusion coefficient D vs mole fraction of component 1 x_1 of a binary mixture. Traditionally, the self-diffusion coefficient D_{self} describes mass diffusion resulting only from like-particle interactions and is determined only for pure substances. However, with molecular dynamics simulation techniques, where particle motion may be tracked, the label $D_{self,i}$ may be used synonymously with the intradiffusion coefficient, which describes the mass diffusion of one component in another component. At the infinite dilution limit, where only a few molecules of one component are present in a nearly pure fluid composed of the second component, $D_{self,i}$ is equal to the tracer diffusion coefficient and the mutual diffusion, or interdiffusion coefficient described by Fick's law D_{11} converges to $D_{self,i}$. This work is only concerned with diffusion coefficients close to the infinite dilution limit. Limit proximity is highly mixture-dependent and is assumed here when below $x_i \approx 0{,}1$ [10,11].

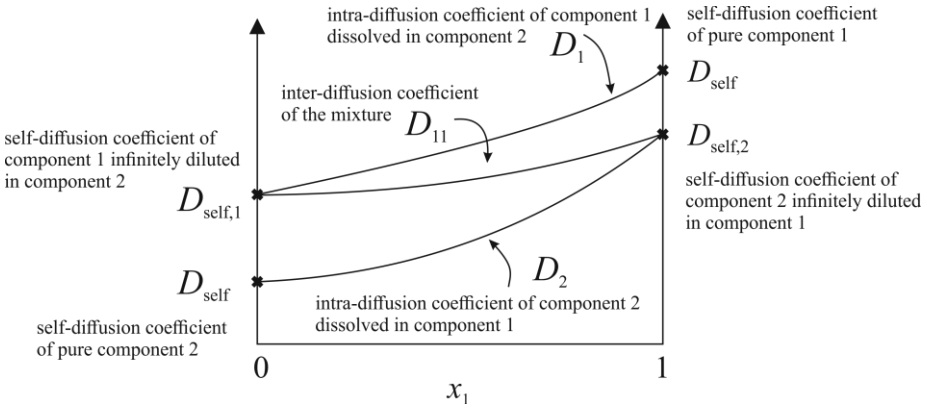

Figure 2.1: Exemplary drawing of mass diffusion coefficients as a function of mixture composition x_i for an arbitrary binary mixture.

To date, the availability of experimental data is quite limited. Most data available for Fick diffusion coefficients in binary mixtures are for gaseous mixtures [12-21]. Much of the available data for mixtures consisting of a liquid with a dissolved gas are well-outside the infinite dilution limit, where investigations are performed over a wider composition range [14-22]. This is particularly true for mixtures containing IL solvents, where solubilities between the IL and investigated gas – typically carbon dioxide CO_2 or refrigerants – are known and generally larger [23-25]. Higher solute concentrations are therefore more easily obtainable within the limits of the experimental apparatuses. The motivation behind investigations of binary mixtures consisting of a liquid with a dissolved gas often include characterization of the potential working fluid class for oil recovery processes [10,22], or gas separation processes, e.g. carbon capture or sequestration [10,24,26,27]. Diffusion coefficients are therefore determined for mixtures where the solvent is typically water, an *n*-paraffin, or an electrolyte [14,28,29]. In such cases, attempts to correlate the data are then limited to a specific fluid class [23,26]. Regarding solutes, the majority of available data is associated overwhelmingly with CO_2 or light gases such as nitrogen N_2 or oxygen O_2. There have been no known investigative efforts for the determination of diffusion coefficients for the explicit purpose of characterizing the diffusive mass transport process over a wide range of fluid classes.

2.1.1 Experimental Methods

The experimental determination of the Fick diffusion coefficient of binary mixtures consisting of a liquid solvent with a dissolved gas is possible with

a variety of techniques, however, most of them rely on the presence of a macroscopic gradient to measure molecular diffusion by analyzing a time-dependent absorption of the solute gas into the liquid. This causes limitations in the application of the technique or the accuracy of the results, in part, because the determined mutual diffusion coefficient is averaged over a concentration range covered over the duration of the experiment, rather than at a specified concentration. Despite this, these conventional techniques are widely used and quite reliable. One category of conventional techniques is that of capillary methods, which rely on real-time mixing of different components. A well-known example of a capillary method is the Loschmidt cell or the closed-tube method, where two – usually symmetric and identical – tube sections are isolated but joined at a pivot point. The individual sections are filled with the different mixture components at identical pressure and temperature. Then, the sections are aligned, and the diffusive process begins [13,14]. The evaluation procedure is based on Fick's second law of diffusion, which monitors a change in concentration with time. However, the Loschmidt cell method is more often used for gaseous mixtures, rather than the mixture of a liquid with a dissolved gas [13,30]. In 1968, Malik and Hayduk [31] presented a steady state capillary cell method for measuring diffusion coefficients of gas-liquid mixtures. They have a small capillary of approximately 0.3 mm diameter which broadens at the base to a diameter of approximately 1.0 mm. Diffusion is measured by monitoring the upward movement of the liquid line in the larger capillary and the downward movement of a solute-saturated bead of liquid, which was placed on the open end of the small capillary. This bead maintains the gaseous atmosphere inside the capillary as gas molecules are absorbed into the liquid below. Unfortunately, the accuracy of diffusivity results with this method is highly reliant on solubility data, which is often even more scarcely available in the literature than diffusion coefficients. It may also be worth investigating the impact of gravity on bead movement and measured diffusivity. In 2015, Kugler et al. [30] surmised that the acceleration due to gravity could have an impact on results. Although their work focused on the Loschmidt cell method for binary gas mixtures, both techniques rely on mass transfer along a vertically oriented capillary.

Another category of conventional diffusion measurement techniques uses chromatography. One of the most prominent chromatography methods is the Taylor Dispersion method [14,29]. Here, a small sample volume is injected into the laminar flow of a fluid contained in a microcapillary and the dispersion of this plug is analyzed. The injected fluid will spread out

radially due to both axial convection and molecular diffusion. The distribution of the solute can be detected with a differential refractive index detector once a sufficiently long time has passed and the flow is fully developed. For the measurement of self-diffusion and intra-diffusion coefficients, the nuclear magnetic resonance (NMR) spin-echo technique and the pulsed field gradient NMR technique are prominent methods, popular for their fast application and reasonable accuracy. Here, with use of an applied magnetic field, information about the time-dependent displacement of molecules can be obtained. Typical relative uncertainties are 1-2% but can reach up to 10%, especially at larger pressures [11,14].

An emerging optical technique for the determination of not only mass diffusivity, but also, simultaneously, the thermal diffusivity, kinematic viscosity, and Soret coefficient is the shadowgraph technique [32]. This is categorized as a photo correlation spectroscopy and heterodyne near-field scattering technique. Here, a stationary macroscopic temperature gradient is applied to the sample, which results in thermodiffusion driving a concentration gradient, or, the Soret effect. A high-speed camera captures the scattered light signal arising from the fluctuations in density, which result from the non-equilibrium fluctuations in temperature, concentration, and fluid velocity resulting from the stationary concentration gradient. Stacks of images are then analyzed to determine an autocorrelation structure function reflecting both the static and the dynamic behavior of these non-equilibrium fluctuations in density [32,33]. There are limitations in applying the technique related to the sign of the Soret coefficient and the magnitude of the Lewis number *Le*, which can be linked to an insufficient separation of the fluctuations in temperature and concentration or possible solute convection. In a recently submitted manuscript from AOT-TP investigating the application of the Shadowgraph technique to mixtures of a liquid with dissolved gas, typical relative expanded uncertainties ($k = 2$) associated with diffusivities are around (10 to 20)% [34].

A non-conventional technique for the determination of Fick diffusion coefficients is the optical technique dynamic light scattering (DLS). Here, a monochromatic, coherent laser irradiates a dielectric medium and is scattered in all directions. Changes in the dielectric susceptibility due to local diffusive flux results in fluctuations in the scattered light intensity. There is no macroscopic gradient applied. In fact, the fluid is in macroscopic thermodynamic equilibrium and the scattered light intensity fluctuates due to microscopic fluctuations in entropy or temperature, concentration, and pressure in the fluid caused by the Brownian motion of molecules. By analyzing the scattered light intensity resulting from

microscopic fluctuations in temperature or entropy and concentration, this experimental technique allows the simultaneous determination of the thermal diffusivity and the Fick diffusion coefficient with typical expanded (k = 2) experimental uncertainties for both properties between (1 and 10)%. It has been used extensively within the present work and is discussed in further detail in Chapter 4. DLS can also be used to determine a fluid's sound attenuation and the speed of sound by analyzing the scattered light intensity resulting from microscopic fluctuations in pressure, however this is not addressed in this work [35,36].

2.1.2 Computer Simulation

Since the first computer simulation of a liquid in 1953 [37], computational power and data processing capabilities have advanced rapidly. Modern simulation approaches are able to incorporate multi-threading for utilization of high-performance computer clusters. This results in highly efficient calculations, which permits simulations to consider far more complex molecular representations on a larger scale. While a particularly important application of molecular dynamics (MD) simulations is for biomolecular systems, i.e. proteins at physiological temperatures [38-42], they are also used extensively in thermophysical property research [43-47]. The most prominent simulation styles for predicting binary diffusion coefficients are non-equilibrium molecular dynamics (NEMD) simulations, and equilibrium molecular dynamics (EMD) simulations [48,49]. Both methods model the evolution of a statistical ensemble on the nanometer scale using time-reversible equations of motion. The fluid to be modelled is placed in a simulation volume and parameters such as temperature, pressure, or volume, are set before the simulation begins. As the dynamics of the system unfold, these properties are monitored to maintain the energy distribution in the system, effectively solving the many-body problem of statistical mechanics.

As the name suggests, the NEMD approach is used for systems out of thermodynamic equilibrium. This is achieved by applying a macroscopic gradient in the form of a defined perturbation. However, in order to detect a microscale response, such as the local fluctuations in concentration which govern mass diffusivity, a large perturbation strength is needed at the macroscale in order to overcome the surrounding statistical noise of the system [50]. EMD simulations on the other hand are performed under macroscopic thermodynamic equilibrium conditions. Dynamic or transport properties can be calculated using the Green-Kubo formulism, which relates the local fluctuations in temperature, pressure, or concentration to

their respective driving forces. It is based on the fluctuation-dissipation theorem from statistical thermodynamics, which accepts that every elementary process in an equilibrium state will be perfectly matched against its reversible process. An investigation of neat Lennard-Jones fluids by Irma et al. [51] showed that the methods employed by EMD simulations for calculating the Maxwell-Stefan diffusion coefficient are less time-consuming and yield more accurate results than the NEMD simulations. Additionally, from a single EMD simulation, Fick diffusivity, thermal conductivity, and dynamic viscosity can be calculated, whereas an NEMD simulation will apply a perturbation akin to the fluctuation that will be evaluated, gaining access to only one property [52-54]. EMD simulations have been used extensively within the present work and are discussed in further detail in Chapter 4.

The basis of MD simulations is the molecular force field (FF) describing the inter- and intramolecular potentials of molecules at each simulation time step. Some of the most prominent FFs in the literature today include the generalized FFs L-OPLS [41,42] – an extension of the FF Optimized Potentials for Liquid Simulations (OPLS) to long-chained hydrocarbons, CHARMM36– a version of the Chemistry at HARvard Macromolecular Mechanics (CHARMM) FF recommended for protein simulations [39], and GAFF [38,55-57] – the generalized form of the Assisted Model Building with Energy Refinement (AMBER) FF, due to their excellent versatility of application and improved performance in the prediction of transport properties compared to other available FFs [43]. Each of these FFs were developed and predominantly used for the study of biological processes and, therefore, are only intended to be used at physiological temperatures [38-40,42]. When used to investigate higher temperatures, simulation results can deviate significantly from experimental reference [44,58].

To improve upon the predictive capabilities of MD simulations, efforts are often focused on improving FF descriptions of molecules. Typically, molecular FFs for individual molecules or fluid classes are proposed when the more well-known FFs fail outside the scope of their applicability. However, the atom descriptions contained in empirically derived FFs for specific molecules may not be fully transferable. A more accurate but computationally expensive approach considers reparameterization of the intramolecular or electrostatic potentials. This is usually achieved with quantum mechanical or optimized *ab initio* calculations, which are then additionally followed by an empirically based optimization of the Lennard-Jones (LJ) parameters [45,46,59].

2.1.3 Prediction Models

Another method of finding the diffusion coefficient in binary fluid mixtures close to infinite dilution of one component is through prediction models. It is less costly in terms of both time and money than experiments or simulations and could yield very accurate results when applied appropriately. The basis of prediction model development is split into purely theoretical, purely empirical, or semi-empirical development. In every development technique, as well as in the choice and application of prediction models for engineering purposes, there is a necessary trade-off to consider between the ease of application and the accuracy of results.

The basis of many theoretically derived models relies on the assumption that fluid molecules are spherical. Hydrodynamic theory, for example, is based on the Stokes-Einstein formula for the intra- or self-diffusivity of spherical particles in a fluid

$$D = \frac{k_B T}{\pi r_1 \eta_2 n_{SE}}, \tag{2.2}$$

where, k_B is Boltzmann's constant, T is the temperature, η_2 is the viscosity of the solvent, and r is the radius of the spherical solute particles. The parameter n_{SE} is the Stokes–Einstein number determined by a boundary condition at the surface of the spherical particles [60,61]. When solute molecules are of similar size to the solvent molecules, $n_{SE} = 4$. However, if the solute size is much larger than the size of a solvent molecule, $n_{SE} = 6$ [60]. With this incredibly simple model, the diffusion coefficient is described by only the thermal energy, solute size, an interaction coefficient (n_{SE}), and the solvent viscosity. For real fluids, the radius of non-spherical solute particles can be described by the effective hydrodynamic radius σ_{eff}, often also denoted a in other works. Cadogan et al. report an empirically derived linear expression for $\sigma_{eff,2}$, given in nm as

$$\sigma_{eff,2} = 0.489 - 0.127 \frac{\rho_2}{\rho_{c,2}}, \tag{2.3}$$

relating this property to the reduced solvent density, with respect to the critical density of the solvent $\rho_{c,2}$ [22]. The more elusive an accurate determination of σ_{eff} becomes, e.g. variability due to a pressure dependence or multiple possible gauss conformations due to increased kinetic energy, the

less accurately the model can predict the binary or self-diffusion coefficient. The work of Cadogan et al. applied the Stokes-Einstein equation to binary mixtures of CO_2 or N_2 dissolved in water [29], CO_2 dissolved in brines [10], and CO_2 dissolved in eight different hydrocarbon solvents [22], and compared it to their experimental data. Here, σ_{eff} is correlated as a weak function of temperature as an alternative to introducing an exponent on η_2. Experimental D_{11} results were obtained using either the Taylor dispersion method at temperatures up to 423 K and pressures up to 69 MPa or the ^{13}C pulse-field gradient NMR method around 298 K and 0.1 MPa. While the absolute relative deviation (ARD) was typically less than 5%, the model could not accurately predict the binary Fick diffusion coefficient of the mixture of squalane (2,6,10,15,19,23-hexamethyltetracosane; CAS 111-01-3) with dissolved CO_2. This was attributed to the flexibility of squalane and the subsequent complexity of the hydrodynamic radius of this solvent. They then applied a modified version of the rough-hard-sphere theory [13], a modeling approach based on the smooth-hard-sphere theory developed by Assael et al. [62], correlating the mixture diffusivity with a dimensionless reduced self-diffusion coefficient D^*

$$D^* = \frac{[nD_{SHS}]}{[nD]_{\rho\to 0}}\left(\frac{V}{V_0}\right)^{2/3}. \tag{2.4}$$

Here, D_{SHS} is the smooth hard-sphere self-diffusion coefficient derived from corrected Enskog theory, n is the particle number density, the subscript $\rho\to 0$ on $[nD]$ in the denominator refers to the zero-density limit, V is the volume, and V_0 is the core volume or the volume of close-packed spheres, dependent on the hard-sphere core diameter σ

$$V_0 = \frac{N_A\sigma^3}{\sqrt{2}}. \tag{2.5}$$

According to the kinetic theory expression for the dilute-gas limit, $[nD]_{\rho\to 0}$ can be described as

$$[nD]_{\rho\to 0} = \left(\frac{3}{8\sigma^2}\right)\sqrt{\frac{RT}{\pi M}}, \tag{2.6}$$

which results in the expression for D^* [63]

$$D^* = \frac{8}{3} D_{\text{self}} \left(\frac{2N_A}{V} \right)^{1/3} \left(\frac{M\pi}{RT} \right)^{1/2}, \tag{2.7}$$

This dimensionless diffusion coefficient falls on a universal curve and is correlated only as a function of the reduced volume $V^* = V/V_0$. The smooth-hard-sphere theory is extended to rough hard spheres with the inclusion of a roughness or coupling factor A to account for the exchange of rotational and translational energy in particle collisions. This theory is also derived for the thermal conductivity and dynamic viscosity [62,64] and has been successfully applied to several pure fluids considering simple molecular liquids [65], alkanes [66], aromatic hydrocarbons [67], alcohols [68] with a roughly 5% relative deviation [64] between the calculated self-diffusivities and experimental reference. It has also been applied to benzene and carbon tetrachloride in supercritical CO_2 with an average absolute relative deviation AARD of under 8% [69]. In 2016, Cadogan et al. [22] defined the dimensionless reduced diffusion coefficient for hard-sphere theory applied to real fluids as

$$D^* = \frac{[nD_{11}]}{[nD_{11}]_0} \left(\frac{V}{V_{0,12}} \right)^{2/3} \left(\frac{V_{0,12}}{V_{0,2}} \right)^{1/3}, \tag{2.8}$$

for the determination of the tracer diffusion coefficient, or the self-diffusion coefficient of component i infinitely diluted in component j $D_{\text{self},i}$, which is also equal to the binary Fick diffusion coefficient D_{11} at this low-concentration limit. $V_{0,2}$ and $V_{0,12}$ can be calculated with Eq. 2.5, using the hard-sphere diameter of the solvent σ_2 and the arithmetic mean diameter σ_{12} of σ_2 and the hard-sphere solute diameter σ_1 [22]. The final expression for the reduced mutual diffusion coefficient is then

$$D_{11}^* = \frac{8}{3} \frac{D_{11}}{A} \left(\frac{2M_{12}\pi}{RT} \right)^{1/2} \left(\frac{2N_A}{V} \right)^{1/3} \left(\frac{V_{0,12}}{V_{0,2}} \right)^{2/3}, \tag{2.9}$$

where M_{12} is the reduced molar mass calculated by

$$M_{12} = \frac{M_1 M_2}{M_1 + M_2}. \tag{2.10}$$

The challenge of applying this model is in determining V_0 and A. Assael et al. correlated these values for a variety of hydrocarbon-based solvents using experimental data [65-68,70]. They have also been reported for refrigerants and other dense fluids [71-74], but for application of the hard-sphere theory model for predicting viscosity and thermal conductivity. Cadogan et al. [22] uses V_0 values for squalane reported by Ciotta et al. [74], which were derived from viscosity measurements. For their mixture of CO_2 infinitely diluted in squalane at temperatures between (298 and 423) K and pressures up to 67 MPa, Cadogan et al. report an average absolute relative deviation of 1.5%, which would suggest that V_0 is transferable when derived from another transport coefficient. However, Dymond, co-author on many of the early publications on the hard-sphere model approach, notes that the characteristic volume used for predicting the self-diffusion coefficient must be about 5% larger than that fit for the thermal conductivity or the viscosity [75]. It is unclear how this may impact D_{11} of other mixtures and, although there is a sound theoretical basis for the hard-sphere theory approach, empirically-derived correlations are still required for application of the model.

Several hard-sphere theory-based model modification or improvements pop up in the literature, but perhaps the most notable one is by Lito et al. [12] from 2013. They boast validation of their model with "the largest database ever compiled" for binary tracer diffusion coefficients comprising of 487 mixture combinations for roughly 300 different molecules and 8293 data points covering polar, weakly polar, and non-polar mixtures as well as gaseous, liquid, and supercritical fluid mixtures. Their results are also quite impressive. They report a global average absolute relative deviation of less than 3%, outperforming the ten other models they applied for comparison. Unfortunately, the application of their model requires an 11-step process, outlined in their publication, which includes acquiring the critical properties of mixture components and potentially fitting two parameters – the minimum-energy distance parameter of the 6-12 Lennard-Jones potential for the solvent $\sigma_{i,LJ}$ and the activation energy of the diffusion process E_D – to experimental data. Although they provide this information in the Supporting Information of their work for the vast array of data they have amassed, determining these parameters for novel mixtures would prove difficult. Additionally, to derive E_D, the solute and solvent hard-sphere effective diameters are still needed.

Of the ten models that Lito et al. [12] compared their results against, one was that of Wilke and Chang [76], published in 1955. This is perhaps the most famous and widely-used prediction model for dilute binary fluid mixtures. It is given as

$$D_{11,\mathrm{calc}} = 7.4 \times 10^{-8} \frac{T(\chi M)^{0.5}}{\eta V_{\mathrm{b}}^{0.6}}, \tag{2.11}$$

where M is the molecular weight of the solvent, η is the viscosity of solution given in centipoise, V_{b} is the molal volume of the solute at its normal boiling point given in $cm^2 \cdot g^{-1} \cdot mol^{-1}$ and χ is an association factor for the solvent, with χ of several substances including water and benzene included in their work. The model is originally conceptualized from Eyring theory and the Stokes-Einstein relation but was developed and evaluated based on the experimental data of 285 state points considering 251 solute-solvent combinations, including many acids and aromatic substances. In 2018, Giraudet et al. [77] showed that the predicted $D_{11,\mathrm{calc}}$ values calculated using the Wilke-Chang model were significantly underestimated for mixtures of *n*-alkanes with the small, light gases H_2 and helium He. They then proposed a modified version empirically fit to 175 data points of binary Fick diffusion coefficients of liquid *n*-alkanes with dissolved H_2, He, N_2, or carbon monoxide CO close to infinite dilution. Their model has the form

$$D_{11,\mathrm{calc}} = 1.274 \times 10^{-8} \frac{TM_2^{0.5}}{\nu_2^{0.9}\left(M_1\left(0.45 + \omega_1\right)\right)^{0.25}}, \tag{2.12}$$

with subscripts 1 and 2 corresponding to the solute and solvent, ν is the kinematic viscosity, M is the molar mass, and ω is the acentric factor. Empirical or semi-empirical prediction models are typically limited to the fluid class of the associated data. For example, due to the large number of experiments which have been performed on mixtures of an *n*-alkane with a dissolved gas, usually CO_2 or a small-chain alkane, several prediction models exist which perform well for mixtures with *n*-alkane or paraffin-based solvents but fail when applied to e.g. more associative fluids such as alcohols. This, and its simple application, is what made the model by Wilke-Chang so appealing throughout the decades. The general failure of empirically-based models when applied beyond the scope of their development was observed in the 2019 publication by Wu et al. [78] They update their model [77] – published a year prior – now considering 204 binary Fick diffusion coefficients, which also include 1-alcohol solvents and the dissolved gas CO_2. This new form includes an association factor Ψ to account for the polar interactions of the alcohols with inclusion of the dipole moment of the solvent μ_2. It is given as

$$D_{11,\mathrm{calc}} = 5.249 \times 10^{-17} \frac{T\left(\Psi M_2\right)^{0.5}}{v_2^{0.8}\left(M_1\left(0.45+\omega_1\right)\right)^{0.25}}, \tag{2.13}$$

$$\Psi = 1 + 1.388 \times 10^{6} \frac{v_2^{0.3}\mu_2}{M_2 T}. \tag{2.14}$$

Their model has been applied to dense fluids with diffusivities on the order of 10^{-7} to 10^{-9} $m^2 \cdot s^{-1}$ and their reported average absolute relative deviation between predicted and experimentally determined binary Fick diffusion coefficients for 305 data points considering *n*-alkane and 1-alcohol solvents was less than 10%. The work contained in this cumulative thesis begins as an extension of their work following the 2019 publication of Wu et al. [78].

3 Aim of this Thesis

The characterization of diffusive mass transport in liquids with dissolved gas is achieved through synergy between predicted and experimentally determined Fick diffusion coefficients D_{11}. Experimental results for D_{11} in binary fluid mixtures consisting of a liquid solvent with a dissolved gas solute close to the infinite dilution limit are determined via DLS experiments at the Institute of Advanced Optical Technologies – Thermophysical Properties (AOT-TP) of Friedrich-Alexander Universität (FAU) and are used as validation and reference for EMD simulations and prediction model development. These investigations are made possible through the financial support of the German Research Foundation (Deutsche Forschungs-gemeinschaft, DFG) via the project grants FR 1709/15-1 and FR 1709/11-2. The aim of this thesis is to cumulate the results, which have led to an improved knowledge and understanding of the influences driving molecular diffusion. In particular, the predictive techniques and the improvement of prediction methods are addressed as well as the strong relationship between mass diffusion and dynamic viscosity.

The EMD simulations for investigating $D_{\mathrm{self},1}$ or D_{11} are performed at similar state points to the DLS measurements so that results can be directly compared and the accuracy of resultant thermophysical properties are validated. Investigated temperatures and pressures range from (298 to 423) K and up to 6.3 MPa. The apparent fluid-property relationships which arise during data analysis are further evaluated with the use of radial distribution functions (RDFs). A qualitative interpretation of results is performed as well as a quantitative analysis of hydrogen-bonding statistics. To improve upon this predictive method, an empirically based correction to the used molecular force fields (FFs) is developed. The FF forms the basis of EMD simulations and the accuracy of simulation results depends on the molecular descriptions and resultant interactions contained therein. In total, 45 mixture combinations including 13 solvents and 11 solutes are simulated as part of this cumulative work. The solvent fluid classes covered here include linear alkanes of varying chain length up to a carbon number $N_c = 28$, 1-alcohols up to $N_c = 10$, and an acid, ester, and cyclic and aromatic hydrocarbons with $N_c = 6$. The investigated solutes vary in terms of molecular weight, size and shape, and polarity. All molecules which are used in the simulations are described in the next chapter in the section on Model Systems of Interest.

While EMD simulations allow a unique interpretation of results by offering insight into the fluid structure on a molecular level, another predictive method for estimating mass diffusivities which is incorporated in this work is the development and application of prediction models. Many models in the literature are limited to the range of fluid class and thermodynamic states upon which they were developed. Additionally, most research has been performed for gaseous mixtures, rather than mixtures of a liquid solvent with dissolved gas solute. Prior efforts within this project series resulted in the development of a prediction model which incorporated *n*-alkane and 1-alcohol solvents and five different dissolved gas solutes [78]. With the wide variety of investigated fluid classes and gases as well as a systematic variation of solvent and solute combinations, an assessment of the present data allows for a more comprehensive analysis of the influences affecting diffusive mass transport. A further 44 mixture combinations considering *n*-alkane, 1-alcohol, or ionic liquid (IL) solvents and six different dissolved gas solutes are incorporated in prediction model development, since they were also experimentally determined with DLS at AOT-TP within this project series.

Following analysis of diffusivity results, the influence of a molecular core volume is reintroduced. A simple approach to estimating the core volume of any molecule is then proposed. Here, the molar core volume of a molecule is determined by representing the atoms as hard-spheres and calculating the volume of overlapping spheres with simple geometry, based on the work of Bondi [79,80]. The solvent and solute core volume are then used to develop an exceptionally simple predictive engineering model for binary Fick diffusion coefficients of liquids with dissolved gas close to the infinite dilution regime. This model is additionally applied to 49 further mixtures from the literature, spanning seven orders of magnitude for D_{11} and including 11 binary gaseous mixtures.

4 Applied Strategy and Used Methods

In the following sections, the most important techniques used for acquiring, predicting, and evaluating mass diffusivities in binary mixtures close to infinite dilution of one component are given. Further details are provided in the respective publications related to this thesis. At first, the model systems of interest are detailed. Then, a brief description of the experimental techniques dynamic light scattering (DLS) and surface light scattering (SLS) are provided. Although the SLS method is not applied for the determination of mass diffusivity, it is discussed here in connection with measurements performed for the determination of dynamic viscosity η. As a transport property – which can be thought of as diffusion of momentum governed by shear forces – the behavior of η is closely related to that of mass diffusivity. This relationship has been utilized for the purpose of improving molecular FF in EMD simulations. A discussion of FF development comes in a later chapter, but the application of EMD simulations, the various post processing techniques utilized for the prediction of diffusivities, and further analysis techniques providing insight into the fluid structure are provided.

4.1 Model Systems of Interest

Investigations for the binary Fick diffusion coefficient are performed over a wide range of temperatures from (298 to 423) K and pressures up to 10.86 MPa. In total, 451 binary Fick diffusion coefficients spanning 89 binary mixture combinations with 17 liquid solvents and 11 dissolved gases are evaluated. To conscientiously study the influence of fluid behavior on mass diffusion, it is necessary to establish a systematic variation of the molecular characteristics of mixture components. The liquid solvents considered in this work comprise of multiple different fluid classes including: linear and branched alkanes with a carbon number N_c between 6 to 28, linear alcohols with N_c between 6 to10, an acid, an ester, the cyclic and aromatic hydrocarbons cyclohexane and benzene, and ionic liquid salts with three unique cations and two unique anions. This selection of solvents provides a range of liquid densities and dynamic viscosities between roughly (650 to 1350) kg·m^{-3} and (0.3 to 120) mPa·s at 298 K. The second component of the binary mixture constitutes a dissolved gas, whose concentration should be small enough such that assumptions of the infinite dilution limit are considered valid. Solutes are chosen to consider the impact on diffusion resulting from molecular weight and size, coulombic

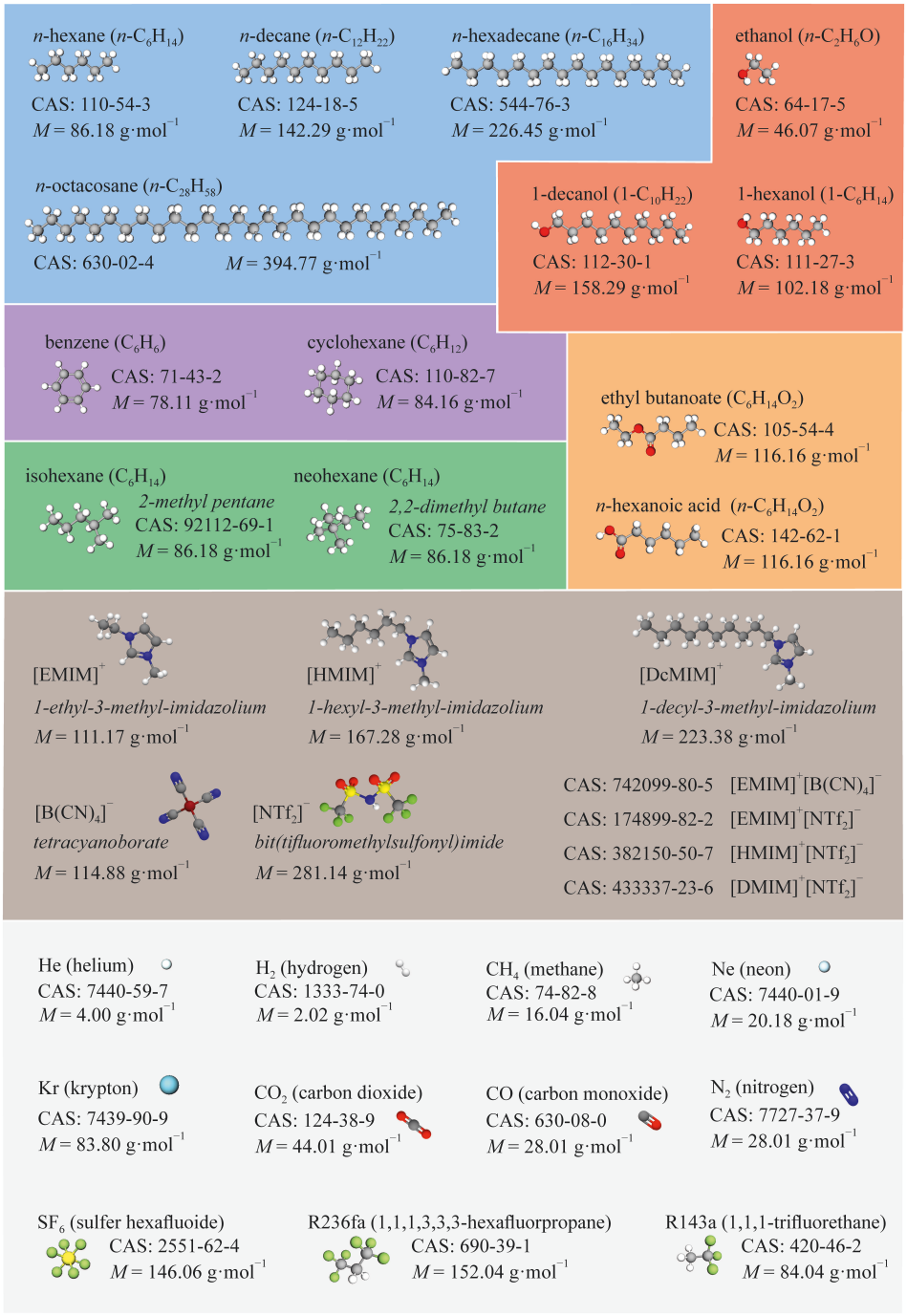

Figure 4.1: Selected solvent and solute mixture components investigated via DLS experiments and EMD simulations.

potential, and complexity or non-sphericity of structure. Illustrations for all solvent and solute molecules are given in Figure 4.1 along with their chemical abstracts service (CAS) number and molecular weight *M*. The gaseous solutes are shown at the bottom with a grey background. Solvent fluid classes are separated by color: blue for *n*-alkanes, purple for ring-structures, green for branched alkanes, red for 1-alcohols, orange for the acid and ester, and brown for the ionic liquids. This color scheme for the solvents will be consistent throughout this thesis.

4.2 Dynamic Light Scattering

The experimental determination of D_{11} is achieved through the optical technique dynamic light scattering DLS. This technique is contactless, does not require calibration, and has been applied extensively for the simultaneous determination of D_{11} and the thermal diffusivity a of a variety of fluid mixtures [36,81-84]. The fundamental basis of DLS is briefly described in the following section. For further details regarding the theory behind DLS, please refer to the literature [85-87] and for details regarding its implementation, the setup, or the used experimental parameters, please refer to the adjoining publications of this cumulative thesis [88-93]. It should be noted that the DLS method utilized in these studies determines the mixture Fick diffusivity accessible via the scattered light signal arising from molecules. Another common application of DLS is for the determination of seed particle diameter accessible via the determination of the translational particle diffusion coefficient [94]. In such a case, the presence of particles would dominate the scattered light signal and molecular signals would not be resolvable. Therefore, no seed particles were used in the determination of the molecular diffusion coefficient. In fact, great care was taken during experimental preparation to assure no particles were present in the investigated mixtures.

4.2.1 Light Scattering from Bulk of Fluid Body

A fluid in macroscopic thermodynamic equilibrium will still experience microscopic fluctuations in temperature or entropy, pressure, and concentration due to the natural Brownian motion of molecules. The mean lifetimes of these fluctuations are accessible through photon correlation spectroscopy and their relaxation follows the same laws as macroscopic fluctuations. With a clearly defined scattering geometry, the temporal behavior of scattered light intensity, which contains information about the temporal behavior of these microscopic fluctuations, can be detected and analyzed. The scattering geometry is identified by q and determined by the

fluid's index of refraction n_D, the laser wavelength in vacuum λ_o, and the scattering angle Θ_s, which is determined by the experimental set-up. It can be calculated with

$$q = \left|\vec{q}\right| = \frac{4\pi n_{\text{fluid}}}{\lambda_o} \cdot \sin\left(\frac{\Theta_s}{2}\right). \tag{4.1}$$

Figure 4.2 shows a schematic representation of the spectrum of scattered light in the frequency domain $S(\omega_f)$, which is accessible via DLS. The Brillouin doublet shown in blue for accessing the sound attenuation D_s and the speed of sound c_s result from propagating fluctuations in pressure. For further information, please refer to references 35 and 95. The relevant component for this work is the unshifted central peak, or the Rayleigh component, which can be decomposed into contributions from fluctuations in concentration (green) and temperature (red). To access the corresponding transport properties D_{11} and the thermal diffusivity a the characteristic scattered light signal is analyzed in the Fourier domain, where the characteristic decay times associated with fluctuations in concentration $\tau_{C,c}$ or temperature $\tau_{C,t}$ are determined. D_{11} and a can then be calculated using the working equations

$$a = \left(\tau_{C,t} q^2\right)^{-1} \tag{4.2}$$

and

$$D_{11} = \left(\tau_{C,c} q^2\right)^{-1}. \tag{4.3}$$

The determination of $\tau_{C,c}$ and $\tau_{C,t}$ is achieved by performing a second-order correlation function of the scattered light intensity in the time domain with photon correlation spectroscopy. The second order correlation function can be evaluated based on either a homodyne or a heterodyne detection scheme. In the former, only the scattered light resulting from fluctuations in the investigated fluid may be analyzed. Homodyne conditions may therefore be difficult to realize due to unwanted stray light resulting from dust particles or the experimental setup. In a heterodyne detection scheme, coherent reference light is intentionally superimposed with the light scattered by the fluid bulk, usually in the form of coherent laser light rerouted around the experimental sample cell following a beam splitter.

With this detection scheme, any coherent stray light, which would otherwise affect the homodyne case, is simply counted towards the reference light.

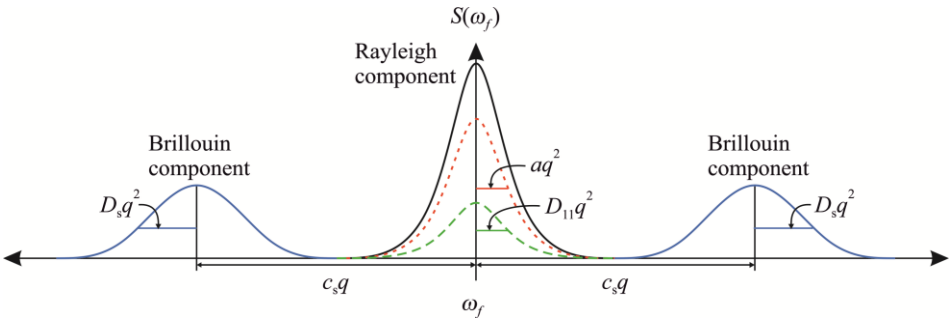

Figure 4.2: Schematic representation of the spectrum of scattered light for a binary mixture in DLS experimental investigations.

All DLS investigations included as part of this cumulative thesis were performed using a heterodyne detection scheme. The normalized correlation function $g^{(2)}(\tau)$ is described by

$$g^{(2)}(\tau) = b_0 + b_1 \cdot \exp\left(\frac{-\tau}{\tau_{C,t}}\right) + b_2 \cdot \exp\left(\frac{-\tau}{\tau_{C,c}}\right), \qquad (4.4)$$

where τ is the correlation time and b_i are equation constants. b_0 will be a function of the optical array, i.e. mirrors, dust, other stray light sources. b_1 and b_2 determine the signal contrast and depend on the change in refractive index with fluctuations in temperature or concentration. For examples on fitting to $g^{(2)}(\tau)$ results, please refer to the publications within this work [88,89] as well as the literature [36].

It should be noted that fluctuations and the resultant signal related to mass diffusivity can only be resolved when microscopic concentration fluctuations are large; i.e in mixtures. It is therefore possible that D_{11} is not resolvable for mixtures with exceptionally small solute concentrations. However, this greatly depends on the mixture components. The determination of D_{11} is only possible if the change of refractive index with a change in composition is large enough. Additionally, the change in osmotic compressibility, which is a function of the change in chemical potential, plays a role. For many of the mixtures included in this work, solute

compositions are lower than 3 mol%, with the lowest being 0.2 mol% for *n*-hexane with dissolved R143a at 303.12 K [93]. Fluctuations in temperature governing a can be analyzed for neat fluids as well as mixtures. Provided the ratio between the decay times of the two signals is sufficiently large, such that each exponential may be resolved, D_{11} and a can be simultaneously determined. Where this is not possible, an effective diffusivity D_{11}^* is reported instead which encompasses both D_{11} and a.

4.2.2 Light Scattering from Surface Waves

The fundamental theory behind DLS can be applied to surface waves at an interface for the determination of interfacial or surface tension γ and η. For a fluid in macroscopic thermodynamic equilibrium, it is still possible to find surface fluctuations or ripplons due to the Brownian motion of molecules. The decay time of these fluctuations, and the thermophysical properties which they govern, can be accessed by analyzing the temporal behavior of light, scattered as a result of the molecular motion motivating these fluctuations. In surface light scattering (SLS), rather than the fluid bulk, the scattering volume is placed at the vapor-liquid or liquid-liquid interface to access surface fluctuations, or capillary waves. The interface is composed of a near-infinite number of superimposed waves. With a carefully defined scattering geometry, all waves with the wave number q can be accessed. In this case, the characteristic scattered light signal is composed of a frequency-unshifted Rayleigh line and a frequency-shifted Brillouin doublet, similar to the spectrum acquired from DLS and shown in Figure 4.2. However, the spectrum components in this case correspond to the probed surface mode. Either an over-damped or an oscillatory decay of the probed fluctuation is possible and can be identified by the capillary number Y [86]

$$Y = \frac{\rho\gamma}{4\eta^2 q}, \tag{4.5}$$

where γ is the surface or interfacial tension, ρ and η are the bulk liquid density and dynamic viscosity, and q is the scattering vector given by Eq. 4.1 for SLS in the transmission direction.

When $Y \leq 0.145$, an overdamped behavior is observed corresponding to the frequency-un-shifted Rayleigh line. In this case, the ratio of γ to η can be determined from the half-width half-maximum using a first-order approximation of the spectral power density $S(\omega_f)$, shown in Figure 4.3. At

$Y > 0.145$, an oscillatory decay of the related surface fluctuation is observed corresponding to a frequency shift which results in the Brillouin doublet. Here, both γ and η can be determined using the first-order approximation of $S(\omega_f)$ from the frequency shift and half-width half-maximum of the peak.

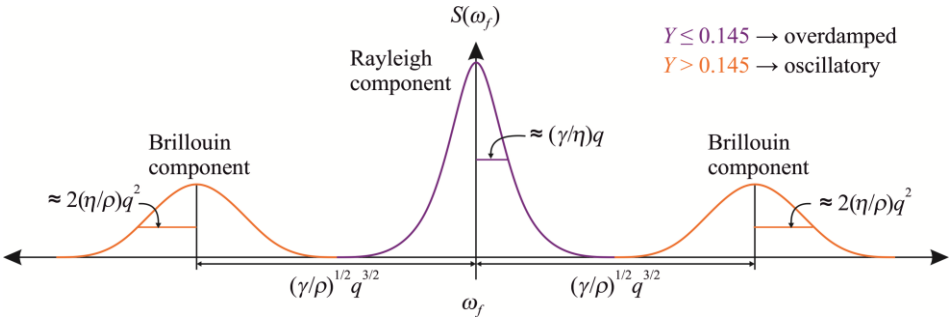

Figure 4.3: First-order approximation of the spectrum of scattered light in SLS experimental investigations.

In the heterodyne detection scheme, the normalized intensity correlation function for analyzing the spectrum in the time domain will depend on the probed surface mode. For propagating surface fluctuations related to an oscillatory decay and $Y > 0.145$,

$$g^{(2)}(\tau) = b_0 + b_1 \cdot \cos\left(\omega_q \tau - c\right) \cdot \exp\left(\frac{-\tau}{\tau_C}\right). \tag{4.6}$$

The equation constants b_0 and b_1 are related to the baseline scattered light signal and the ratio of scattered light to reference light in the heterodyne detection scheme. Within the cosine function, c is a phase term to account for deviations of the spectrum from the Lorentzian form. For a given q, the mean lifetime and frequency of propagation of a fluctuation are equal to τ_C and ω_q. In the overdamped case with $Y \leq 0.145$ and using heterodyne measurement conditions, $g^{(2)}(\tau)$ will have the form

$$g^{(2)}(\tau) = b_0 + b_1 \cdot \exp\left(\frac{-\tau}{\tau_C}\right). \tag{4.7}$$

Again, b_0 and b_1 are adjustable constants depending on the measurement conditions. For further information on the application of the SLS tech-

nique, please refer to the relevant publications listed as part of this cumulative thesis [58,96,97]. For information related to the theory behind propagating surface waves or the scattering geometry and experimental realization of the technique, please refer to the literature [86,98].

Although this application of the DLS method to capillary waves does not yield mass-diffusion coefficients, the experimental determination of the dynamic property η has been used as validation for the development and testing of molecular force fields used in simulations. Additionally, as will be shown in the following sections, η is closely related to diffusivity.

4.3 Molecular Dynamics Simulations

A prominent method within the field of thermophysical property research is that of molecular dynamics (MD) simulations. Within the context of this thesis, only equilibrium MD (EMD) simulations have been performed. Here, each investigated state point exists in macroscopic thermodynamic equilibrium, i.e. there are no applied gradients in temperature, pressure, or chemical potential. Similar to the concept of DLS, the relevant thermophysical properties are derived from evaluating fluctuations caused by microscopic gradients, which result from molecular interactions.

The basis of MD simulations is the calculation of Newtonian equations of motions at each simulation timestep. The potential energy function is composed of electrostatic, intramolecular, and Lennard-Jones (LJ) potentials and has the form

$$\begin{aligned} U = \sum_{i}^{N} U_i = & \sum_{\text{bond}} \frac{k_r}{2}\left(r - r_0\right)^2 + \ldots . \\ & \ldots \sum_{\text{angle}} \frac{k_\Theta}{2}\left(\Theta - \Theta_0\right)^2 + \sum_{\text{torsion}} k_\chi \left(1 + \cos\left(\eta\chi - \delta\right)\right)^2 + \ldots \\ & \ldots \sum_{i}^{N-1}\sum_{j>i}^{N} \frac{1}{4\pi\varepsilon_0}\frac{q_i q_j}{r_{ij}} + \sum_{i}^{N-1}\sum_{j<i}^{N} 4\varepsilon_{ij}\left[\left(\frac{\sigma_{ij}}{r_{ij}}\right)^{12} - \left(\frac{\sigma_{ij}}{r_{ij}}\right)^{6}\right]. \end{aligned} \tag{4.8}$$

Here, k is a force constant associated with the corresponding bond-stretching, angle-bending, or dihedral-angle-rotation of the molecular geometry, q_i and q_j are partial charges, r is a distance parameter, and ε_{ij} and σ_{ij} are the potential well depth and minimum-energy distance of the 6-12 LJ potential. The subscripts i and j correspond to interaction sites i and j. This equation is the basis of EMD simulations and its components are described

by molecular force fields (FF). All investigations of mixture diffusivity have been performed with all-atom (AA) FFs, where each atom is explicitly described with a unique q_i, ε_i, etc., and an interaction site corresponds to a single atom. This selection was made based on results of a separate study investigating the thermophysical properties dynamic viscosity and surface tension via EMD simulations [58]. The united-atom and course-grain FFs – where an interaction site corresponds to more than one atom – do not perform as well as the AA FF in terms of prediction accuracy for the dynamic properties. For more information on these other FF classes, please refer to the literature [44,58,99,100].

The GROMACS [101] simulation software is chosen due to its incredible versatility, ease of use, and online troubleshooting community. Version 5.1.2 is used initially, then updated to version 2021.1 to utilize GPUs available through the university compute cluster [88]. Aside from the reduced computational cost, the only notable change this incurred is the change of barostat to set and equilibrate the pressure during simulation runs in an isobaric-isothermal (*NpT*) ensemble. Here, larger fluctuations in pressure were observed, which, in actuality, correspond to a more realistic representation of the simulated fluid [88]. This had no noticeable effect on the accuracy of thermophysical property prediction. Post-processing efforts also utilize highly efficient parallel computing for the calculation of correlation functions. All simulation details regarding equilibration procedure, timestep, saving frequency, etc. can be found in the respective publication, where the data is originally presented and will not be repeated here.

4.3.1 Data Evaluation

At each simulation time step, Newton's equations of motion are performed to calculate the interaction potential between interaction sites. This determines the movement of molecules and the forces present in the fluid at any given snapshot in time. Through rigorous post-processing methods, various thermophysical properties may be calculated from this information. In the following sections, calculation procedures in EMD simulations for the thermophysical properties dynamic viscosity η, self-diffusivity of a pure substance D_{self} or the mixture self-diffusion coefficient of component 1 infinitely diluted in component 2 $D_{\mathrm{self,1}}$, and the binary mixture mutual diffusion coefficient D_{11} will be discussed.

Dynamic Viscosity

In EMD simulations, a common, well-established approach for determining dynamic properties of a fluid is the Green-Kubo method, derived from

fluctuation-dissipation theory. Here, η is accessible via the pressure tensor $\vec{P}$ by considering the integral of the autocorrelation function of the off-diagonal elements of $\vec{P}$ as a function of the correlation time τ. For a cubic volume V, η is calculated by

$$\eta = \frac{V}{k_B T} \lim_{\tau' \to \infty} \int_0^{\tau'} \left\langle p_{xy}(\tau + \tau_0) \cdot p_{xy}(\tau_0) \right\rangle \mathrm{d}\tau \qquad (x \neq y). \tag{4.9}$$

Figure 4.4 shows the evolution of the dynamic viscosity for increasing τ. For large τ, η will plateau and this value corresponds to the fluid viscosity. Unfortunately, identifying the start of the plateau region is subjective, which may have implications for liquids which have large viscosity, i.e. require large τ before a plateau is reached. In such a case, the simulation is dependent on the permissible computational expense which can be taken to ensure long-enough runtimes.

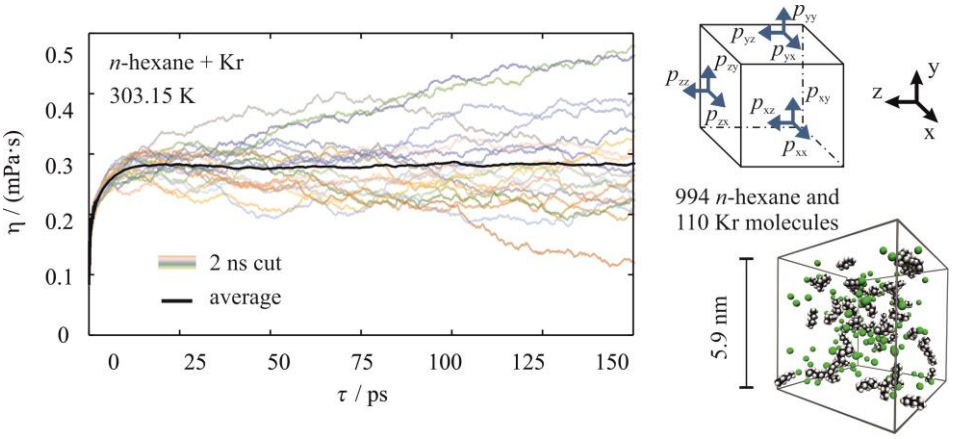

Figure 4.4: (left) Evolution of the liquid dynamic viscosity η for the binary mixture of *n*-hexane with dissolved Kr close to infinite dilution at 303.15 K as a function of the correlation time τ according to the time decomposition method of Zhang et al. [102] Colored lines represent 2 ns long sections of the simulation run. The black line shows the final average considering the evolution of all 2 ns long sections. (right) Representative simulation boxes showing (top) the elements of the pressure tensor for the calculation of η and (bottom) a screenshot of the investigated system during the run. Only 50 *n*-hexane molecules are shown.

The reported value and statistical uncertainty ($k = 2$) for η in the publications of this cumulative work are the average value and twice the

standard deviation of five independent simulation runs. There have been two methods used to determine η from a single simulation run. Originally, a single plateau evaluated over the complete simulation runtime, which would be 30-60 ns, is considered. This may result in large uncertainties due to the poor convergence of this approach when statistical information is limited due to large viscosities and too-short runtimes. In Lenahan et al. [89], the time-decomposition method of Zhang et al. [102] is used to evaluate an average viscosity from a single run cut into 2 to 5 ns segments. An example of this can be seen in Figure 4.4. With this method, overall statistical uncertainty across the multiple independent simulations is reduced.

The Self-Diffusion Coefficient

Evaluation of the self-diffusion coefficient $D_{\mathrm{self},i}$ is achieved by tracking a molecule's movement as a simulation progresses. The mean square displacement MSD of all molecules of a species i is related to $D_{\mathrm{self},i}$, here denoted $D_{\mathrm{o},i}$, with the Einstein relation [49]

$$\begin{aligned} D_{\mathrm{o},i} &= \frac{1}{6N_i}\lim_{\tau\to\infty}\frac{\mathrm{d}}{\mathrm{d}\tau}\left\langle\sum_{k=1}^{N_i}\left(r_{i,k}\left(t+\tau\right)-r_{i,k}\left(t\right)\right)^2\right\rangle\ldots \\ \ldots &= \frac{1}{6N_i}\lim_{\tau\to\infty}\frac{\mathrm{d}\left(\mathrm{MSD}_i\right)}{\mathrm{d}\tau}\,. \end{aligned} \tag{4.10}$$

This is valid for a neat fluid and mixtures, where N_i is the total number of molecules of species i and r_k(t) is the center-of-mass position of the k-th molecule at time t. The angular brackets denote an ensemble averaging considering multiple possible t for each correlation time τ. Eq. 4.10 is only valid when the MSD is linear in time, which can be evaluated using $\beta = \mathrm{d}(\log(\mathrm{MSD})) / \mathrm{d}(\log(\tau))$ and checking its convergence to unity. This approach for calculating $D_{\mathrm{self},i}$ is considered to be relatively computationally inexpensive although computational cost increases for longer simulation runtimes or larger simulation volumes, i.e. more molecules, which are required for improved statistics. For a mixture close to infinite dilution of component i, $D_{\mathrm{self},i}$ is considered equal to the Fick or mutual diffusion coefficient D_{12}. Therefore, due to the lower computational effort associated with post-processing, $D_{\mathrm{self},i}$ is determined and reported whenever anomalous behavior due to non-ideality can be neglected and the mixture is considered to be close to infinite dilution of one component.

In 2004, Yeh and Hummer [103] investigated finite size effects influencing the calculation of self-diffusion coefficients and viscosities in simulations of water, LJ, and hard-sphere fluids. They developed a relation to account for the observed system-size dependence, which has since become a standard for the calculation of $D_{\mathrm{self},i}$ for real fluids simulated with periodic boundary conditions.

$$D_{\mathrm{self},i} = D_{\mathrm{o},i} - \frac{k_B T \xi}{6\pi\eta L}. \tag{4.11}$$

Here, $D_{\mathrm{o},i}$ is the uncorrected diffusion coefficient acquired from EMD simulations, L is the length of one side of the cubic simulation volume with periodic boundary conditions applied, and $\xi = 2.837297$. The dynamic viscosity η is also required. Jamali et al. extended their study in 2018 to correct for finite size effects influencing the calculation of the Maxwell-Stefan diffusion coefficient, which will be discussed further in the next section.

The Fick-Diffusion Coefficient

Departing the vicinity of the infinite dilution limit, assumptions pertaining to the ideality of the mixture fail. In this case, it is no longer accurate to equate the Fick or mutual diffusion coefficient D_{11} to the self-diffusivity of the low-concentration component i in the mixture $D_{\mathrm{self},i}$. This is exemplarily shown in Figure 2.1. Rather, D_{11} must be calculated from EMD simulations via the product of the Maxwell-Stefan diffusion coefficient $Đ_{12}$ and the thermodynamic factor Γ_{ij} [104], which is a more computationally demanding approach. While D_{11} describes movement of mass due to a concentration gradient, $Đ_{12}$ is governed by gradients in chemical potential and can be calculated from an EMD simulation using the Onsager coefficients Λ_{ij} [105].

$$\Lambda_{ij} = \lim_{t\to\infty} \frac{1}{6Nt} \left\langle \left(\sum_{k=1}^{N_i} \left(r_{k,i}(t) - r_{k,i}(0) \right) \right) \times \left(\sum_{l=1}^{N_j} \left(r_{l,j}(t) - r_{l,j}(0) \right) \right) \right\rangle, \tag{4.12}$$

where N is the total number of molecules in the volume, N_i and N_j are the number of molecules of species i and j and $r_{k,i}(\mathrm{t})$ is the center-of-mass position of the k-th molecule of species i at time t. This is a cross-correlation of molecule displacement considering the two species i and j. Then, $Đ_{12}$ is calculated as

$$Đ_{12} = \frac{x_2}{x_1}\Lambda_{11} + \frac{x_1}{x_2}\Lambda_{22} - 2\Lambda_{12}\,, \tag{4.13}$$

where x_i is the mole fraction of species i in the mixture. The cross-correlations between like molecules of species i can be expressed as $\Delta\Lambda_{ii} = x_j\,(\Lambda_{ii} / x_i - D_{self,i})$ and between unlike species as $\Delta\Lambda_{12} = 2\Lambda_{12}$. These individual contributions to the calculation of $Đ_{12}$ are highlighted in Figure S3 of the Supporting Information in reference 91 and is repeated here as Figure 4.5.

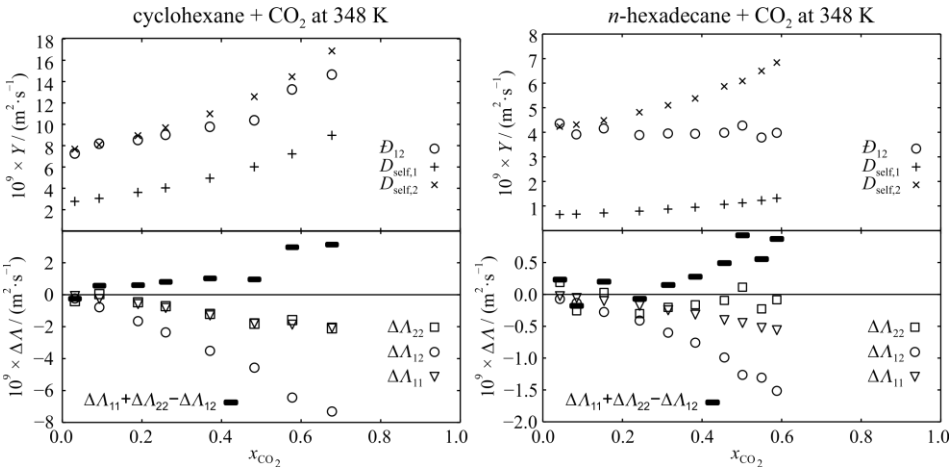

Figure 4.5: Comparison of the kinetic contributions to the diffusion process of a binary liquid mixture for (left) cyclohexane or (right) *n*-hexadecane with dissolved CO_2 over a wide composition range at 348 K. This figure is adapted from Figure S3 of the Supporting Information of reference 91.

As the concentration of dissolved CO_2 increases, the greatest contribution to $Đ_{12}$ is from cross-correlations between unlike species. Looking at the magnitudes of $\Delta\Lambda_{12}$ in the lower plots of Figure 4.5, it also appears that the mixture of 40 mol% *n*-hexadecane and 60 mol% CO_2 will have behavior more closely resembling an ideal mixture than that of 40 mol% cyclohexane and 60 mol% CO_2. Although these effects should not be observable in close vicinity to the infinite dilution limit, an awareness of how cross-correlations between unlike species may influence D_{11} can still aid in interpreting data.

The second component necessary for determining D_{11} is the thermodynamic factor Γ_{ij}, which is a property used to account for the deviation of a mixture from ideality. In an ideal mixture, $\Gamma_{ij} = 1$. For simulations of binary mixtures where one component is present in very low compositions, an evaluation of Γ_{ij} can be a good indicator of proximity to the infinite dilution limit. To calculate Γ_{ij}, the running-Kirkwood-Buff integral approach of Ganguly and van der Vegt [106] is used, with

$$\Gamma_{11} = 1 - x_1 \frac{c_2 \left(G_{11}^{\infty} + G_{22}^{\infty} - G_{12}^{\infty} \right)}{1 + c_2 x_1 \left(G_{11}^{\infty} + G_{22}^{\infty} - G_{12}^{\infty} \right)} . \tag{4.14}$$

The infinity superscript on the Kirkwood-Buff coefficients G_{ij} represents an extrapolation to macroscopic systems, and c_2 is the molar concentration of species 2.

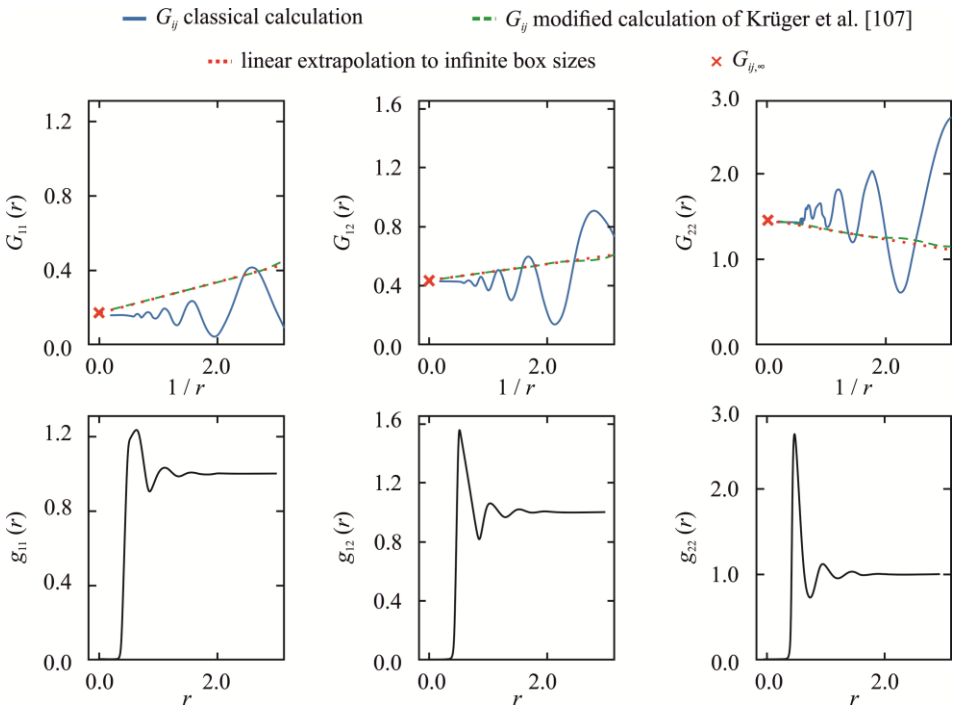

Figure 4.6: Radial distribution functions $g_{ij}(r)$ and Kirkwood-Buff integrals $G_{ij}(r)$ with corrections applied shown representatively for the binary mixture of *n*-hexane with 10% dissolved SF_6 at 323 K.

Kirkwood-Buff integrals are derived from radial distribution functions RDFs and an example of each is shown in Figure 4.6 from the binary mixture of *n*-hexane with 10% dissolved SF_6 at 323 K. In the lower part of the figure, the RDF is shown, where $g_{ij}(r)$ gives the ratio between the local number density (of component *i* at a distance *r* from component *j*) and the global number density. The Kirkwood-Buff integrals of Ganguly and van der Vegt [106] $G_{ij}(r)$ are more accurately extrapolated to macroscopic systems using a correction for finite size effects reported by Krüger et al. in 2013 [107]. Γ_{ij} calculated for this mixture at this state point is 0.96, which is very close to the value of unity for an ideal mixture. This gives a good indication that binary mixtures of *n*-hexane containing 10% or less dissolved SF_6 are fairly close to the infinite dilution limit.

4.3.2 Structure Analysis through Radial Distribution Functions

In addition to accessing macroscopic thermophysical properties, EMD simulations allow insight into the fluid structure on a molecular level. Radial distribution functions (RDF)s, which were previously discussed in connection with Kirkwood-Buff coefficients and calculating Γ_{ij}, have also been used to assess qualitative fluid behavior, calculate hydrogen bond statistics, and determine molecular effective diameters σ_{eff} [92]. The lattermost use is discussed in the following chapter, where σ_{eff} for the substances within the model systems of interest are provided. In this section, a general, qualitative analysis of RDFs will be given with a focus on interpretation of hydrogen bonding.

In fluid analysis, RDFs can quantify the reduced density by providing the ratio between the local number density and the global number density. Figure 4.7 shows some exemplary RDFs between the center-of-mass COM of solute molecules dissolved in either *n*-hexane or 1-hexanol close to the infinite dilution limit $g_{\text{solute-solute}}(r)$. This image is taken and modified from Piszko et al. [92] It represents the likelihood of finding the COM of one solute molecule a distance *r* from the COM of another molecule. On the left part of Figure 4.7, the impact of temperature can be addressed. From 303 K to 423 K, there is a broadening of the peak, a reduction in amplitude, and a slight rightward shift of the peak maximum. The larger system temperature corresponds to an increase in the kinetic energy of the molecule, which is reflected in stronger bond vibrations and rotational momentum. This results in a slightly larger average size of the molecule, sampled over the length of the simulation. The shifted peak corresponds to a slight increase in the average distance between the COM of the two solute molecules. When the molecule is represented as a sphere, the peak location

indicates the effective diameter σ_{eff} of molecule. The peak broadening suggests an increased likelihood of finding the COM of the two solute molecules both closer together and farther apart than σ_{eff}, which has to do with primarily with solute shape. Likewise, the reduced peak amplitude corresponds to a reduced likelihood of finding the two COM of the solute molecules at a distance σ_{eff} away from each other.

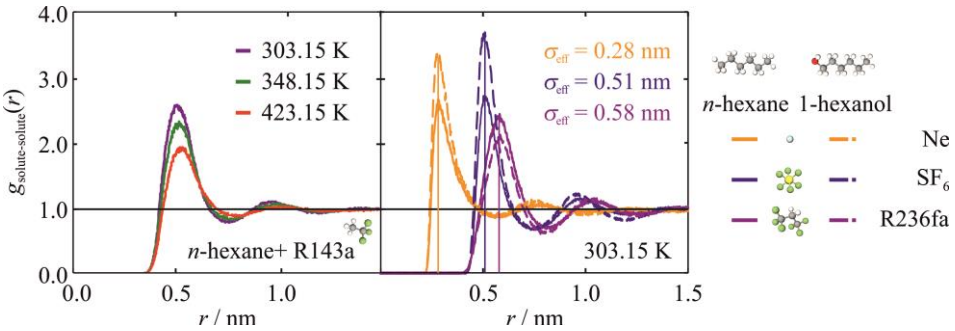

Figure 4.7: Exemplary radial distribution functions RDFs between the center-of-mass COM of solute molecules close to the infinite dilution limit $g_{solute\text{-}solute}(r)$. (left) *n*-hexane with dissolved R143a at three different temperatures. (right) Ne, SF_6 or R236fa dissolved in either *n*-hexane or 1-hexanol at 303.15 K. This image is modified from Piszko et al. [92].

The right part of Figure 4.7 shows RDFs again for the COM of solute molecules, but now for Ne, SF_6 or R236fa dissolved in either *n*-hexane or 1-hexanol close to infinite dilution. The different σ_{eff} of the different solutes are highlighted and are unchanged whether dissolved in the linear alkane or alcohol. This suggests a successful approach in using EMD simulations to interpret the molecular size of the solute. The spherical shape of Ne and SF_6 result in relatively narrow peaks, whereas R236fa is broader and with a lower amplitude. Between the two solvents, Ne and SF_6 have higher peak amplitudes in 1-hexanol compared to *n*-hexane, while the opposite is true for R236fa. A possible interpretation is that the hydrogen-bonding of the hydroxyl-groups in the alcohol inhibit solute movement in their vicinity. The solutes are more likely to diffuse around the alkane tail and are therefore more likely to encounter another solute molecule. This is not observed in R236fa, whose asymmetry encourages coulombic interactions with the hydroxyl-group of the alcohol.

It is also possible to calculate RDFs between atoms and an example of this is shown in Figure 4.8. Here, RDFs between either Ne or R236fa solute COM and the COM of either the alkyl-tail end-carbon atom C or the hydroxyl-

group oxygen atom O in 1-hexanol $g_{\text{solute-atom}}(r)$ are calculated. Such analysis allows a closer investigation of the influence of the hydroxyl group in the 1-alcohol. For both solutes, there is a strong peak when the reference atom is C. This supports the aforementioned theory that hydrogen-bonding between the hydroxyl-groups of the alcohol limit the presence of solutes in their vicinity. The dashed-orange line in Figure 4.8 indicates that Ne is unlikely to be in close vicinity to an O atom, because $g_{\text{Ne-O}}(r) < 1$. On the other hand, $g_{\text{R236fa-O}}(r)$ has a prominent peak above unity at a distance r smaller the $g_{\text{R236fa-C}}(r)$ peak. The closer packing of molecules due to coulombic forces could be the reason for this.

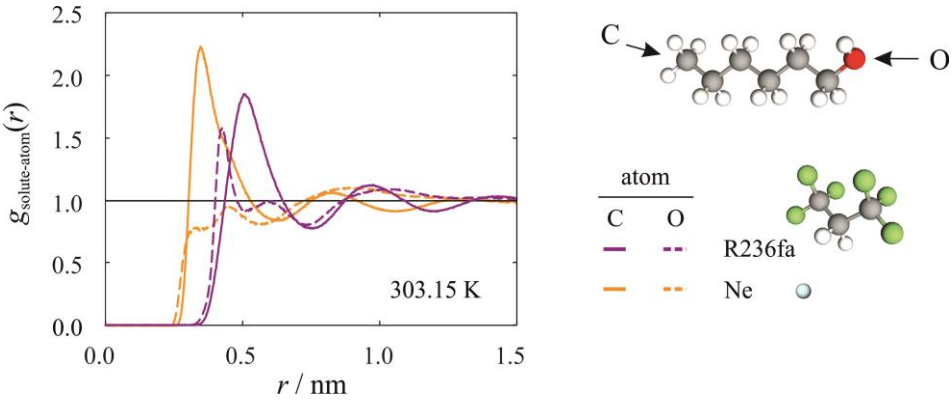

Figure 4.8: Exemplary radial distribution function between the center-of-mass COM of the solute and the COM of either the indicated carbon C or oxygen O atom $g_{\text{solute-atom}}(r)$ for Ne or R236fa dissolved in 1-hexanol at 303.15 K. This image is modified from Piszko et al. [92].

A quantitative analysis of hydrogen bonding is possible with RDFs by calculating the coordination number of appropriately selected interactions. Figure 4.9 shows RDFs between the oxygen O and hydrogen H atoms comprising the hydroxyl-group of the solvent 1-hexanol in a binary mixture with dissolved R236fa close to infinite dilution [92] $g_{\text{O-H}}(r)$, along with the average number of hydrogen bonds formed $\langle n_{\text{O-H}} \rangle$ within the first coordination shell. By analyzing the probability distribution function between the two atoms which form the hydrogen bond, $\langle n_{\text{O-H}} \rangle$ can be calculated with [108]

$$\langle n_{\text{O-H}} \rangle = 4\pi \frac{N_{\text{solvent}}}{L^3} \int r^2 g_{\text{O-H}}(r) \mathrm{d}r \,, \tag{4.15}$$

where $N_{solvent}$ is the number of 1-hexanol molecules and L is the box edge length of the cubic simulation vomule. By integrating over the complete box, $\langle n_{O\text{-}H} \rangle / z^3 = N_{solvent}$. To determine $\langle n_{O\text{-}H} \rangle$ within the first coordination shell, the upper bound of the integral should correspond to the first minimum following the initial peak. This is shown in Figure 4.9 for both temperatures around $r = 0.27$ nm. It should be noted $g_{O\text{-}H}(r)$ calculates a sharp, high-amplitude peak, which occurs at a distance corresponding to the bond length between O and H. This is omitted from Figure 4.9 and $\langle n_{O\text{-}H} \rangle$ calculations because it is the covalent bond within the 1-hexanol molecule rather than a hydrogen-bond.

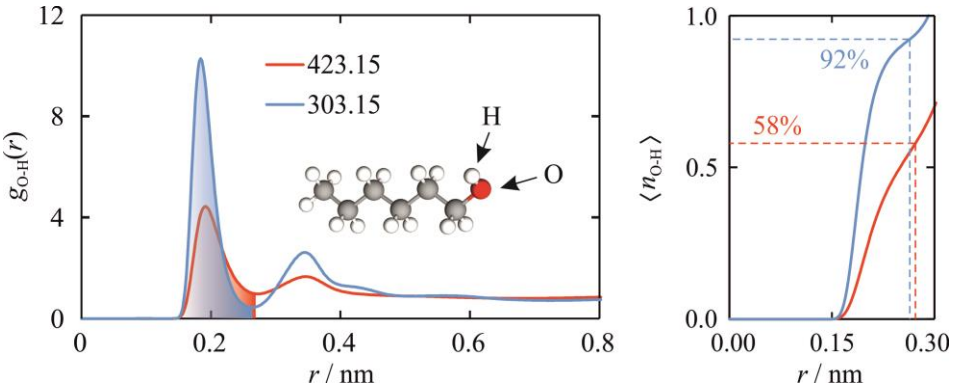

Figure 4.9 R236fa dissolved in 1-hexanol close to the infinite dilution limit at 303.15 and 423.15 K. (left) Exemplary radial distribution functions RDF between the center-of-mass COM of the indicated oxygen O and hydrogen H atoms $g_{O\text{-}H}(r)$. (right) Average number of hydrogen bonds formed $\langle n_{O\text{-}H} \rangle$ with values corresponding to the first coordination shell indicated for each temperature.

For a single 1-hexanol molecule, $\langle n_{O\text{-}H} \rangle = 1$ within the coordination shell corresponds to 100% of all hydroxyl groups included in $g_{O\text{-}H}(r)$ contributing to a hydrogen-bond. For this particular system, analyzing the RDFs at two different temperatures and calculating $\langle n_{O\text{-}H} \rangle$ with Eq. 4.15 shows a decrease of 36% in the average number of hydrogen bonds formed by a single 1-hexanol molecule. This confirms the common understanding that the hydrogen bond network within a polar solvent breaks down with increasing temperature.

5 Results and Discussion

In this chapter, the results of this cumulative work are given. First, the advancements made in FF development for simulations are presented and discussed. Here, the strong correlation between the two transport properties – viscosity and mass diffusivity – are highlighted and a shortcoming of EMD simulations is addressed. Next, results pertaining to the observed influence of molecular and fluid characteristics on diffusive mass transport are discussed. Since the EMD simulations modeled the same mixtures at approximately the same state points as were experimentally investigated via DLS and the main findings and developments from simulations have been discussed in the previous section, only results pertaining to DLS data are discussed. Results from EMD simulations generally agree well with experiments and usually are predicted within combined uncertainty of DLS results. For further details pertaining to how diffusivity results of a specific mixture compare between simulations and experiments, please refer to the respective publication.

Within the six publications presenting results on diffusion of a binary fluid mixture consisting of a liquid solvent and dissolved gas solute which are included as part of this cumulative work, 236 mass diffusivities spanning 45 different mixture combinations are given and will be consolidated in this section. Additionally, results consisting of 215 further diffusivities spanning 44 mixture combinations considering *n*-alkane [77,109], 1-alcohol [78], and IL [110,111] solvents with the dissolved gases H_2, He, N_2, CO, CO_2, and Kr are included for a more comprehensive discussion, since they are also determined using DLS at AOT-TP as part of the same project.

Following the discussion of the observed influences impacting diffusive mass transport, the development and application of predictive engineering models is discussed. An updated model to the one proposed by Wu et al. [78] is presented and its applicability is discussed. Finally, a simpler solution is proposed.

5.1 Development and Optimization of Force Fields

The basis of MD simulations is the molecular FF describing the potential energy between interaction sites for each calculation step as the simulation unfolds. This potential energy function is described by Eq. 4.8 in the previous chapter. The parameters of the electrostatic, intramolecular, and Lennard-Jones (LJ) potentials comprising the function are given in the

unique FF description for each molecule. This section will discuss improvements to the highly transferable OPLS-based FFs for application up to process-relevant conditions well beyond physiological temperatures. This is done with empirically-based modifications to the atomistic description of the LJ potential. First, in 2020 a simple temperature-dependent modification is proposed based solely on ρ data of *n*-dodecane for the improved prediction of surface or interfacial tension, η, and D_{self} in neat fluids. The transferability is evaluated with application to binary liquid mixtures [97], ternary mixtures of liquids and dissolved gases [96], and binary mixtures of a liquid with dissolved gas [88,90-93]. Then, in 2023 an updated model is proposed which incorporates the substance critical temperature T_c and extends the applicable temperature range [89]. At the end of this section, an improvement to the cyclohexane FF is briefly discussed as well.

The work of Klein et al. [58] combined SLS investigations and EMD simulations for the evaluation of ρ, surface or interfacial tension, and η of 12 linear and branched alkanes and alcohols. Simulating *n*-dodecane using the L-OPLS FF close to the saturation line predicted a critical point already at 573 K, when the critical temperature calculated using the equation of state of Lemmon and Huber [112] is 658 K. In response to this strong temperature dependency of predicted thermophysical properties, Klein et al. introduced an empirically-developed temperature correlation for ε_{ii} of the LJ-potential of the L-OPLS FF and applied it to the 11 further linear and branched alkanes and alcohols up to a carbon number of 40 with excellent results in the prediction of liquid density, surface tension, and dynamic viscosity. The correlation is based solely on the saturated ρ of *n*-dodecane and is applicable between (298.15 and 573.15) K. The correlation is given as

$$\varepsilon_i(T) = \varepsilon_{i,\text{L-OPLS}} \cdot \left(1 + \sum_{n=0}^{2} C_n T^n \right) \tag{5.1}$$

and $C_0 = -0.1914$, $C_1 = 8.167\times10^{-4}\ \mathrm{K^{-1}}$, and $C_2 = -5.857\times10^{-7}\ \mathrm{K^{-2}}$. The new predicted critical temperature for *n*-dodecane with the modified FF is 673 K. Although the correlation is not based on a physical description of the temperature dependency of ε_{ii}, the empirical optimization of parameters by comparing to experimental reference values is a cost-effective way to extend the applicability of well-established FFs to process-relevant conditions.

Albeit the FF modification proposed in Klein et al. was developed solely on the saturated ρ of *n*-dodecane, it was possible to eliminate the temperature-dependency of the observed deviations between simulated and experimental values for the surface tension γ, and the dynamic properties η and D_{self} as well [58]. In 2021, Lenahan et al. [97] applied this modification to binary liquid mixtures and found it to be fully transferable across the complete composition range, as the pure-substance FFs were each L-OPLS based and carried over similar statistical uncertainties and deviations from experimental values as for simulations of the neat fluids for σ and η. This was observed again in the publications of Klein et al. [113], Kankanamge et al. [114], and Lenahan et al. [96] when applied to binary and ternary mixtures involving liquids and dissolved gases. In these cases, the solute FF is often not OPLS-based and therefore, the temperature-dependent modification is only applied to the solvent. By removing the temperature-dependent deviations inherent to the original solvent FF, the influence of the dissolved gas on γ and the dynamic property η could be resolved. Around the same time, this modification was additionally applied to 34 mixtures considering 8 solutes close to infinite dilution and 13 solvents for the determination of $D_{self,i}$ [90,92]. As expected, the improved predictive capability with regard to η over a large temperature range extended to $D_{self,i}$.

Lenahan et al. [89] extended the work of Klein et al. [58] with a new correlation utilizing the same procedure as in the original work as well as the original ρ data of *n*-dodecane, now extended up to 648.15 K. This corresponds to a reduced temperature $T_R = T/T_c$ of about 0.98.

$$\varepsilon_i(T) = \varepsilon_{i,\mathrm{OPLS}} \cdot \left(1 + 3.94 \cdot \left(\frac{T_c^2}{T T_o} \cdot \frac{\left(T - T_o\right)}{\left(T_c - T_o\right)} \right) \right). \tag{5.2}$$

The new correlation incorporates a substance's critical temperature T_c and the temperature at which the OPLS FF parameters were developed T_o. This enables application of the FF modification to ethane, which was developed at T_o = 184.52 K [41]. For all other liquids where the OPLS FF is applied, the original parameters are evaluated at 298.15 K [41]. Relative deviations in ρ, η and D_{self} of neat ethane compared to experimental results again showed a strong temperature dependency with the original FF of (0.05, 6.8, and –22)% at 184.51 K and (–11, –22, and –2.4)% at 273.15 K. The original FF did not simulate a liquid phase at 298.15 K close to saturation pressure. With the modification of Eq. 5.2 applied, the relative deviations in ρ, η and D_{self} at 273.15 K are (1.7, 7.8, and –29)%. Figure 5.1 shows the results of Eq.

5.2 applied to several *n*-alkanes, up to N_C = 40 and T_c = 904 K [58,115]. The maximum absolute temperature for each substance corresponds to a T_R of roughly 0.98. The original FF modification published by Klein et al. and given by Eq. 5.1 is shown in black and does not significantly deviate from the results of Eq. 5.2 within their applicable temperature range of (298 to 573) K. The dashed black line indicates an extrapolation of their correlation to 873.15 K, which corresponds to T_R = 0.97 for *n*-tetracontane.

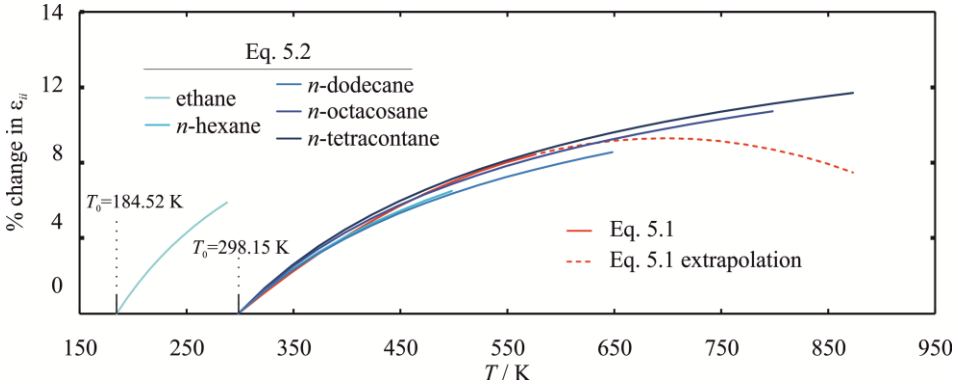

Figure 5.1: Proposed change in the epsilon parameter of the Lennard-Jones potential in atomic descriptions of OPLS-based force fields as a function of temperature. The temperature-dependent modification reported by Klein et al. [58] and described in the main text by Eq. 5.1 is shown in black. The dashed line represents an extrapolation of this correlation beyond 573.15 K. All other lines show results of the temperature-dependent and substance-specific correlation reported by Lenahan et al. [89] and described by Eq. 5.2 in the main text.

Although such modifications have shown to significantly improve the predictive quality of simulations for neat fluids and are fully transferable to mixtures in regard to equilibrium and dynamic thermophysical property prediction, they are still not sufficient at capturing more complex fluid behavior approaching the critical point. The work of Lenahan et al. [89], where this new modification is proposed, additionally investigates ethane (2) with 3 mol% dissolved N_2 (1) and found $D_{self,1}$ to be over 650% overpredicted at 298.15 K, relative to an experimental investigation of D_{11}. Although the temperature-dependent FF modification significantly improved the prediction of η and D_{self} in the neat fluid, it failed to accurately describe the mixture Fick diffusion coefficient approaching a critical point. This could be due to the hydrodynamic fluctuations in the fluid, which become infinitely large approaching the critical point. It is these fluctuations which govern dynamic fluid behavior. In this case, the

failure to accurately predict D_{11} is then likely a result of the limited simulation box size, rather than the used FF. With improved hardware and access to more efficient computational resources, an assessment of this claim could be possible in the future.

In addition to the temperature-dependent modification to the energy term of the LJ potential, a static change is suggested specifically for the OPLS-based FFs describing cycloalkanes. Investigations of $D_{self,i}$ in mixtures of cyclohexane with dissolved He or Kr showed underpredictions of nearly 30% [90] and investigations of η in the liquid organic hydrogen carrier dicyclohexylmethane showed overpredictions of up to 55% [47]. To remedy this, the second LJ parameter σ_{ij} describing the zero-energy distance between two interaction sites *i* and *j* is reduced by 2% for both the C and H atom descriptions in the cyclohexane FF [91]. This results in a close to 20% reduction in the relative deviation between simulated and experimentally determined values for both η and D_{self} of neat cyclohexane between (298 and 448) K. Additionally, $D_{self,1}$ values from simulations of cyclohexane with dissolved CO_2 [91], CH_4, or R143a [88] have a relative deviation from experimental D_{11} values of typically less than 15%, which is a notable improvement.

5.2 Diffusion Coefficient in Binary Mixtures of a Liquid and a Dissolved Gas

All figures given in this section are created from the published data given in references 77, 78, 88, 90-93 and 110 from the investigations performed at the Institute of Advanced Optical Technologies – Thermophysical Properties of FAU. In some instances, multiple data given on a plot are separated by color according to either solute or solvent. The solute color scheme is given as follows – H_2: dark red, He: purple, CH_4: light red, Ne: light blue, N_2: blue, CO: orange, CO_2: yellow, Kr: green, SF_6: peach, R143a: grey, R236fa: dark green. The solvent color scheme is represented in Figure 4.1 and given as follows – *n*-alkanes: blue, branched alkanes; green, cyclic alkanes: purple, 1-alcohols: red, acid/ester: orange, IL: brown. To begin, the influence on the binary Fick diffusion coefficient D_{11} of varying *n*-alkane solvent chain length N_c is addressed for five different dissolved gases. A graphical representation of this is given in Figure 5.2. Then, a comparison between the solvents *n*-hexane and its hydrogenated counterpart 1-hexanol is given at two different temperatures to address the observed influence of hydrogen bonding on D_{11}. This comparison is additionally shown in Figure 5.3 for 11 different gas solutes. Next, the discussion moves away from

addressing the influence of specific molecular characteristics and instead focuses on how T, and solvent η and ρ are related to the binary mixture's D_{11}. Finally, greater attention is given to the relationship between η and D_{11}.

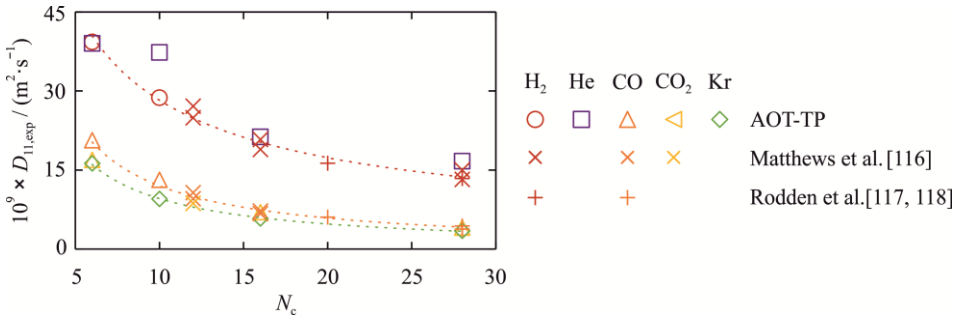

Figure 5.2. The binary Fick diffusion coefficient D_{11} of mixtures consisting of an *n*-alkane and a dissolved gas plotted against number of carbons atoms N_c in the solvent molecule. Solvent gas is separated by color. Open symbols represent experimental data determined by DLS at AOT-TP from references 77 and 90-92. Other symbols represent data acquired from the literature [116-118]. Lines are a simple power-law fit to aid the eye. All results are around 373.15 K and the datum for D_{11} of the mixture *n*-hexane and CO_2 is extrapolated to 373.15 K.

The linear alkanes included in this work have carbon numbers N_c ranging from 6 to 28 and were investigated with primarily five different solutes. Figure 5.2 shows D_{11} data at 373.15 K plotted against N_c for each of these mixtures with the five different solvents indicated by color. To aid the eye, a simple power-law correlation is fitted through the data sets for H_2, CO, and CO_2, where literature data was available. There is a clear non-linear decrease of D_{11} with increasing N_c. Although the influence of M_{solute} is apparent from Figure 5.2, it is also not linear. As noted already by Giraudet et al. [77], while M_{helium} is twice as large as $M_{hydrogen}$, this is not reflected in the D_{11} of mixtures containing these gases. The proposed explanation to this observance was that the sphericity of the dissolved solute molecules plays a significant role and can be represented in the form of the acentric factor ω.

It should be noted that the relative experimental uncertainties of the data for *n*-hexane and *n*-decane with dissolved He determined by DLS at AOT-TP are (50.6 and 24.0)%. This could account for the seemingly large value for D_{11} in the *n*-decane and He mixture. Additionally, the datum for *n*-hexane and CO_2 is extrapolated to 373.15 K from the data by Klein et al. [109] using a second-order polynomial fit to temperature.

To address the influence of hydrogen bonding, several primary 1-alcohol solvents, the acid *n*-hexanoic acid, and the ester ethyl butyrate were investigated. The results shown in Figure 5.3 are only for the solvents with $N_c = 6$, to limit the influence on D_{11} caused by solvent molecule size and ideally isolate the impact caused by the presence of the highly electronegative oxygen atom O. Results for two temperatures are shown to capture the influence of hydrogen bonding, since this effect is known to strongly weaken with increasing temperatures. In the previous chapter, the quantitative assessment of hydrogen-bonding statistics through RDF analysis is detailed.

For better visualization of results between different solvents and gaes, the D_{11} axis is given on log-base 10 scale. In the left part of Figure 5.3, D_{11} of binary mixtures containing the solvent 1-hexanol is compared to those with *n*-hexane for all 11 investigated gas solutes. The magnitude of the difference in D_{11} at 303 K compared to those at 348 K is larger for the 1-alcohol compared to the *n*-alkane, which is exactly as expected given the breakdown of the hydrogen bond network affecting the alcohol. Only the mixture with dissolved He does not appear to be affected.

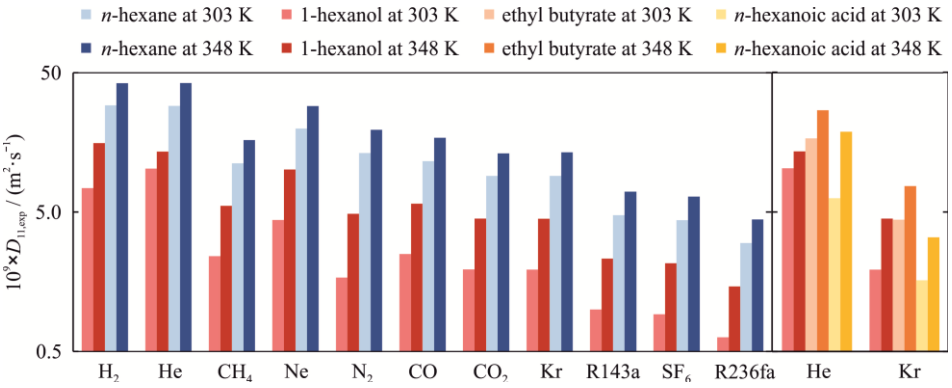

Figure 5.3. Evaluating the impact of hydrogen bonding on diffusive mass transport by comparing binary mass diffusion coefficients $D_{11,exp}$ at 303 K and 348 K for several solvents with $N_c = 6$. (left) Comparison between mixtures with *n*-hexane or 1-hexanol as the solvent considering all 11 solutes. (right) Comparison between *n*-hexane, 1-hexanol, and the two solvents containing a carbonyl group. Solutes are labeled in order of increasing atomic mass from left to right.

In the right part of Figure 5.3, data at 303 K and 348 K for D_{11} of mixtures containing the acid or ester are compared to those with 1-hexanol. No other solutes were investigated with these solvents. Here, it would be expected that D_{11} in mixtures containing one of the two solvents containing a

carbonyl group in addition to a hydroxyl group would have a stronger temperature response than the 1-alcohol, which only has a hydroxyl group. Instead, the ester is comparable to the alcohol and the acid shows the strongest response. This could be because the acid has a carboxyl group, whereas in ethyl butyrate, the double-bonded O forming its carbonyl group is shifted down the alkane tail by one carbon atom. This should slightly increase the bulkiness of ethyl butyrate compared to *n*-hexanoic acid and could also result in a weaker dipole, since the highly electronegative O atoms are not as concentrated on one side of the molecule.

The impact of the solvent molecular structure is also observed in the solvent properties η and ρ. Four further solvents with $N_c = 6$ which can be included here are the branched alkanes 2-methylpentane (also called isohexane) and 2,2-dimethylbutane (also called neohexane), and the cyclic molecules cyclohexane and benzene, which is an aromatic ring. Figure 5.4 shows D_{11} plotted against (A) temperature T, (B) ρ, and (C) η for all solvents with $N_c = 6$ with dissolved Kr across the investigated temperature range from Piszko et al. [92] and Lenahan et al. [90] Observing all three influences, it appears that the relationship between D_{11} and η is the most closely linked and that the trend is relatively independent of the solvent. For instance, the alcohol and acid solvents have the highest ρ and η but the lowest mixture D_{11} due to the presence of hydrogen bonding. The ester has a large ρ for this same reason, but a lower η and larger mixture D_{11} due to the branching of its carbonyl-group. Between oxygenated solvents and the alkanes, which have the lowest η and ρ, there is a gap above 0.7 g·cm^{-3} for ρ but the plot of η shows a relatively smooth transition over the investigated range. Similar η leads to similar values for D_{11}, but this is not reflected by ρ. This relationship is also apparent from the D_{11} results for benzene or cyclohexane with dissolved Kr. Here ρ of the phenyl-ring solvent is much larger than that of cyclohexane. Yet, the mixture D_{11} is slightly lower and therefore follows a more similar trend as the solvent η.

From Figure 5.4(C), the relationship between D_{11} and η appears to be independent of solvent fluid class. This is explored further with Figure 5.5, where D_{11} is again plotted against η using data from Giraudet et al. [77], Wu et al. [78], Klein et al. [110], Piszko et al. [92], and Lenahan et al. [90]. Figure 5.5(A) shows results for binary mixtures of *n*-hexane with six different dissolved gas solutes whereas Figure 5.5(B) shows D_{11} results for four different gases in up to 15 different solvents at the same temperature of 348 K. Again, solvent fluid class is shown to have a very similar influence on D_{11} as for η. The range of η at 348 K shown here is from 0.19 mPa·s for isohexane with

dissolved He to about 18 mPa·s for the mixture of [DMIM][NTf_2] with dissolved Kr. In this upper range, where the ILs have very high η and the smallest D_{11}, the relationship between D_{11} and η weakens. For large changes in η, only small changes in D_{11} are reported, often within uncertainty. Therefore, D_{11} may be independent of η, when η is so large.

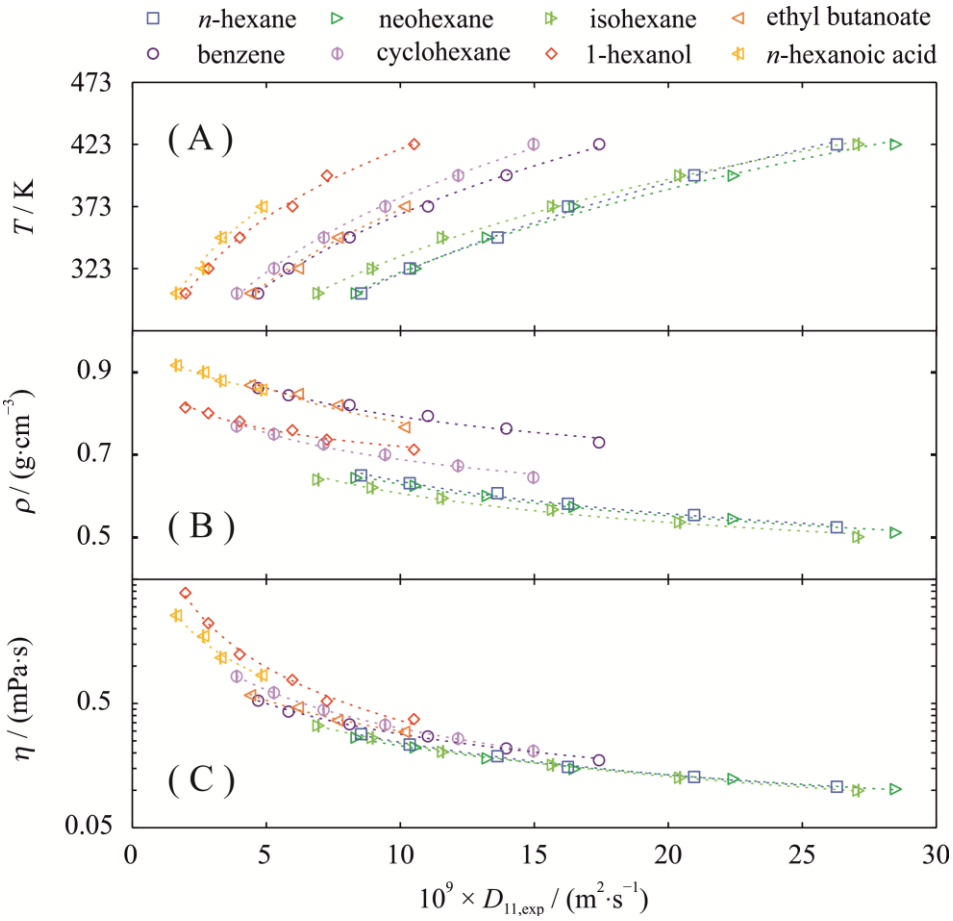

Figure 5.4. Experimental results for D_{11} of binary mixtures of Kr dissolved in solvents with N_C = 6 plotted against (A) temperature, (B) solvent density, and (C) solvent viscosity. Colors indicate the solvent. Lines are a simple power-law fit to aid the eye. No uncertainties are given for legibility.

On the other hand, the relationship between D_{11} and η is strongly dependent on the solute. In 1971, Hayduk and Cheng [28] assessed the relationship between diffusivity and solvent viscosity for several mixtures

with an *n*-alkane solvent and ethane or CO_2 close to infinite dilution. They also found that the viscosity dependence is likely strongly related to the solute. The transferability of this relationship across different solvent fluid classes is observable in Figure 5.5(B) as well.

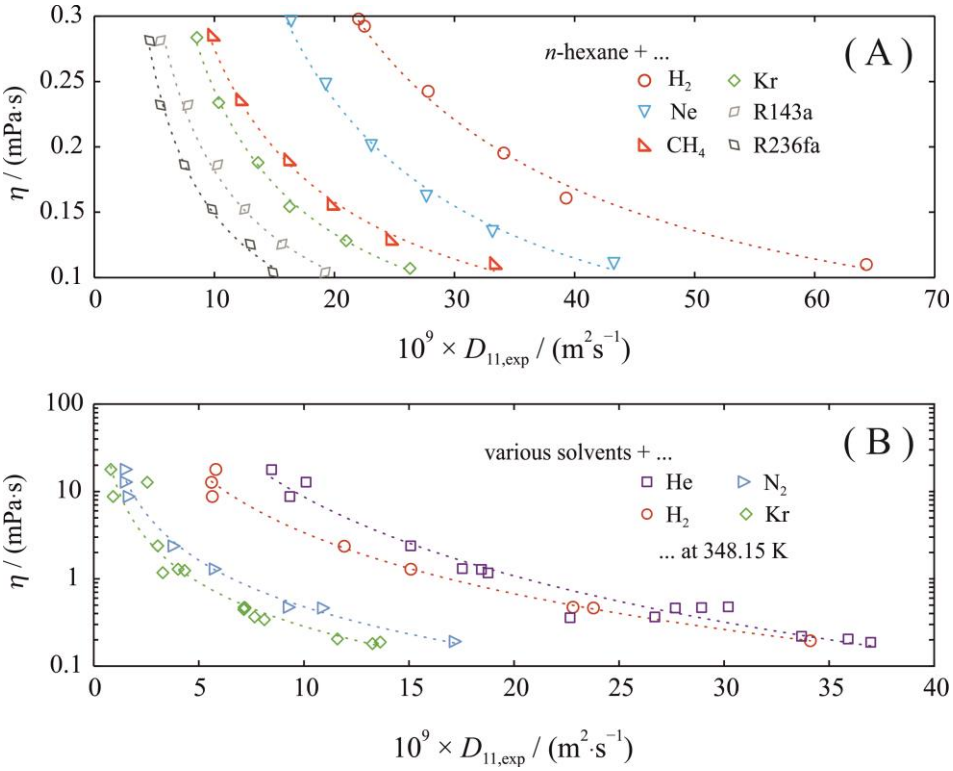

Figure 5.5. Solvent viscosity η plotted against binary mass diffusivities $D_{11,exp}$ for (A) *n*-hexane with six different solutes and (B) various solvents with four different solutes at 348 K. Colors indicate the solute. Lines are a simple power-law fit to aid the eye. No uncertainties are given for legibility.

The influence of molar mass is readily apparent in Figure 5.5(A). Results of mixtures containing *n*-hexane with the light gases H_2 and Ne dissolved have larger D_{11} values and show a steeper dependency on η compared to mixtures containing the heavier refrigerants or Kr. Curiously, R143a and Kr have very similar molecular weights, with M_{R143a} = 84.0 g·mol^{-1} and M_{Kr} = 83.8 g·mol^{-1}, but this is not reflected in the results for D_{11}. A similar observation was made by Giraudet et al. [77], investigating *n*-alkane solvents, Wu et al. [78],

investigating 1-alcohol solvents, and Klein et al. [110], investigating IL solvents. They each found that, although M_{He} is about twice as large as M_{H_2}, D_{11} in binary mixtures with He or H_2 as the solute in the same solvent are comparable. It is likely that the solute shape and size also influence the diffusive process and the relationship between D_{11} and η, which would explain the larger diffusivity observed for *n*-hexane with dissolved Kr as compared to *n*-hexane with dissolved R143a.

5.3 Prediction Models for the Binary Fick Diffusion Coefficient close to the Limit of Infinite Dilution

The influencing factors behind mutual diffusivity in binary mixtures of a liquid with a dissolved gas has been investigated through systematic variation of selected solute and solvent combinations. This chapter summarizes the main findings of three recent publications which investigate binary mixtures of a liquid with a dissolved gas at compositions assumed close to infinite dilution [88,90,92]. Within these three publications, 35 mixture combinations are investigated at approximately three to six temperatures each, resulting in 193 experimentally investigated state points. Also within this project series, the Fick diffusion coefficient of binary mixtures across a wider composition range extending to well outside the infinite dilution regime are measured. Evaluating the impact of composition on diffusion is beyond the scope of the present thesis, however, results for D_{11} at the lower composition range of these studies – assumed to be in the vicinity of the infinite dilution regime – are included here. This comprises a further two publications, encompassing 10 mixture combinations, and 47 experimentally investigated state points.

As mentioned in the section Model Systems of Interest in Chapter 4, mixture combinations vary substantially in terms of solute and solvent characteristics. Therefore, the solvents will be separated based on their fluid class; alkane: linear, branched, cyclic; oxygenated: primary alcohol, acid/ester; or ionic liquid. Initial investigations focused only on linear alkanes and primary alcohols and from these, a simple predictive engineering model was developed by Wu et al. [78], which is provided in the State of the Art by Eq. 2.13-2.14. The training set is now extended to include not only all D_{11} data mentioned above from the publications included in this cumulative work, but also further data published in references 77 and 78, which were used as part of the testing set by Wu et al. [78] This is, in total, 451 diffusivities. Reported effective diffusivities D_{11}^*, where Le is close to unity, are not included in the training set. Additionally,

data predicted via EMD simulations are not included. Although simulation results show accurate trends with respect to dynamic fluid behavior and generally agree well when compared to experiments, D_{11} values are typically underpredicted compared to their respective experimental reference and including them here would be moot.

Solute and solvent input data to the models for the mixtures comprising the training set can be found in the respective publications where the model is applied, except for [EMIM][B(CN)$_4$]. Here, the solvent properties were acquired from the Ionic Liquid Database – ILThermo (v2.0) [6,7]. Predicted binary Fick diffusion coefficients $D_{11,calc}$ using Eq. 2.13-2.14 for the complete data set are shown in a parity plot against the respective experimental diffusivity $D_{11,exp}$ in Figure 5.6(A). Shortcomings of the model have been highlighted in the publications Piszko et al. [92] and Lenahan et al. [90]. In particular, their model performs poorly for mixtures of highly polar sub-stances. The largest deviations between $D_{11,calc}$ and $D_{11,exp}$ are found for mixtures of 1-hexanol with a refrigerant, or mixtures with ethyl-butanoate or an IL as the solvent. The overall bias and AARD considering all 451 diffusivities is (14.11 and 28.17)%. Attempts at developing an improved, modified version of the model published in Wu et al. [78] yielded the result:

$$D_{11,calc} = 6.93 \times 10^{-18} \frac{T\Psi^2}{\left(1.75 + \omega_1\right)^{1.87}} \left(\frac{\rho_2^{1.14}}{\eta_2^{0.75}}\right)\left(\frac{M_2}{M_1}\right)^{0.27}, \tag{5.3}$$

$$\Psi = 1 + 2.10 \times 10^6 \frac{\nu_2^{0.5}\left|\mu_1 - \mu_2\right|}{TM_1M_2}. \tag{5.4}$$

Greater variation of individual parameters was permitted in the form of separate exponents on η_2 and ρ_2 in Eq. 5.3, and the inclusion of M_1 and μ_1 in Ψ. Parameterization is optimized through a steepest-decent algorithm using the MATLAB software.

The results for $D_{11,calc}$ acquired using Eq. 5.3-5.4 are shown in a parity plot with experimental data in Figure 5.6(B). There is no considerable improvement in the prediction of D_{11} with this approach. The new bias and AARD considering all 451 diffusivities are (8.00 and 25.11)%. Where improvements could be observed, they are compensated for with larger deviations elsewhere. For example, reduced deviations between $D_{11,calc}$ and $D_{11,exp}$ for mixtures containing 1-hexanol and R143a, R136fa, or SF_6 come at

the expense of larger deviations for other mixtures with 1-alcohol solvents. Figure 5.8(A) and (B) illustrate the calculated bias using the model of Wu et al. from Eq. 2.13-2.14 and that presented here with Eq. 5.3-5.4 to visualize how deviations are distributed by solvent fluid class. Although the updated model has accepted greater complexity of implementation in order to incorporate the greater variety of molecular characteristics, there is no apparent reward in regard to accuracy of prediction.

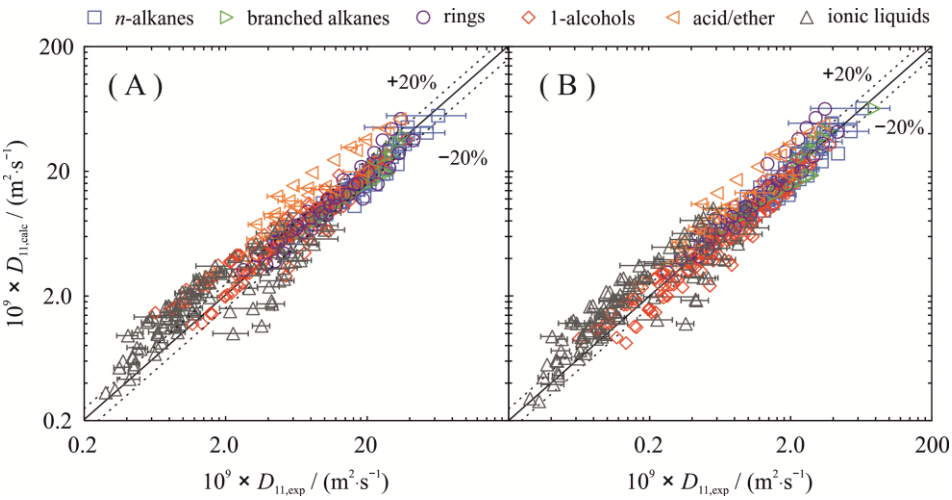

Figure 5.6. Parity plots for 451 binary Fick diffusion coefficients predicted $D_{11,calc}$ or experimentally determined $D_{11,exp}$ for all data used in the training set. (A) $D_{11,calc}$ is predicted using the semi-empirical prediction model published by Wu et al. [78] and shown as Eq. 2.13-2.14 in the main text. (B) $D_{11,calc}$ is predicted with an updated, re-parameterized version of the model by Wu et al., given with Eq. 5.3-5.4 in the main text. Symbol color indicates the solvent fluid class and only some error bars are shown for legibility purposes.

Giraudet et al. [77], the precursor to Wu et al. [78], state that their model is a modified version of that proposed by Wilke and Chang [76], which is also discussed in the State of the Art of this thesis and given by Eq. 2.10. They state that their inclusion of the acentric factor was the main contributor to improving the prediction of diffusivities in mixtures containing H_2 and He and that the impact of solvent density is captured by their inclusion of the kinematic viscosity. The model by Wilke and Chang incorporates the solute molal volume at the boiling point, which Giraudet et al. and Wu et al. have removed. Additionally, the model based on hard-sphere theory by Assael et al. [62] and described by Eq. 2.3 correlates the dimensionless reduced diffusivity as a function of the ratio between system

volume and the close-packed hard-sphere diameter. Cadogan et al. [22] extended their efforts to real fluids by considering the molar core volumes of both solute and solvent molecules. Their modification is described by Eq. 2.8. During efforts to identify and correct for failures in improving the model by Wu et al., a simple solution was found, which re-introduces the parameter of the core volume.

5.3.1 The Core Volume

For an incompressible fluid in macroscopic thermodynamic equilibrium, the volume occupied by the fluid V depends on its molar mass M and the liquid density at the relevant state point ρ, $V = M / \rho$. However, this volume includes both the space occupied by fluid molecules themselves, and the "free volume" between molecules, resulting from and allowing for molecular vibrations. It is through this "free volume" that gaseous solutes can diffuse. For this reason, a molecular characteristic describing size of molecules is developed to assess the impact on D_{11}. In this work, it is dubbed the core volume V_0 and represents the 3-dimmensional space occupied by a molecule.

The method detailed below is based on the overlapping-sphere concept given by Bondi [79,80] and uses van der Waals radii and covalent bond lengths which are available for every atom and atom pair [119-121]. This method does not account for non-sphericity due to occupied or shared atomic shell orbitals. It is assumed that all atoms are hard spheres and that the occupied molecular volume can be built by adding singular atomic volumes until the complete molecule is described. The geometry behind calculating core volumes is shown in Figure 5.7. The left part of the figure and the following equations are modified from the work of Bondi [79,80].

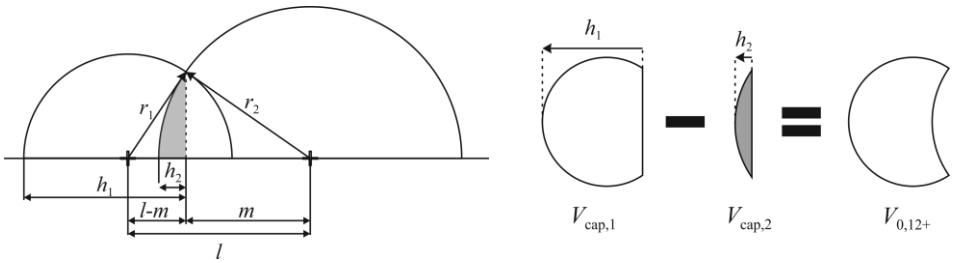

Figure 5.7. Two-dimensional geometry of spheres overlapping. $V_{0,12+}$ represents the core volume addition when adding a new atom to a molecule build.

radii correspond to atomic van der Waals radii r_i and $i = 1$ for the atom to be added. The bond length is designated l and an intermediate variable m is acquired from the Pythagoras's Theorem using l, r_1, and r_2 with

$$m = \frac{r_2^2 - r_1^2 + l^2}{2l}. \tag{5.5}$$

The volumes indicated in the right part of Figure 5.7 are acquired using the formula for the volume of a spherical cap:

$$V_{\text{cap},i} = \pi h_i^2 \left(r_i - \frac{h_i}{3} \right). \tag{5.6}$$

Here, h_i is the indicated height of the cap with

$$h_1 = r_1 + l - m \quad \text{and} \quad h_2 = r_2 - m. \tag{5.7}$$

The final volume $V_{o,12+} = N_A \times (V_{\text{cap},1} - V_{\text{cap},2})$ is in units of ($cm^3 \cdot mol^{-1}$) and contributes to a group contribution method for specific bonded-atom pairs.

Within this work, every atom pair which is encountered has had $V_{o,12+}$ calculated and the corresponding values are given in Table 5.1. For example, when building *n*-alkanes, the full spherical volume of an end-C-atom, $V_{(C-)} = 4\pi/3 \times r^3$ is the starting point. The other volume additions to consider in such a molecule are those of H-atoms connected to C-atoms $V_{o,(H-c)+}$ and C-atoms connected to C-atoms $V_{o,(C-c)+}$. In an *n*-alkane, there are ($N_C \times 2+2$) $V_{o,(H-c)+}$ and (N_C-1) $V_{o,(C-c)+}$. The final V_o for each molecule indicated in the section Model Systems of Interest is provided in Table 5.3 along with comparable molar volumes acquired through other calculation methods.

The Boltzmann diameters reported by Ben-Amotz et al. [122] are treated as hard-sphere core diameters σ for calculating V_o from Eq. 2.5. Fuller et al. [123] reports "diffusion volumes" empirically fit to 340 experimental gas-phase diffusion coefficients. The van der Waals volumes V_w, collected by Yaws [124] or calculated using the available group contribution components provided by Bondi [79] are shown as well in Table 5.3. V_w holds the same definition as V_o, as it is the volume occupied by a molecule described by a collection of overlapping hard spheres with diameters based on the atomic van der Waals radii and sphere overlap based on bond length. Most

solvent V_w values reported by Yaws use the book of Bondi as a reference, so they are indicated in the table as an asterisk for legibility. Many of the V_w values provided by Bondi have a small correction applied based on experimental density data. This may be the cause of the small deviations observed with respect to this work.

Table 5.1: Calculated $V_{0,12+}$ values for every atom pair encountered during molecule build of each solvent and solute identified in the section Model Systems of Interest.

Added atom (1)	Fixed atom (2)	$V_{0,12+}$ / ($cm^3 \cdot mol^{-1}$)	Added atom (1)	Fixed atom (2)	$V_{0,12+}$ / ($cm^3 \cdot mol^{-1}$)
Single bonded			Double bonded		
H	H	1.70	C	C	6.95
H	C	1.10	C	N	7.27
H	O	1.36	O	C	4.16
H	N	1.48	O	S	4.73
C	C	7.67			
C	O	8.26	Triple bonded		
C	N	8.35	C	O	7.24
C	S	8.31	N	C	4.07
C	B	6.76	N	N	4.71
O	C	4.72			
N	C	5.35			
F	C	4.21			
F	S	4.78			
S	N	11.3			

Molar volumes acquired with EMD simulations are calculated with Eq. 2.5 using effective molecule diameters σ_{eff} determined from RDFs. Here, σ_{eff} of a molecule describes the average diameter value of a sphere occupied by the molecule during the simulation run. It is acquired from the first peak position of an RDF calculated between the COM of like-molecules. For small molecules, it works quite well. However, identifying peak location becomes more difficult as peaks broaden for larger and less-spherical

molecules. The linear alkane *n*-octacosane, with $N_C = 28$, did not have a peak at all and σ_{eff} could not be determined. For each of the substances investigated with EMD simulations, where a COM-COM RDF was generated, σ_{eff} is extracted and given in Table 5.2.

Table 5.2: Effective Molecular Diameter σ_{eff} Acquired from Peak Position in Radial Distribution Functions.

Solute Molecule	σ_{eff} / nm	Solvent Molecule	σ_{eff} / nm
H_2	0.30	ethane	0.49
He	0.25	*n*-hexane	0.61
CH_4	0.40	*n*-decane	0.77
NH_3	0.30	*n*-hexadecane	0.87
Ne	0.28	isohexane	0.59
CO	0.44	neohexane	0.59
N_2	0.39	cyclohexane	0.62
CO_2	0.40	benzene	0.58
Kr	0.39	ethanol	0.46
R143a	0.51	1-hexanol	0.61
SF_6	0.51	1-decanol	0.75
R236fa	0.58	*n*-hexanoic acid	0.63
		ethyl-butanoate	0.66

It should be noted that increasing temperatures typically results in a broadening of the peak and lower peak amplitude, but it does not significantly shift the peak position. This coincides with expectation. As kinematic energy increases, molecules have stronger vibrations and more movement, resulting in a reduced likelihood that any one configuration occurs more often than another.

The molar core volumes of this work are comparable to but generally smaller than the volume parameters acquired from the literature. In particular, the occupied volume estimated with Eq. 2.5 using an effective hard-sphere diameter and those empirically fit to diffusivity data by Fuller et al. [123] are considerably larger.

Table 5.3: Volume Parameters Representing The Space Occupied by a Molecule for The Purpose of Predicting Diffusion Coefficients in Units of ($cm^3 \cdot mol^{-1}$)[a] for Every Solute and Solvent Identified in The Section Model Systems of Interest.

Substance	This work	Yaws [124]	Bondi [79]	EMD	Ben-Amotz et al. [122]	Fuller [123]
H_2	6.06	6.21		11.50		7.07
He	6.92	6.92		6.65		2.88
CH_4	16.80	17.05		27.25		24.42
NH_3	13.83	13.80		11.50		14.9
Ne	9.21	10.33		9.35	6.85	5.59
CO	16.10	16.20		36.27	17.82	18.9
N_2	14.10	15.80		25.26	17.50	17.9
CO_2	20.71	19.70		27.25	20.67	26.9
Kr	20.79			25.26	18.62	22.8
R143a	35.99		35	56.49		
SF_6	43.38	46.80		56.49		
R236fa	55.19		66.56	83.08		
H_2O	11.58	12.37		11.50	10.62	12.7
ethane	26.67	*	27.34	50.10		45.62
n-hexane	66.17	*	68.26	96.66	90.11	128.82
n-decane	105.66	*	109.18	194.41		212.02
n-hexadecane	164.89	*	170.56	280.41	244.63	336.82
n-octacosane	283.37	*	293.32			586.41
isohexane	66.17	*	68.25	87.46		128.82
neohexane	66.17	*	68.24	87.46		128.82
cyclohexane	59.24	61.40	58.68[b]	101.49	76.60	124.80
benzene	50.46	48.40	45.84	83.08	63.11	112.72
ethanol	31.66	*	31.94[c]	41.45	37.15	51.20
1-hexanol	71.15	*	72.86[c]	96.66	96.89	134.39
1-decanol	110.64	*	113.78[c]	179.65		217.59

Substance	This work	Yaws [124]	Bondi [79]	EMD	Ben-Amotz et al. [122]	Fuller [123]
n-hexanoic acid	73.10		78.03[d]	106.48		135.94
ethyl-butanoate	68.71		73.23	122.42		135.94
$B(CN)_4$	92.53					
NTf_2	108.43		84.28[e]			
EMIM	54.35		55.57			
HMIM	93.85		96.49			
DMIM	133.34		137.41			

An asterisk in the column of Yaws indicates that Bondi is their reference and the values are identical. [a]the work of Fuller et al. identifies a "diffusion volume" with "dimensions of atomic volumes" but does not provide a unit. The values given here are multiplied by 10^2. [b]value taken from Table 8.4 in reference rather than from group contribution method. [c]$\delta V_w = 0$. [d]no V_w value is given for [-C(=O)-OH], so [-C(=O)-H] + [-OH] is used instead. [e][N-S] and [C-S] connections are unaccounted for and [-NH_2] is used instead of [S-NH-S].

5.3.2 A Simple Model

The mixtures included in this work are comprised of a wide range of fluid classes and gaseous solutes. This variation has allowed investigation of how macroscopic fluid properties are influenced by the microscopic molecular characteristics of mixture components. During model development, it became clear that a single, simple, predictive engineering model describing all available mixture combinations to within 10-15% of the respective experimental data is impossible. The limitation here is the word "simple". Instead, a prediction model is proposed to cumulate this work, which accepts an approximately 20% AARD with some systematics present, but only relies on the molar mass of each component M_i, the solvent dynamic viscosity η_2 and density ρ_2, and the molar core volume of each component $V_{0,i}$, which can be calculated from the method described in the previous section. The model is given as

$$D_{11} = 5.3 \times 10^{-11} \frac{T}{\eta_2^A \rho_2^{0.95}} \frac{V_{0,2}^{1/3}}{V_{0,1}}, \tag{5.9}$$

$$A = \left(\frac{V_{0,2}}{M_2} \right)^{1/M_1} - 0.44\,. \tag{5.10}$$

This equation has been parameterized using the aforementioned training set, which contains all DLS experimental Fick diffusivity data $D_{11,exp}$ reported in references 77, 78, 88 and 90-93, except for those where the Lewis number Le is close to 1 and the reported D_{11}^{*} is the effective diffusivity. The training set consists of 451 data points. Bias and AARD between $D_{11,calc}$ predicted with Eq. 5.9-5.10 and $D_{11,exp}$ is reported in Table 5.4 for the complete training set. It is also shown separately for the seven different fluid classes and 11 different dissolved-gas solutes. Additionally, the bias is graphically represented in Figure 5.8(C) next to the calculated bias for the model proposed by Wu et al. [78] in Figure 5.8(A), and their model reparametrized with the new training set in Figure 5.8(B). A parity plot for $D_{11,calc}$ predicted with Eq. 5.9-5.10 against $D_{11,exp}$ is given in the left part of Figure 5.9. The right part of Figure 5.9 is an extended parity plot also containing data from a testing set including binary gaseous mixtures.

The *n*-alkane (blue) and 1-alcohol (red) solvents were the only solvent fluid classes included in the training set of the original model by Wu et al. [78]. Figure 5.8(A) shows a strong positive deviation, i.e. an overprediction of $D_{11,calc}$, for 1-alcohols. This data mostly corresponds to the investigations in Piszko et al. [92] for the heavy and bulky refrigerants R143a, R236fa, and SF_6. The reparameterization of their model with the new training set improved these predictions but could not accurately predict several other fluid classes and therefore introduced a systematic bias to compensate for this. This is shown in Figure 5.8(B), where the blue and red curves fall to the left of the zero line. Most predictions for *n*-alkanes and 1-alcohols with this model are slightly underpredicted, but within 20%. The new model proposed in this work from Eq. 5.9-5.10 also shows some systematic deviations between solvent fluid classes.

In particular, the general overprediction of $D_{11,calc}$ in mixtures with *n*-alkane solvents as compared to those with 1-alcohol solvents can be seen both in Figure 5.8(C) and the parity plot in the left of Figure 5.9. This observation was also made by Wu et al. [78] in their application of their original model, which was published a year prior and developed using only experimental D_{11} data of binary mixtures with *n*-alkane solvents [77]. Wu et al. remedied this issue with the introduction of the solvent dipole moment in Ψ, described by Eq. 2.13-2.14. In this work, the dipole moment is not considered to maintain the exceptionally easy application of the model. The influence on D_{11} of associative interactions experienced by polar molecules in a fluid should be reflected in other macroscopic properties, such as η. For example, the viscosity of *n*-hexane compared to that of 1-hexanol at 303 K around atmospheric pressure is over a factor of 10

smaller. This emphasis away from incorporating further substance-specific parameters and instead relying on the relationship between the two transport properties D_{11} and η is the basis of this model development.

Table 5.4. Bias and AARD for all binary mixtures included in the training set given in total as well as separated by fluid class and dissolved gaseous solute along with the number of data points in each category.

	Number of data points	Bias	AARD		Number of data points	Bias	AARD
all	451	0.08	18.85	H_2	41	7.08	15.77
n-alkanes	133	10.32	17.89	He	72	–12.99	19.35
branched alkanes	19	10.92	11.82	CH_4	23	2.93	9.81
rings	40	–11.89	13.40	Ne	12	17.26	23.29
1-alcohols	138	–8.96	14.49	N_2	47	0.82	15.83
acid/ester	25	–3.78	15.61	CO	30	18.63	21.05
ionic liquids	96	2.72	30.95	CO_2	57	–8.00	14.41
				Kr	102	4.28	15.14
				R143a	34	–9.57	10.99
				SF_6	9	–9.27	10.67
				R236fa	12	–21.21	22.60

Although some systematics remain, there is a clear improvement in predicting $D_{11,calc}$, particularly for binary mixtures which have one of the two solvents containing a carbonyl-group or an ionic liquid solvent. The largest deviation observed between $D_{11,calc}$ and $D_{11,exp}$ was 122% for the mixture of [EMIM][NTf_2] and H_2 at 298 K. Curiously, only the mixtures containing IL solvents and the lightest molecules He and H_2 were poorly predicted by the model with bias and AARD of (–42.22 and 47.11)% for He and 65.08% both for H_2, considering all state points. Without the data of these mixtures included, the bias and AARD between $D_{11,calc}$ and $D_{11,exp}$ for all other binary mixtures in the training set containing an IL solvent are (–3.10 and 17.23)%. It could be that due to the high viscosity of the ILs (close to 20 times larger than η of 1-hexanol and over 200 times larger than η of *n*-hexane at 303 K

and atmospheric pressure) and the small size and light weight of the gases, H_2 and He diffuse through the solvent as though they are moving through a porous media. It is unclear why $D_{11,calc}$ for mixtures containing He are underpredicted, but are overpredicted for mixtures containing H_2. However, it likely has to do with the representation of the molar mass in the model, since they are nearly the same size.

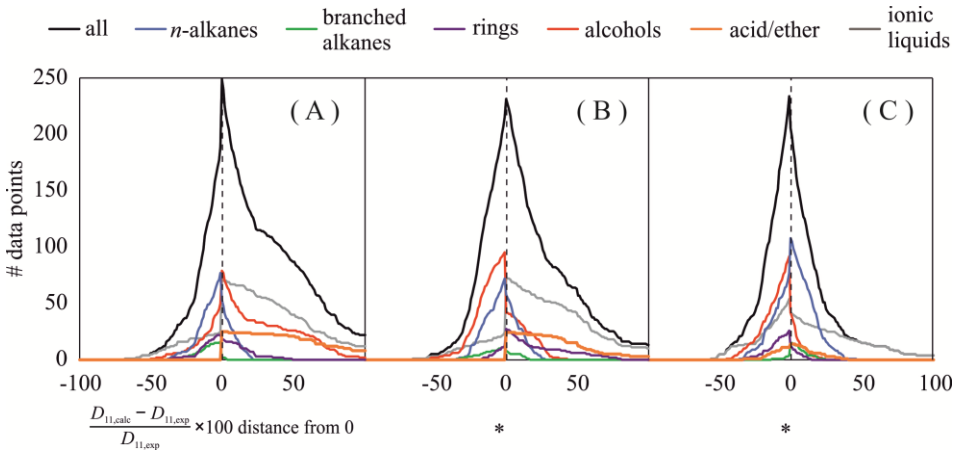

Figure 5.8. Evaluation of model bias for (A) Wu et al. [78], shown with Eq. 2.13-2.14 (B) the model of Wu et al. re-parameterized according to Eq. 5.3-5.4, and (C) Eq. 5.9-5.10 of this work. Solvent fluid class of the training set are indicated by color and selected data for training the models is discussed in the main text.

As a next step, the new model is applied to 314 diffusivities acquired from the literature comprising the testing set. Solvent and solute input data for η and ρ are acquired from the REFPROP software version 10.0 by the National Institute of Standards and Technology (NIST) [125], except for 1-propanol, *n*-hexadecane, *n*-octacosane and *n*-eicosane, which were not available. Here, η and ρ are calculated using the correlation provided by Ruth et al. [126], and data measured by Mathews et al. [116], Rodden et al. [117,118], and Klein et al. [58]. Experimental diffusivities for the testing set can be found in references 14-21, 81, 83, 116-118, and 127-138. Although more data is available in the literature, particularly for gaseous mixtures, it is not applied here because a more comprehensive application of the model would be beyond the scope of this thesis. The development and testing of this simple, predictive engineering model is meant to cumulate the results characterizing diffusive mass transport in binary mixtures of a liquid solvent with a dissolved gas solute close to infinite dilution.

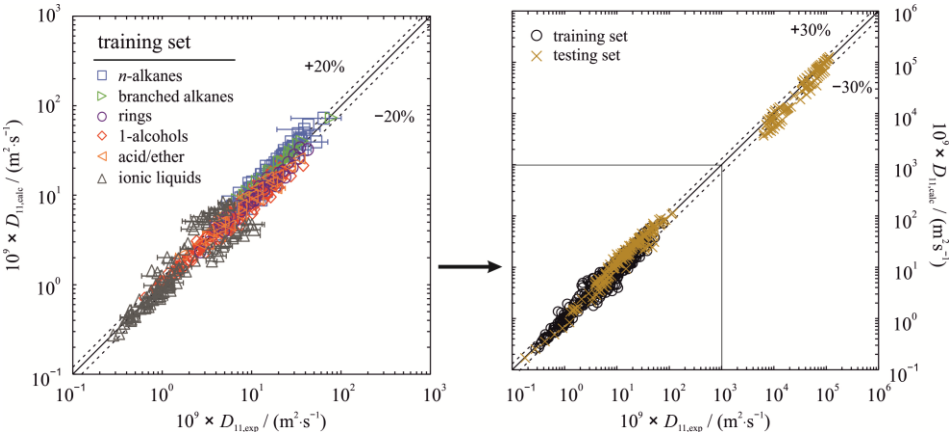

Figure 5.9. Parity plots of binary Fick diffusion coefficients predicted using the proposed model described by Eq. 5.9-5.10 in the main text $D_{11,calc}$ and those determined via experiments $D_{11,exp}$. (Left) 451 diffusivities comprising the data used in the training set, where symbol color indicates the solvent fluid class. (Right) The 451 diffusivities of the training set with 314 diffusivities comprising the testing set for Eq. 5.9-5.10.

A parity plot of $D_{11,calc}$ and $D_{11,exp}$ for the training set and testing set are shown in the right part of Figure 5.9. Diffusivities in the training set spanned two orders of magnitude from 2.9×10^{-10} mPa·s for [DMIM][NTf_2] with dissolved Kr at 298 K to 7.8×10^{-7} mPa·s for neohexane with dissolved He at 423 K. The testing set includes 219 data from liquid or supercritical fluid mixtures, with the lowest diffusivity value being 1.1×10^{-11} mPa·s for propanol with dissolve methane at 153 K. There are also 95 data from gaseous mixtures included and the largest diffusivity value is 1.1×10^{-4} mPa·s for He with dissolved N_2 at 400 K. The testing set therefore spans seven orders of magnitude. The bias and AARD for all 314 diffusivities comprising the testing set are (6.7, 23.6)%. The maximum absolute relative deviation is 92.3% from the supercritical fluid mixture of CO_2 with propanol at 343 K and 8 MPa.

6 Conclusions

Mass diffusion is important for process design and optimization in many fields of engineering. In particular, in the areas of chemical and energy engineering, many working fluids consist of liquids with dissolved gas and accurate knowledge of diffusion in these systems can aid in production efficiency. The number of potential working fluids or mixture combinations as well as all the possible thermodynamic states which could be relevant for process design and optimization are nearly limitless. Although a fundamental understanding of how the molecular characteristics of mixture components influence diffusion is necessary to characterize the diffusive mass process in binary fluid mixtures, it would be impossible to experimentally investigate everything. Therefore, it is necessary to be able to screen candidate working fluids in new and modernized technologies.

Experimental results are the gold standard in terms of accurate determination of fluid properties, but simulations are ever improving and are a cost-effective option next to experiments. Additionally, EMD simulations allow a unique interpretation of results by offering insight into the fluid structure on a molecular level. Another predictive method for estimating mass diffusivities is the application of prediction models. While many models available in the literature are empirically based and therefore limited to the range of fluid class and thermodynamic states upon which they were developed, there are also those available which are built from a theoretical basis. However, when applied to real fluid mixtures, it becomes necessary to incorporate an empirically based correction to the theory for improved accuracy of results. Accordingly, there is then always a trade-off between achieving an accurate prediction and the ease of application of the prediction model.

In an effort to develop our fundamental understanding of diffusion in fluids, diffusive mass transport in binary fluid mixtures consisting of a liquid solvent with a dissolved gas solute close to the infinite dilution limit is characterized using DLS experiments and EMD simulations. Investigations for the binary Fick diffusion coefficient

are performed over a wide range of temperatures and pressures, namely from (298 to 423) K and up to 10.86 MPa. In total, 451 binary Fick diffusion coefficients spanning 89 mixture combinations, 17 liquid solvents, and 11 dissolved gases are evaluated to assess the influence of molecular characteristics on diffusion. The solvents vary by fluid class considering *n*-alkanes with N_c = 6 to 28, 1-alcohols with N_c = 2 to 10, cyclic or aromatic hydrocarbons, branched alkanes, an acid, an ester, and ionic liquids including three different cations and two different anions. The dissolved gasses vary by molecular weight from M_{H_2} = 2.02 g·mol^{-1} to M_{R236fa} = 152 g·mol^{-1}, as well as by size, shape, and polarity. Many of the selected gases, such as H_2, CO_2, or the refrigerants, for example, have relevance in the fields of chemical engineering and energy technology.

An assessment of the influence of molecular characteristics on the diffusion coefficients acquired by DLS experiments highlights the strong relationship between mass diffusion and the solvent dynamic viscosity. The impact of hydrogen bonding is analyzed by evaluating diffusivities in the linear alkane *n*-hexane, the primary alcohol 1-hexanol, the acid *n*-hexanoic acid, and the ester ethyl butanoate – four solvents with N_c = 6 – at 303 K and a higher temperature of 348 K, where the impact of hydrogen bonding is significantly reduced. It is surmised that the polarity of a substance, and the resultant electrostatic forces therein e.g. hydrogen bonding, would be reflected in another thermophysical property that could be related to the diffusivity.

Diffusion coefficients of all solvents with N_c = 6, including the branched and cyclic hydrocarbons as well, with dissolved Kr are then related to temperature, solvent density, and solvent viscosity to address how these properties relate to diffusive mass transport over different solvent fluid classes. The relationship between binary mixture diffusion coefficients and the solvent dynamic viscosity appeared relatively independent of solvent fluid class. The impact of solute characteristics on the relationship between mass diffusivity and solvent viscosity is then evaluated by analyzing the binary mixtures of 15 different solvents with six different solutes. Here, a strong impact of solute molar mass and shape or size could be identified.

To improve upon the predictive methods used in diffusion research, DLS results are used as validation for EMD simulation results. Although simulations have, in general, a systematic underprediction of diffusion coefficients compared to DLS results, they can accurately predict the observed trends of mass diffusion with respect to e.g., temperature, viscosity, or solute type. Therefore, EMD simulations are further utilized to calculate hydrogen-bond statistics and analyze fluid behavior on a microscopic level via radial distribution functions. The validation of simulation results provided by experimental DLS results also allows evaluation of the molecular FFs used in simulations. To improve the predictive capabilities of EMD simulations approaching the critical temperature of the investigated solvent, a FF modification was developed in the form of a substance-specific temperature-dependent modification to the energy parameter of the Lennard-Jones potential. This correlation requires only the critical temperature of the substance and is applicable up to a reduced temperature $T_R = T/T_c$ of 0.98. Additionally, the cyclohexane FF is modified with a static change to the sigma parameter to improve predictions of the dynamic properties η and D_{self} up to 448 K.

Another predictive method beyond simulation techniques addressed in this work is that of prediction models. The previously published model by Wu et al. [78], which is discussed in the State of the Art, is re-parameterized according to a training set identified by the 451 diffusivities included in the discussion on how diffusive mass transport is impacted by molecular characteristics. This new model does not have significantly improved accuracy and it is clear that the basis of the model is, again, limited to the fluid classes of its original development. To improve upon the model in the same way for the wide variety of new mixture combinations that are included in the training set would introduce greater complexity to the model which would greatly reduce the appeal of applying it. Instead, the concept of accounting for a fluid's "free volume" is readdressed. This has been proposed and applied by several well-known models in the literature based on hydrodynamic theory or hard-sphere theory [22,62,76]. A simple approach to estimating the core volume of any molecule is proposed. Here, the molar core volume of a molecule is determined

by representing the atoms as hard-spheres and calculating the volume of overlapping spheres with simple geometry, based on the work of Bondi [79,80]. The solvent and solute core volume are then used to develop an exceptionally simple predictive engineering model for binary Fick diffusion coefficients of liquids with dissolved gas close to the infinite dilution regime. This model also includes the molar masses of both mixture components as well as the solvent dynamic viscosity and density. This model is developed using the 451 diffusivities of the training set and has an overall bias and average absolute relative deviation from experimental results of (0.08 and 18.85)%. The only clear outliers are binary mixtures of the ionic liquids containing the anion [NTf_2] with dissolved H_2 or He. Here, it can be deduced that the two gases are diffusing in the solvent similarly to diffusion through a porous media due to the very large viscosity of the solvent coupled with the small size and light weight of the gases. This hypothesis is not evaluated.

The model is then applied to a testing set comprising of 314 diffusivities acquired from the literature considering 49 mixture combinations, including 11 binary gaseous mixtures. Although much more data is available in the literature, especially for gaseous mixtures, only select combinations were chosen in order to diversify model application and avoid a biased evaluation. As such, the total bias and average absolute relative deviation of the testing set is (6.7 and 23)%. Considering both the training and testing sets, totaling 765 binary Fick diffusion coefficients and spanning seven orders of magnitude, the bias and AARD are (2.8 and 21)%.

In conclusion, furthering our fundamental understanding of diffusive mass transport has been achieved through analysis of experimentally determined binary Fick diffusion coefficients, validation of EMD simulation techniques and improvements in FF development, and the development of a simple, predictive engineering model. The strong relationship between the two dynamic properties viscosity and diffusivity is readily apparent and better understood following these investigations. Given the reasonable accuracy and exceptional ease of implementation for this model as well as the broad variation of solvent fluid class and solute characteristics of the mixtures which

went into its development, it is a valuable tool for the prediction of binary Fick diffusivities at the limit of infinite dilution. Next steps would be to investigate how the model performs for more diverse or complex real systems and to test the range of applicability of the core volume calculation to novel substances. Evaluating the performance of the new model for multicomponent mixtures, which can be treated as a binary system, is of interest. This has already been done here for the mixtures containing ILs. Furthermore, testing the applicability of the new model to binary mixtures beyond the infinite dilution regime could be addressed with inclusion of different component concentrations and the activity coefficient or thermodynamic factor of the mixture.

References

(1) Scheuermann, S. S.; Eibl, S.; Bartl, P., Detailed Characterisation of Isomers Present in Polyalphaolefin Dimer and the Effect of Isomeric Distribution on Bulk Properties. *Lubr. Sci.* **2011,** *23*, 221-232.

(2) Linke, P.; Papadopoulos, A. I.; Seferlis, P., Systematic Methods for Working Fluid Selection and the Design, Integration and Control of Organic Rankine Cycles—A Review. *Energies* **2015,** *8*, 4755-4801.

(3) Rao, P. C.; Yoon, M., Potential Liquid-Organic Hydrogen Carrier (LOHC) Systems: A Review on Recent Progress. *Energies* **2020,** *13*, 6040.

(4) Niermann, M.; Drünert, S.; Kaltschmitt, M.; Bonhoff, K., Liquid Organic Hydrogen Carriers (LOHCs) – Techno-Economic Analysis of LOHCs in a Defined Process Chain. *Energy Environ. Sci.* **2019,** *12*, 290-307.

(5) IUPAC Solubility Data Series (online) - IUPAC-NIST Solubility Database, Version 1.1. Office of Data and Informatics of the National Institute of Standards and Technology (NIST) Material Measurement Laboratory (MML): online, 2012.

(6) Qian, D.; Chris, M.; Andrei, K.; Vladimir, D.; Joe, M.; Jason, W.; Robert, C.; Kenneth, M.; Michael, F., ILThermo: A Free-Access Web Database for Thermodynamic Properties of Ionic Liquids. *J. Chem. Eng. Data* **2007**.

(7) Andrei, K.; Joe, M.; Robert, C.; Vladimir, D.; Kenneth, K.; Chris, M.; Michael, F., Ionic Liquids Database - ILThermo (v2.0). Ionic Liquids Database - ILThermo (v2.0): 2013.

(8) Fick, A., V. On Liquid Diffusion. *Lond. Edinb. Dublin Philos. Mag. J. Sci.* **1855,** *10*, 30-39.

(9) Taylor, R., *Multicomponent Mass Transfer*. John Wiley & Sons: 1993; Vol. 2.

(10) Cadogan, S. P.; Hallett, J. P.; Maitland, G. C.; Trusler, J. P. M., Diffusion Coefficients of Carbon Dioxide in Brines Measured Using 13C Pulsed-Field Gradient Nuclear Magnetic Resonance. *J. Chem. Eng. Data* **2015,** *60*, 181-184.

(11) Etesse, P.; Chapman, W. G.; Kobayashi, R., Nuclear Magnetic Resonance Measurement of Spin-Lattice Relaxation and Self-Diffusion in Supercritical CO_2-*n*-Hexadecane Mixtures. *Mol. Phys.* **1993,** *80*, 1145-1164.

(12) Lito, P. F.; Magalhães, A. L.; Gomes, J. R. B.; Silva, C. M., Universal Model for Accurate Calculation of Tracer Diffusion Coefficients in Gas, Liquid and Supercritical Systems. *J. Chromatogr. A* **2013,** *1290*, 1-26.

(13) Marrero, T. R.; Mason, E. A., Gaseous Diffusion Coefficients. *J. Phys. Chem. Ref. Data* **1972,** *1*, 3-118.

(14) *Gases in Gases, Liquids and Their Mixtures*. Springer Berlin, Heidelberg: 2007; p VIII, 411.

(15) Wilhelm, E.; Battino, R., Binary Gaseous Diffusion Coefficients. 1. Methane and Carbon Tetrafluroide with *n*-Hexane, *n*-Heptane, *n*-Octane, and 2, 2, 4-Trimethylpentane at One-Atmosphere Pressure at 10-70 deg. *J. Chem. Eng. Data* **1972,** *17*, 187-189.

(16) Dunlop, P. J.; Bignell, C., Diffusion and Thermal Diffusion in Binary Mixtures of Methane with Noble Gases and of Argon with Krypton. *Physica A: Stat. Mech. Appl.* **1987,** *145*, 584-596.

(17) Trengove, R.; Harris, K.; Robjohns, H.; Dunlop, P. J., Diffusion and Thermal Diffusion in Some Dilute Binary Gaseous Systems Between 195 and 400 K: Tests of Several Asymmetric Potentials Using the Infinite Order Sudden Approximation. *Physica A: Stat. Mech. Appl.* **1985,** *131*, 506-519.

(18) Robjohns, H.; Dunlop, P. J., Diffusion and Thermal Diffusion in Some Binary Mixtures of the Major Components of Air. *Ber. Bunsenges. Phys. Chem.* **1984,** *88*, 1239-1241.

(19) Wilhelm, E.; Battino, R.; Carpenter, R. L., Binary Gaseous Diffusion Coefficients. II. Methane and Carbon Tetrafluoride with Cyclohexane, Methylcyclohexane, Benzene, and Toluene at 1 atm at 10-70. deg. *J. Chem. Eng. Data* **1974,** *19*, 245-247.

(20) Loiko, A.; Ivakin, B.; Suetin, P., Temperature Dependence of Trace Diffusion Coefficients of Certain Gases. *Sov. Phys. JETP* **1974,** *19*, 434.

(21) Seager, S. L.; Geertson, L. R.; Giddings, J. C., Temperature Dependence of Gas and Vapor Diffusion Coefficients. *J. Chem. Eng. Data* **1963,** *8*, 168-169.

(22) Cadogan, S. P.; Mistry, B.; Wong, Y.; Maitland, G. C.; Trusler, J. P. M., Diffusion Coefficients of Carbon Dioxide in Eight Hydrocarbon Liquids at Temperatures between (298.15 and 423.15) K at Pressures up to 69 MPa. *J. Chem. Eng. Data* **2016,** *61*, 3922-3932.

(23) Morgan, D.; Ferguson, L.; Scovazzo, P., Diffusivities of Gases in Room-Temperature Ionic Liquids: Data and Correlations Obtained Using a Lag-Time Technique. *Ind. Eng. Chem.* **2005,** *44*, 4815-4823.

(24) Huang, J.; Rüther, T., Why are Ionic Liquids Attractive for CO_2 Absorption? An Overview. *Aust. J. Chem.* **2009,** *62*, 298-308.

(25) Asensio-Delgado, S.; Pardo, F.; Zarca, G.; Urtiaga, A., Vapor–Liquid Equilibria and Diffusion Coefficients of Difluoromethane, 1,1,1,2-Tetrafluoroethane, and 2,3,3,3-Tetrafluoropropene in Low-Viscosity Ionic Liquids. *J. Chem. Eng. Data* **2020,** *65*, 4242-4251.

(26) Moganty, S. S.; Baltus, R. E., Diffusivity of Carbon Dioxide in Room-Temperature Ionic Liquids. *Ind. Eng. Chem.* **2010,** *49*, 9370-9376.

(27) Ramdin, M.; de Loos, T. W.; Vlugt, T. J. H., State-of-the-Art of CO2 Capture with Ionic Liquids. *Ind. Eng. Chem.* **2012,** *51*, 8149-8177.

(28) Hayduk, W.; Cheng, S. C., Review of Relation between Diffusivity and Solvent Viscosity in Dilute Liquid Solutions. *Chem. Eng. Sci.* **1971,** *26*, 635-646.

(29) Cadogan, S. P.; Maitland, G. C.; Trusler, J. P. M., Diffusion Coefficients of CO_2 and N_2 in Water at Temperatures between 298.15 K and 423.15 K at Pressures up to 45 MPa. *J. Chem. Eng. Data* **2014,** *59*, 519-525.

(30) Kugler, T.; Jäger, B.; Bich, E.; Rausch, M. H.; Fröba, A. P., Systematic Study of Mass Transfer in a Loschmidt Cell for Binary Gas Mixtures. *Int. J. Thermophys.* **2015,** *36*, 3116-3132.

(31) Malik, V.; Hayduk, W., A Steady'state Capillary Cell Method for Measuring Gas-Liquid Diffusion Coefficients. *Can. J. Chem. Eng.* **1968,** *46*, 462-466.

(32) Wu, W.; Jander, J. H.; Rausch, M. H.; Fröba, A. P.; Giraudet, C., Simultaneous Determination of Multiple Transport Properties over a Wide Range of Temperatures and Pressures from the Analysis of Non-Equilibrium Fluctuations by the Shadowgraph Method. *J. Chem. Phys.* **2020,** *153*.

(33) Schmidt, P. S.; Wu, W.; Rausch, M. H.; Fröba, A. P., Fick diffusion coefficients probed by the shadowgraph method considering confinement and advection. *J. Chem. Phys.* **2023,** *158*.

(34) Wu, W.; Schmidt, P. S.; Piszko, M.; Giraudet, C.; Rausch, M. H.; Fröba, A. P., Determination of Diffusivities in Binary Fluid Mixtures with Various Lewis Numbers as well as Positive and Negative Soret Coefficients by the Shadowgraph Method. In *J. Chem. Phys.*, 2023.

(35) Fröba, A.; Botero, C.; Leipertz, A., Thermal Diffusivity, Sound Speed, Viscosity, and Surface Tension of R227ea (1,1,1,2,3,3,3-Heptafluoropropane). *Int. J. Thermophys.* **2006,** *27*, 1609-1625.

(36) Fröba, A. P. *Dynamic Light Scattering (DLS) for the Characterization of Working Fluids in Chemical and Energy Engineering*. Habilitation Thesis., Friedrich-Alexander-Universität Erlangen-Nürnberg, Erlangen, 2009.

(37) Metropolis, N.; Rosenbluth, A. W.; Rosenbluth, M. N.; Teller, A. H.; Teller, E., Equation of State Calculations by Fast Computing Machines. *J. Chem. Phys.* **1953,** *21*, 1087-1092.

(38) Cornell, W. D.; Cieplak, P.; Bayly, C. I.; Gould, I. R.; Merz, K. M.; Ferguson, D. M.; Spellmeyer, D. C.; Fox, T.; Caldwell, J. W.; Kollman, P. A., A Second Generation Force Field for the Simulation of Proteins, Nucleic Acids, and Organic Molecules. *J. Am. Chem. Soc.* **1995,** *117*, 5179-5197.

(39) MacKerell, A. D.; Bashford, D.; Bellott, M.; Dunbrack, R. L.; Evanseck, J. D.; Field, M. J.; Fischer, S.; Gao, J.; Guo, H.; Ha, S.; Joseph-McCarthy, D.; Kuchnir, L.; Kuczera, K.; Lau, F. T. K.; Mattos, C.; Michnick, S.; Ngo, T.; Nguyen, D. T.; Prodhom, B.; Reiher, W. E.; Roux, B.; Schlenkrich, M.; Smith, J. C.; Stote, R.; Straub, J.; Watanabe, M.; Wiórkiewicz-Kuczera, J.; Yin, D.; Karplus, M., All-Atom Empirical Potential for Molecular Modeling and Dynamics Studies of Proteins. *J. Phys. Chem. B* **1998,** *102*, 3586-3616.

(40) Guvench, O.; MacKerell, A. D., Comparison of Protein Force Fields for Molecular Dynamics Simulations. In *Molecular Modeling of Proteins*, Kukol, A., Ed. Humana Press: Totowa, NJ, 2008; pp 63-88.

(41) Jorgensen, W. L.; Maxwell, D. S.; TiradoRives, J., Development and Testing of the OPLS All-Atom Force Field on Conformational Energetics and Properties of Organic Liquids. *J. Am. Chem. Soc.* **1996,** *118*, 11225-11236.

(42) Jorgensen, W. L.; Madura, J. D.; Swenson, C. J., Optimized Intermolecular Potential Functions for Liquid Hydrocarbons. *J. Am. Chem. Soc.* **1984,** *106*, 6638-6646.

(43) Glova, A. D.; Volgin, I. V.; Nazarychev, V. M.; Larin, S. V.; Lyulin, S. V.; Gurtovenko, A. A., Toward Realistic Computer Modeling of Paraffin-Based Composite Materials: Critical Assessment of Atomic-Scale Models of Paraffins. *RSC Adv.* **2019,** *9*, 38834-38847.

(44) Papavasileiou, K. D.; Peristeras, L. D.; Bick, A.; Economou, I. G., Molecular Dynamics Simulation of Pure *n*-Alkanes and Their Mixtures at Elevated Temperatures Using Atomistic and Coarse-Grained Force Fields. *J. Phys. Chem. B* **2019,** *123*, 6229-6243.

(45) Raabe, G., Parameterization Approach for a Systematic Extension of the Hydrofluoroolefin Force Field to Fluorinated Butenes and Hydrochlorofluoroolefin Compounds. *J. Chem. Eng. Data* **2020,** *65*, 1234-1242.

(46) Raabe, G.; Maginn, E. J., A Force Field for 3,3,3-Fluoro-1-propenes, Including HFO-1234yf. *J. Phys. Chem. B* **2010,** *114*, 10133-10142.

(47) Kerscher, M.; Klein, T.; Schulz, P. S.; Veroutis, E.; Dürr, S.; Preuster, P.; Koller, T. M.; Rausch, M. H.; Economou, I. G.; Wasserscheid, P.; Fröba, A. P., Thermophysical Properties of Diphenylmethane and Dicyclohexylmethane as a Reference Liquid Organic Hydrogen Carrier System from Experiments and Molecular Simulations. *Int. J. Hydrog. Energy* **2020,** *45*, 28903-28919.

(48) Tildesley, D. J.; Allen, M. P., *Computer Simulation of Liquids*. Clarendon Oxford: 1987.

(49) Frenkel, D.; Smit, B., *Understanding Molecular Simulation: from Algorithms to Applications*. Elsevier: 2001; Vol. 1.

(50) Hoover, W. G.; Hoover, C. G., Nonequilibrium Molecular Dynamics. *Condens. Matter Phys.* **2005,** *8*, 247-260.

(51) Irma M. J. J. Van De Ven-Lucassen Thijs J. H. Vlugt Antonius J. J. Van Der Zanden Piet J. A. M, K., Using Molecular Dynamics to Obtain Maxwell-Stefan Diffusion Coefficients in Liquid Systems. *Mol. Phys.* **1998,** *94*, 495-503.

(52) Schelling, P. K. a. P., Simon R. and Keblinski, Pawel, Comparison of Atomic-Level Simulation Methods for Computing Thermal Conductivity. *Phys. Rev. B* **2002,** *65*, 144306.

(53) Müller-Plathe, F., Reversing the Perturbation in Nonequilibrium Molecular Dynamics: an Easy Way to Calculate the Shear Viscosity of Fluids. *Phys. Rev. E* **1999,** *59*, 4894.

(54) Lu, G.; Duan, Y.-Y.; Wang, X.-D., Surface Tension, Viscosity, and Rheology of Water-Based Nanofluids: a Microscopic Interpretation on the Molecular Level. *J. Nanopart. Res.* **2014,** *16*, 2564.

(55) Wang, J.; Hou, T., Application of Molecular Dynamics Simulations in Molecular Property Prediction. 1. Density and Heat of Vaporization. *J. Chem. Theory Comput.* **2011,** *7*, 2151-2165.

(56) Wang, J.; Wolf, R. M.; Caldwell, J. W.; Kollman, P. A.; Case, D. A., Development and Testing of a General Amber Force Field. *J. Comput. Chem.* **2004,** *25*, 1157-1174.

(57) Jämbeck, J. P. M.; Lyubartsev, A. P., Update to the General Amber Force Field for Small Solutes with an Emphasis on Free Energies of Hydration. *J. Phys. Chem. B* **2014,** *118*, 3793-3804.

(58) Klein, T.; Lenahan, F. D.; Kerscher, M.; Rausch, M. H.; Economou, I. G.; Koller, T. M.; Fröba, A. P., Characterization of Long Linear and Branched Alkanes and Alcohols for Temperatures up to 573.15 K by Surface Light Scattering and Molecular Dynamics Simulations. *J. Phys. Chem. B* **2020,** *124*, 4146-4163.

(59) Neumann, J.; Golub, B.; Odebrecht, L.-M.; Ludwig, R.; Paschek, D., Revisiting Imidazolium Based Ionic Liquids: Effect of the Conformation Bias of the [NTf_2] Anion Studied by Molecular Dynamics Simulations. *J. Chem. Phys.* **2018,** *148*.

(60) Himmelblau, D. M., Diffusion of Dissolved Gases in Liquids. *Chem. Rev.* **1964,** *64*, 527-550.

(61) Day, M. A., The No-Slip Condition of Fluid Dynamics. *Erkenntnis* **1990,** *33*, 285-296.

(62) Assael, M. J.; Dymond, J. H.; Tselekidou, V., Correlation of High-Pressure Thermal Conductivity, Viscosity, and Diffusion Coefficients for *n*-Alkanes. *Int. J. Thermophys.* **1990,** *11*, 863-873.

(63) Aljeshi, Y. A.; Taib, M. B. M.; Trusler, J. P. M., Modelling the Diffusion Coefficients of Dilute Gaseous Solutes in Hydrocarbon Liquids. *Int. J. Thermophys.* **2021,** *42*, 140.

(64) Assael, M. J.; Dymond, J. H.; Patterson, P. M., Correlation and Prediction of Dense Fluid Transport Coefficients. IV. A Note on Diffusion. *Int. J. Thermophys.* **1992,** *13*, 729-733.

(65) Assael, M. J.; Dymond, J. H.; Papadaki, M.; Patterson, P. M., Correlation and Prediction of Dense Fluid Transport Coefficients: II. Simple Molecular Fluids. *Fluid Phase Equilib.* **1992,** *75*, 245-255.

(66) Assael, M. J.; Dymond, J. H.; Papadaki, M.; Patterson, P. M., Correlation and Prediction of Dense Fluid Transport Coefficients. I. *n*-Alkanes. *Int. J. Thermophys.* **1992,** *13*, 269-281.

(67) Assael, M. J.; Dymond, J. H.; Patterson, P. M., Correlation and Prediction of Dense Fluid Transport Coefficients. V. Aromatic Hydrocarbons. *Int. J. Thermophys.* **1992,** *13*, 895-905.

(68) Assael, M. J.; Dymond, J. H.; Polimatidou, S. K., Correlation and Prediction of Dense Fluid Transport Coefficients. VI. *n*-alcohols. *Int. J. Thermophys.* **1994,** *15*, 189-201.

(69) Erkey, C.; Gadalla, H.; Akgerman, A., Application of Rough Hard Sphere Theory to Diffusion in Supercritical Fluids. *J. Supercrit. Fluids* **1990,** *3*, 180-185.

(70) Assael, M. J.; Dymond, J. H.; Papadaki, M.; Patterson, P. M., Correlation and Prediction of Dense Fluid Transport Coefficients. III. *n*-Alkane Mixtures. *Int. J. Thermophys.* **1992,** *13*, 659-669.

(71) Assael, M. J.; Dymond, J. H.; Polimatidou, S. K., Correlation and Prediction of Dense Fluid Transport Coefficients. VII. Refrigerants. *Int. J. Thermophys.* **1995,** *16*, 761-772.

(72) Sun, T.; Teja, A. S., Correlation and Prediction of the Viscosity and Thermal Conductivity of Dense Fluids. *J. Chem. Eng. Data* **2009,** *54*, 2527-2531.

(73) Ciotta, F.; Trusler, J. P. M.; Vesovic, V., Extended Hard-Sphere Model for the Viscosity of Dense Fluids. *Fluid Phase Equilib.* **2014,** *363*, 239-247.

(74) Ciotta, F.; Maitland, G.; Smietana, M.; Trusler, J. P. M.; Vesovic, V., Viscosity and Density of Carbon Dioxide + 2,6,10,15,19,23-Hexamethyltetracosane (Squalane). *J. Chem. Eng. Data* **2009,** *54*, 2436-2443.

(75) Dymond, J. H., A Theory-Based Method for Correlation and Prediction of Dense-Fluid Transport Properties. *Int. J. Thermophys.* **1997,** *18*, 303-312.

(76) Wilke, C. R.; Chang, P., Correlation of Diffusion Coefficients in Dilute Solutions. *AIChE J.* **1955,** *1*, 264-270.

(77) Giraudet, C.; Klein, T.; Zhao, G.; Rausch, M. H.; Koller, T. M.; Fröba, A. P., Thermal, Mutual, and Self-Diffusivities of Binary Liquid Mixtures Consisting of Gases Dissolved in *n*-Alkanes at Infinite Dilution. *J. Phys. Chem. B* **2018,** *122*, 3163-3175.

(78) Wu, W.; Klein, T.; Kerscher, M.; Rausch, M. H.; Koller, T. M.; Giraudet, C.; Fröba, A. P., Diffusivities in 1-Alcohols Containing Dissolved H_2, He, N_2, CO, or CO_2 Close to Infinite Dilution. *J. Phys. Chem. B* **2019,** *123*, 8777-8790.

(79) Bondi, A., *Physical Properties of Molecular Crystals, Liquids and Glasses*. John Wiley & Sons, Inc.: New York, 1968; p 502.

(80) Bondi, A., van der Waals Volumes and Radii. *J. Phys. Chem.* **1964,** *68*, 441-451.

(81) Heller, A.; Koller, T. M.; Rausch, M. H.; Fleys, M. S.; Bos, A. R.; van der Laan, G. P.; Makrodimitri, Z. A.; Economou, I. G.; Fröba, A. P., Simultaneous Determination of Thermal and Mutual Diffusivity of Binary Mixtures of *n*-Octacosane with Carbon Monoxide, Hydrogen, and Water by Dynamic Light Scattering. *J. Phys. Chem. B* **2014,** *118*, 3981-3990.

(82) Rausch, M. H.; Heller, A.; Herbst, J.; Koller, T. M.; Bahlmann, M.; Schulz, P. S.; Wasserscheid, P.; Fröba, A. P., Mutual and Thermal Diffusivity of Binary Mixtures of the Ionic Liquids [BMIM][$C(CN)_3$] and [BMIM][$B(CN)_4$] with Dissolved CO_2 by Dynamic Light Scattering. *J. Phys. Chem. B* **2014,** *118*, 4636-4646.

(83) Heller, A.; Fleys, M. S.; Chen, J.; van der Laan, G. P.; Rausch, M. H.; Fröba, A. P., Thermal and Mutual Diffusivity of Binary Mixtures of *n*-Dodecane and *n*-Tetracontane with Carbon Monoxide, Hydrogen, and Water from Dynamic Light Scattering (DLS). *J. Chem. Eng. Data* **2016,** *61*, 1333-1340.

(84) Piszko, M.; Kankanamge, C. J.; Rausch, M. H.; Klein, T.; Fröba, A. P., Dynamic Light Scattering for Studying Mutual Diffusion Coefficients in Electrolyte Systems Comprised Entirely of Ions. *J. Electrochem. Soc.* **2020,** *167*, 133502.

(85) Leipertz, A.; Fröba, A.P., Diffusion Measurements in Fluids by Dynamic Light Scattering. In: *Diffusion in Condensed Matter*. Springer, Berlin, Heidelberg.: 2005; pp 579-618.

(86) Fröba, A. P.; Will, S.; Nagasaka, Y.; Winkelmann, J.; Wiegand, S.; Köhler, W., Optical Methods. In *Experimental Thermodynamics Volume IX: Advances in Transport Properties of Fluids*, The Royal Society of Chemistry: 2014; pp 19-74.

(87) Berne, B. J.; Pecora, R., *Dynamic Light Scattering: With Applications to Chemistry, Biology, and Physics*. Dover Publications: 2000.

(88) Piszko, M.; Lenahan, F. D.; Klein, T.; Fröba, A. P., Diffusivities in Binary Mixtures of Cyclohexane or Ethyl Butanoate with Dissolved CH_4 or R143a Close to Infinite Dilution. *J. Chem. Eng. Data* **2023,** *68*, 339-348.

(89) Lenahan, F. D.; Piszko, M.; Klein, T.; Fröba, A. P., Molecular Dynamics Simulations of Liquid Ethane up to 298.15 K. *Mol. Phys.* **2023**, e2211401.

(90) Lenahan, F. D.; Piszko, M.; Klein, T.; Fröba, A. P., Diffusivities in Binary Mixtures of *n*-Decane, *n*-Hexadecane, *n*-Octacosane, 2-Methylpentane, 2,2-Dimethylbutane, Cyclohexane, Benzene, Ethanol, 1-Decanol, Ethyl Butanoate, or *n*-Hexanoic Acid with Dissolved He or Kr Close to Infinite Dilution. *J. Chem. Eng. Data* **2022,** *67*, 622-635.

(91) Piszko, M.; Lenahan, F. D.; Friedl, L.; Klein, T.; Fröba, A. P., Mutual and Thermal Diffusivities in Mixtures of Cyclohexane, *n*-Hexadecane, *n*-Octacosane, or *n*-Hexanoic Acid with Carbon Dioxide Obtained by Dynamic Light Scattering and Molecular Dynamics Simulations. *J. Chem. Eng. Data* **2022,** *67*, 3059-3076.

(92) Piszko, M.; Lenahan, F. D.; Hahn, S.; Rausch, M. H.; Koller, T. M.; Klein, T.; Fröba, A. P., Diffusivities in Binary Mixtures of *n*-Hexane or 1-Hexanol with Dissolved CH_4, Ne, Kr, R143a, SF_6, or R236fa Close to Infinite Dilution. *J. Chem. Eng. Data* **2021,** *66*, 2218-2232.

(93) Piszko, M.; Lenahan, F. D.; Dennstädt, C.; Klein, T.; Fröba, A. P., Mutual and Thermal Diffusivities in Binary Mixtures of *n*-Hexane or 1-Hexanol with Krypton, R143a, or Sulfur Hexafluoride by Using Dynamic Light Scattering and Molecular Dynamics Simulations. *J. Chem. Eng. Data* **2023**.

(94) Wu, W.; Cui, J.; Sultan, U.; Gromotka, L.; Malgaretti, P.; Damm, C.; Harting, J.; Vogel, N.; Peukert, W.; Inayat, A.; Fröba, A. P., Diffusion of Gold Nanoparticles in Porous Silica Monoliths Determined by Dynamic Light Scattering. *J. Colloid Interface Sci.* **2023,** *641*, 251-264.

(95) Will, S.; Fröba, A.; Leipertz, A., Thermal Diffusivity and Sound Velocity of Toluene over a Wide Temperature Range. *Int. J. Thermophys.* **1998,** *19*, 403-414.

(96) Lenahan, F. D.; Zhai, Z.; Kankanamge, C. J.; Klein, T.; Fröba, A. P., Viscosity and Interfacial Tension of Ternary Mixtures Consisting of Linear Alkanes, Alcohols, and/or Dissolved Gases Using Surface Light Scattering and Equilibrium Molecular Dynamics Simulations. *Int. J. Thermophys.* **2022,** *43*, 116.

(97) Lenahan, F. D.; Zikeli, M.; Rausch, M. H.; Klein, T.; Fröba, A. P., Viscosity, Interfacial Tension, and Density of Binary-Liquid Mixtures of *n*-Hexadecane with *n*-Octacosane, 2,2,4,4,6,8,8-Heptamethylnonane, or 1-Hexadecanol at Temperatures between 298.15 and 573.15 K by Surface Light Scattering and Equilibrium Molecular Dynamics Simulations. *J. Chem. Eng. Data* **2021,** *66*, 2264-2280.

(98) Fröba, A. P.; Leipertz, A., Viscosity and Surface Tension of Saturated Toluene from Surface Light Scattering (SLS). *Int. J. Thermophys.* **2001,** *22*, 41-59.

(99) Martin, M. G.; Siepmann, J. I., Transferable Potentials for Phase Equilibria. 1. United-Atom Description of *n*-Alkanes. *J. Phys. Chem. B* **1998,** *102*, 2569-2577.

(100) Marrink, S. J.; Risselada, H. J.; Yefimov, S.; Tieleman, D. P.; de Vries, A. H., The MARTINI Force Field: Coarse Grained Model for Biomolecular Simulations. *J. Phys. Chem. B* **2007,** *111*, 7812-7824.

(101) Abraham, M. J.; Murtola, T.; Schulz, R.; Páll, S.; Smith, J. C.; Hess, B.; Lindahl, E., GROMACS: High Performance Molecular Simulations through Multi-level Parallelism from Laptops to Supercomputers. *SoftwareX* **2015,** *1-2*, 19 - 25.

(102) Yong Zhang, A. O., Edward J. Maginn, Reliable Viscosity Calculation from Equilibrium Molecular Dynamics Simulations: A Time Decomposition Method. *J. Chem. Theory Comput.* **2015,** *11*, 3537-3546.

(103) Yeh, I.-C.; Hummer, G., System-Size Dependence of Diffusion Coefficients and Viscosities from Molecular Dynamics Simulations with Periodic Boundary Conditions. *J. Phys. Chem. B* **2004,** *108*, 15873-15879.

(104) Liu, X.; Schnell, S. K.; Simon, J.-M.; Krüger, P.; Bedeaux, D.; Kjelstrup, S.; Bardow, A.; Vlugt, T. J. H., Diffusion Coefficients from Molecular Dynamics Simulations in Binary and Ternary Mixtures. *Int. J. Thermophys.* **2013,** *34*, 1169-1196.

(105) Jamali, S. H.; Wolff, L.; Becker, T. M.; Bardow, A.; Vlugt, T. J. H.; Moultos, O. A., Finite-Size Effects of Binary Mutual Diffusion Coefficients from Molecular Dynamics. *J. Chem. Theory Comput.* **2018,** *14*, 2667-2677.

(106) Ganguly, P.; van der Vegt, N. F. A., Convergence of Sampling Kirkwood–Buff Integrals of Aqueous Solutions with Molecular Dynamics Simulations. *J. Chem. Theory Comput.* **2013,** *9*, 1347-1355.

(107) Krüger, P.; Schnell, S. K.; Bedeaux, D.; Kjelstrup, S.; Vlugt, T. J. H.; Simon, J.-M., Kirkwood–Buff Integrals for Finite Volumes. *J. Phys. Chem. Lett.* **2013,** *4*, 235-238.

(108) Muñoz-Muñoz, Y. M.; Guevara-Carrion, G.; Vrabec, J., Molecular Insight into the Liquid Propan-2-ol + Water Mixture. **2018,** *J. Phys. Chem. B,* 8718-8729.

(109) Klein, T.; Wu, W.; Rausch, M. H.; Giraudet, C.; Koller, T. M.; Fröba, A. P., Influence of Liquid Structure on Fickian Diffusion in Binary Mixtures of n-Hexane and Carbon Dioxide Probed by Dynamic Light Scattering, Raman Spectroscopy, and Molecular Dynamics Simulations. *J. Phys. Chem. B* **2018,** *122*, 7122-7133.

(110) Klein, T.; Piszko, M.; Lang, M.; Mehler, J.; Schulz, P. S.; Rausch, M. H.; Giraudet, C.; Koller, T. M.; Fröba, A. P., Diffusivities in Binary Mixtures of [AMIM][NTf_2] Ionic Liquids with the Dissolved Gases H_2, He, N_2, CO, CO_2, or Kr Close to Infinite Dilution. *J. Chem. Eng. Data* **2020,** *65*, 4116-4129.

(111) Koller, T. M.; Heller, A.; Rausch, M. H.; Wasserscheid, P.; Economou, I. G.; Fröba, A. P., Mutual and Self-Diffusivities in Binary Mixtures of [EMIM][$B(CN)_4$] with Dissolved Gases by Using Dynamic Light Scattering and Molecular Dynamics Simulations. *J. Phys. Chem. B* **2015,** *119*, 8583-8592.

(112) Lemmon, E. W.; Huber, M. L., Thermodynamic Properties of *n*-Dodecane. *Energy Fuels* **2004,** *18*, 960-967.

(113) Klein, T.; Lenahan, F. D.; Kerscher, M.; Jander, J. H.; Rausch, M. H.; Koller, T. M.; Fröba, A. P., Viscosity and Interfacial Tension of Binary Mixtures of *n*-Hexadecane with Dissolved Gases Using Surface Light Scattering and Equilibrium Molecular Dynamics Simulations. *J. Chem. Eng. Data* **2021,** *66*, 3205-3218.

(114) Kankanamge, C. J.; Lenahan, F. D.; Klein, T.; Fröba, A. P., Viscosity and Interfacial Tension of Binary Mixtures Consisting of an *n*-Alkane, Branched Alkane, Primary Alcohol, or Branched Alcohol and a Dissolved Gas Using Equilibrium Molecular Dynamics Simulations. *Int. J. Thermophys.* **2022,** *43*, 112.

(115) Nikitin, E. D.; Popov, A. P., Critical Temperatures and Pressures of C40, C44, and C60 Normal Alkanes Measured by the Pulse-Heating Technique. *Fluid Phase Equilib.* **2014,** *379*, 191-195.

(116) Matthews, M. A.; Rodden, J. B.; Akgerman, A., High-Temperature Diffusion of Hydrogen, Carbon Monoxide, and Carbon Dioxide in Liquid *n*-Heptane, *n*-Dodecane, and *n*-Hexadecane. *J. Chem. Eng. Data* **1987,** *32*, 319-322.

(117) Rodden, J. B.; Erkey, C.; Akgerman, A., High-Temperature Diffusion, Viscosity, and Density Measurements in *n*-Eicosane. *J. Chem. Eng. Data* **1988,** *33*, 344-347.

(118) Rodden, J. B.; Erkey, C.; Akgerman, A., Mutual Diffusion Coefficients for Several Dilute Solutes in *n*-Octacosane and the Solvent Density at 371-534 K. *J. Chem. Eng. Data* **1988,** *33*, 450-453.

(119) Mantina, M.; Chamberlin, A. C.; Valero, R.; Cramer, C. J.; Truhlar, D. G., Consistent van der Waals Radii for the Whole Main Group. *J. Phys. Chem. A* **2009,** *113*, 5806-5812.

(120) Pyykkö, P.; Atsumi, M., Molecular Double-Bond Covalent Radii for Elements Li–E112. *Chem. Eur. J.* **2009,** *15*, 12770-12779.

(121) Pyykkö, P.; Atsumi, M., Molecular Single-Bond Covalent Radii for Elements 1–118. *Chem. Eur. J.* **2009,** *15*, 186-197.

(122) Ben-Amotz, D.; Herschbach, D. R., Estimation of Effective Diameters for Molecular Fluids. *J. Phys. Chem.* **1990,** *94*, 1038-1047.

(123) Fuller, E. N.; Schettler, P. D.; Giddings, J. C., New Method for Prediction of Binary Gas-Phase Diffusion Coefficients. *Ind. Eng. Chem.* **1966,** *58*, 18-27.

(124) Yaws, C. L., *Thermophysical Properties of Chemicals and Hydrocarbons*. William Andrew: 2008.

(125) Lemmon, E. W.; Bell, I. H.; Huber, M. L.; McLinden, M. O. *REFPROP, Standard Reference Data Program*, version 10.0 ed.; National Institute of Standards and Technology: Gaithersburg, MD, USA, 2018.

(126) Ruth, A. A.; Lesche, H.; Nickel, B., Temperature Dependence of Viscosity and Density of Cis-1,4/Trans-1,3-Dimethylcyclohexane and Several Other Commonly Used Organic Solvents. *Z. für Phys. Chem.* **2003,** *217*, 707-722.

(127) Sporka, K. H., J.; Růžička, V.; Halousek, M., Diffusion of Gases in Liquids. III. Diffusion Coefficients of Hydrogen in Organic Solvents. *Collect. Czech. Chem. Commun.* **1971,** *36*, 2130-2136.

(128) Dim, A. G., G. R.; Ponter, A. B.; Wood, T., Diffusion of Carbon Dioxide into Primary Alcohols and Methyl Cellulose Ether Solutions. *J. Chem. Eng. Jpn.* **1971,** *4*, 92-95.

(129) Snijder, E. D.; te Riele, M. J.; Versteeg, G. F.; van Swaaij, W. P., Diffusion Coefficients of CO, CO_2, N_2O, and N_2 in Ethanol and Toluene. *J. Chem. Eng. Data* **1995,** *40*, 37-39.

(130) Frank, M. J.; Kuipers, J. A.; van Swaaij, W. P., Diffusion Coefficients and Viscosities of CO_2+ H_2O, CO_2+ CH_3OH, NH_3+H_2O, and NH_3+CH_3OH Liquid Mixtures. *J. Chem. Eng. Data* **1996,** *41*, 297-302.

(131) Erkey, C.; Akgerman, A., Translational-Rotational Coupling Parameters for Mutual Diffusion in *n*-Octane. *AlChE J.* **1989,** *35*, 443-448.

(132) Chen, S.; Davis, H.; Evans, D., Tracer Diffusion in Polyatomic Liquids. II. *J. Chem. Phys.* **1981,** *75*, 1422-1426.

(133) Komarenko, V. G., Manzhelii, V.G., Radtsig, O.V., Temperature Dependence of the Diffusion Coefficient of Methane in Propanol. *Ukr. Fiz. Zh.* **1967,** *12*, 47-51.

(134) Gianturco, F. A.; Paesani, F.; Laranjeira, M. F.; Vassilenko, V.; Cunha, M. A.; Shashkov, A. G.; Zolotoukhina, A. F., Computed and Measured Transport Coefficients for Co-He Mixtures: Testing a Density Functional Approach. *Mol. Phys.* **1998,** *94*, 605-622.

(135) Berezhnoi, A. N.; Shekurov, V. N., Approximation of the Temperature Dependence of the Coefficients of Interdiffusion of Vapor—Gas Systems. *J. Eng. Phys.* **1985,** *49*, 951-955.

(136) Mei, D. H., Liu, H.Q., Wang, W.C., Measurement and Correlation of Diffusion Coefficients for Alcohols in Supercritical CO_2. *J. Chem. Ind. Eng.* **1995,** *46*, 357-364.

(137) Funazukuri, T.; Kong, C.; Kagei, S., Infinite Dilution Binary Diffusion Coefficients of Benzene in Carbon Dioxide by the Taylor Dispersion Technique at Temperatures from 308.15 to 328.15 K and Pressures from 6 to 30 MPa. *Int. J. Thermophys.* **2001,** *22*, 1643-1660.

(138) Chen, B. H.; Chen, S., Diffusion of Slightly Soluble Gases in Liquids: Measurement and Correlation with Implications on Liquid Structures. *Chem. Eng. Sci.* **1985,** *40*, 1735-1741.

Appendix : Publications

Publication A

Tobias Klein, Frances D. Lenahan, Manuel Kerscher, Michael H. Rausch, Ioannis G. Economou, Thomas M. Koller, and Andreas P. Fröba, *Characterization of Long Linear and Branched Alkanes and Alcohols for Temperatures up to 573.15 K by Surface Light Scattering and Molecular Dynamics Simulations*. Journal of Physical Chemistry B **2020** *124* (20), 4146-4163, DOI: 10.1021/acs.jpcb.0c01740.

Publication B

Frances D. Lenahan, Michael Zikeli, Michael H. Rausch, Tobias Klein, and Andreas P. Fröba, *Viscosity, Interfacial Tension, and Density of Binary-Liquid Mixtures of n-Hexadecane with n-Octacosane, 2,2,4,4,6,8,8-Heptamethylnonane, or 1-Hexadecanol at Temperatures between 298.15 and 573.15 K by Surface Light Scattering and Equilibrium Molecular Dynamics Simulations*. Journal of Chemical & Engineering Data **2021** *66* (5), 2264-2280,

Publication C

Maximilian Piszko, Frances D. Lenahan, Simon Hahn, Michael H. Rausch, Thomas M. Koller, Tobias Klein, and Andreas P. Fröba, *Diffusivities in Binary Mixtures of n-Hexane or 1-Hexanol with Dissolved CH_4, Ne, Kr, R143a, SF_6, or R236fa Close to Infinite Dilution*. Journal of Chemical & Engineering Data **2021** *66* (5), 2218-2232, DOI: 10.1021/acs.jced.1c00084

Publication D

Frances D. Lenahan, Maximilian Piszko, Tobias Klein, and Andreas P. Fröba, *Diffusivities in Binary Mixtures of n-Decane, n-Hexadecane, n-Octacosane, 2-Methylpentane, 2,2-Dimethylbutane, Cyclohexane, Benzene, Ethanol, 1-Decanol, Ethyl Butanoate, or n-Hexanoic Acid with Dissolved He or Kr Close to Infinite Dilution*. Journal of Chemical & Engineering Data **2022** *67* (3), 622-635, DOI: 10.1021/acs.jced.1c00922.

Publication E

Frances D. Lenahan, Ziwen Zhai, Chathura J. Kankanamge, Tobias Klein, and Andreas P. Fröba, *Viscosity and Interfacial Tension of Ternary Mixtures Consisting of Linear Alkanes, Alcohols, and/or Dissolved Gases Using Surface Light Scattering and Equilibrium Molecular Dynamics Simulations*. International Journal of Thermophysics **2022** *116* (43), DOI: https://doi.org-/10.1007/s10765-022-03040-x.

Publication F

Maximilian Piszko, Frances D. Lenahan, Lukas Friedl, Tobias Klein, and Andreas P. Fröba, *Mutual and Thermal Diffusivities in Mixtures of Cyclohexane, n-Hexadecane, n-Octacosane, or n-Hexanoic Acid with Carbon Dioxide Obtained by Dynamic Light Scattering and Molecular Dynamics Simulations*. Journal of Chemical & Engineering Data **2022** *67* (10), 3059-3076, DOI: 10.1021/acs.jced.2c00487

Publication G

Maximilian Piszko, Frances D. Lenahan, Tobias Klein, and Andreas P. Fröba, *Diffusivities in Binary Mixtures of Cyclohexane or Ethyl Butanoate with Dissolved CH_4 or R143a Close to Infinite Dilution*. Journal of Chemical & Engineering Data **2023** *68* (2), 339-348, DOI: 10.1021/acs.jced.2c00696

Publication H

Frances D. Lenahan, Maximilian Piszko, Tobias Klein, and Andreas P. Fröba, *Molecular Dynamics Simulations of Liquid Ethane Up to 298.15 K*. Molecular Physics **2023**, e2211401, DOI: 10.1080/00268976.2023.2211401.

Publication I

Maximilian Piszko, Frances D. Lenahan, Tobias Klein, and Andreas P. Fröba, *Mutual and Thermal Diffusivities in Binary Mixtures of n-Hexane or 1-Hexanol with Krypton, R143a, or Sulfur Hexafluoride by Using Dynamic Light Scattering and Molecular Dynamics Simulations*. Accepted for publication in the Journal of Chemical & Engineering Data **2023**, DOI: 10.1021/acs.jced.3c00143.

The aim of this thesis is the characterization of diffusive mass transport in liquids with dissolved gas through analysis of structure-property relationships in a variety of fluid systems. For this, systematically selected binary mixtures of a liquid solvent with a dissolved gas close to infinite dilution have been investigated by dynamic light scattering experiments and molecular dynamics simulations. Within this thesis, details on analyzing the molecular structure of the fluid using simulation results as well as improvements to molecular force fields are given. The evaluation of results is performed over 89 different mixture combinations of a liquid with a dissolved gas, totaling 451 diffusivities. The 17 liquid solvents can be classified as linear, branched, or cyclic alkanes, linear alcohols, an acid, an ester, or an ionic liquid and the 11 different gases vary in terms of molecular weight, size, shape, and polarity. A simple, predictive engineering model is presented, which is empirically developed based on these 451 experimental diffusivity results and requires only the solvent dynamic viscosity and density, the temperature, and the molar mass and core volume of both mixture components. A group contribution method is presented which is used to calculate the molar core volume. The average absolute relative deviation between prediction and experimental results is less than 20%. The model is additionally evaluated against 314 diffusivities from the literature for binary mixtures close to infinite dilution of one component and the average absolute relative deviation is 24%. This positive evaluation includes data for gaseous mixtures, suggesting that the model reflects a realistic behavior, since it is able to perform beyond the scope of its development.

ISBN 978-3-96147-726-5

FAU UNIVERSITY PRESS 2024